THESIS FOR DOCTOR OF ENGINEERING

NOVEL ELECTRODE STRUCTURE FOR THE REDUCTION OF METHANOL CROSSOVER IN A PASSIVE DMFC

MOHAMMAD ALI ABDELKAREEM

2008

Gunma University

Department of Biological and Chemical Engineering

Kiryu 376-8515, Gunma, JAPAN

THESIS FOR DOCTOR OF ENGINEERING

NOVEL ELECTRODE STRUCTURE FOR THE REDUCTION OF METHANOL CROSSOVER IN A PASSIVE DMFC

MOHAMMAD ALI ABDELKAREEM

2008

Gunma University

Department of Biological and Chemical Engineering

Kiryu 376-8515, Gunma, Japan

ABSTRACT

In the last decade, extensive research has been carried out to improve the performance of direct methanol fuel cells (DMFCs). The major problems facing the development of such fuel cells are the slow kinetics of the redox reactions and the crossover of methanol through the membrane which leads to mixed cathode potential and flooding of the cathode as well as high catalyst loading requirements on both electrodes. To get a fuel cell with a reasonable performance and efficiency we need to overcome these two problems. With respect of methanol crossover, a large number of studies were carried out for developing a new proton-conducting membrane or modifying the existing one. A few reports concerned the controlling of the methanol crossover through the backing layer.

This thesis focuses on the controlling of the methanol crossover in a passive direct methanol fuel cell using a novel electrode structure. In this novel structure, a porous carbon plate (PCP) was placed on the anode surface. Experiments have been carried out to investigate and determine the parameters affecting the performance of the DMFCs using this novel electrode structure under both open and closed circuit conditions.

Chapter one, consists of a theoretical back ground about the DMFCs, thermodynamics and kinetics basics, and the motivation of this study.

In chapter two, the effect of porous support properties such as porosity, ε, and water absorptivity, α_w, on the methanol crossover (MCO) and transport phenomena through the membrane electrode assembly (MEA) of a direct methanol fuel cell (DMFC) under open circuit conditions was theoretically and experimentally investigated. Porous plates, made of different materials, with different properties, were used as the support of the DMFC, and the performance of the crossover, i.e., CO_2 production rate at the cathode, cell temperature, fluxes of water and methanol, through the MEA with or without the porous plate were measured and compared to each other. The methanol flux increased with increasing the product of ε and α_w, $\varepsilon\alpha_w$, and the water flux slightly decreased with its increase, in the range where $\varepsilon\alpha_w$ was over a certain value, suggesting that the methanol flux was controlled by the diffusion resistance through the porous plate, whereas the total flux was not affected by it. It was clearly shown that these porous plates prevented the passive DMFC from undergoing a significant loss of methanol due to the crossover, and also being out of temperature control.

In chapter three, the effect of employing porous carbon plate on the performance of a passive direct methanol fuel cell (DMFC) under closed circuit conditions was investigated. The porous carbon plate and a CO_2 gas layer that formed between the anode and the porous plate stably controlled mass transfer of methanol and water from the reservoir to the anode, and they made operation with very high concentrations of methanol, even a neat methanol, possible. i-V and i-t performances of the DMFC with and without porous plate were measured at different methanol concentrations, and the performance was compared with each other. The maximum power density, 24mW/cm^2 at the room temperature, obtained at 2M without porous plate was reproduced at 16M with the porous plate. Also the methanol crossover flux and water flux through the MEA was evaluated and Faraday efficiency of DMFC with and without the porous carbon plate were analyzed. When high concentrations of methanol were used with the porous plate, it was confirmed that the Faraday efficiency was kept high and back diffusion of water from the cathode to the anode through the membrane occurred and that resulted in no flooding at the cathode, contrary to the case without porous plate.

In chapter four, the effect of oxygen and methanol supply modes on the performance and the fluxes of methanol and water through the membrane electrode assembly, MEA, of a DMFC with and without a porous plate was investigated. For the conventional MEA, MEA_C, flowing oxygen and methanol were essential to stabilize the cell performance, avoiding flooding at the cathode and depletion of methanol at the anode. As a result of flowing oxygen, methanol and water fluxes through the MEA_C increased by more than twice that for the air-breathing cell. For the MEA with a porous plate, MEA/PCP, the flow of oxygen and methanol had no significant effect on the cell performance, where the porous carbon plate, PCP, prevented the cathode from flooding by reducing the mass transport through the MEA. Methanol and water fluxes through the MEA/PCP were not affected by flowing oxygen at 0.1l/min. However, the increase in oxygen flow rate from 0.1l/min to 1l/min had a negative effect on the cell performance either in the MEA_C or in the MEA/PCP. This would be due to the cooling effect for MEA_C and the drying effect for the MEA/PCP. A moderate supply of oxygen to the cathode, like air-breathing, was appropriate for the DMFC with a PCP.

In chapter five, the effect of CO_2 discharge from the CO_2 gas layer formed between the anode surface and the porous carbon plate, PCP, was investigated to clear the role of the PCP and the CO_2 gas layer on the performance and the mass transfer in a passive DMFC

using different types of PCPs with different pore structures. The relation between the gas discharge through or not through the PCP and the DMFC performance as well as the effect of the pressure of the gas in the layer were investigated using PCPs with small pore size, 1μm in average diameter, PCPS1, and that with a large pore size, 42μm in average diameter, PCPY1. The formation of the CO_2 gas layer was essential for the strong obstructing of the methanol transport to the anode surface where the gaseous methanol diluted in the CO_2 gas contacted with it. The resistance of the methanol transport across the PCP was affected by the pore structure of the PCP, i.e., the pore size and the bubble point pressure. When the pore size was large, 42μm, the bubble going through the PCP accelerated the methanol transport.

In chapter six, the effect of pore structure and thickness of the porous carbon plate, PCP, as well as gas barrier thickness on the methanol transport and the performance of passive DMFC under different cell voltages 0.1, 0.2 and 0.3V using different methanol concentrations was investigated. As a result of the mass transfer restrictions by employing the PCP, high methanol concentrations over 20M could be used efficiently producing relatively high power density, 30mW/cm^2 for more than 10hrs. The DMFC was operated under limiting current conditions in all the PCPs at 0.1 and 0.2V to more than 20M. The main factors in controlling the methanol transport were the barrier of the gas layer with CO_2 which was formed between the anode surface and the PCP, and the properties of the PCP. At low current densities less than 60mA/cm^2, where CO_2 bubbles did not come out through the PCP, both pore structure and thickness of the PCP did not affect the methanol transport and the current voltage relationship. At higher current densities, CO_2 bubbles were evolved through the PCP; different resistances to methanol transport were shown depending on the PCP pore structure and thickness. CO_2 gas layer between the MEA and the PCP caused a major resistivity for methanol transport and its resistivity was increased with increasing its thickness. By using the PCP at 0.1V, energy density of passive DMFC was significantly increased e.g., more than seven times.

At the end, general conclusions of the studies done through the thesis were summarized.

TABLE of CONTENT

CHAPTER 1

Introduction

1. Fuel cell

1.1. Introduction

A fuel cell is an electrochemical "device" that continuously converts chemical energy into electric energy (and some heat) for as long as fuel and oxidant are supplied. Fuel cells therefore bear similarities both to batteries, with which they share the electrochemical nature of the power generation process, and to engines which — unlike batteries — will work continuously consuming a fuel of some sort. Here is where the analogies stop, though. Unlike engines or batteries, a fuel cell does not need recharging, it operates quietly and efficiently, and — when hydrogen is used as fuel — it generates only power and water, proton exchange membrane fuel cell, PEMFC. Thus, it is a so-called zero emission engine [1].

A fuel cell consists of an anode, a cathode, and an electrolyte. In a typical fuel cell (e.g. a PEMFC, see Fig. 1-1), hydrogen and oxygen gases are supplied to the anode and cathode, respectively. At the anode, protons and free electrons are produced from hydrogen oxidation reaction with the aid of catalyst

$$\mathbf{H_2 \rightarrow 2H^+ + 2e^-} \qquad \mathbf{(1\text{-}1)}$$

The hydrogen ions can be allowed to flow through the electrolyte, but the free electrons can't. At the cathode, the oxygen binds with the hydrogen ions and the free electrons, released at the anode and moving through the external circuit, to form water by catalyst

$$\mathbf{0.5O_2 + 2H^+ + 2e^- \rightarrow H_2O} \qquad \mathbf{(1\text{-}2)}$$

As a result, the movement of electrons from anode to cathode creates a current that can be used to power an electric engine

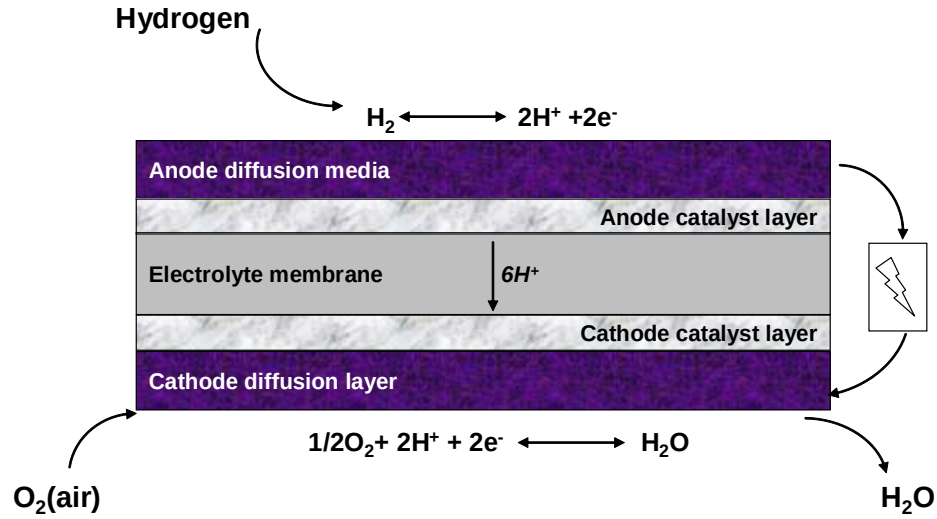

Figure 1-1: Basic description of a fuel cell (e.g. a proton exchange membrane fuel cell)

2. Direct methanol fuel cell

2.1. Introduction

A direct methanol fuel cell (DMFC) is an electrochemical cell that generates electricity based on the oxidation of methanol and reduction of oxygen. Figure 1-2 illustrates the cell construction of a DMFC. At the anode surface methanol and water electrochemically react (i.e., methanol is electro-oxidized) to produce carbon dioxide, protons, and electrons as shown in Eq. (1-3).

$$\mathbf{CH_3OH + H_2O \rightarrow CO_2 + 6H^+ + 6e^- (= 0.046\ V\ anode\ reaction)} \qquad \mathbf{(1\text{-}3)}$$

The protons produced at the anode migrate through the polymer electrolyte, an acidic electrolyte is advantageous to aid CO_2 rejection since insoluble carbonates form in alkaline electrolytes, to the cathode surface where they react with oxygen (usually from air) to produce water as shown in Eq. (1-4).

$$\mathbf{3/2O_2 + 6H^+ + 6e^- \rightarrow 3H_2O\ (=1.23\ V\ cathode\ reaction)} \qquad \mathbf{(1\text{-}4)}$$

These two electrochemical reactions are combined to form an overall cell reaction as:

$$\mathbf{CH_3OH + 3/2O_2 \rightarrow CO_2 + 2H_2O\ (E_{cell} = 1.18\ V\ cell\ voltage)} \qquad \mathbf{(1\text{-}5)}$$

The electrons produced at the anode carry the free energy change of the chemical reaction and travel through the external circuit where they can do useful work, such as powering an electric motor.

Depending on fuel operating strategy, the DMFC technology can be categorized into two groups. One is a vapor-feed DMFC operating at a cell temperature upto130 ºC under a pressurized condition. It is quite encouraging that increased power density up to the level of 250~400mW/cm^2 at 0.5V [2].

The other is a liquid-feed DMFC operating at the atmospheric pressure below 95 ºC. It can be started up at room temperature. The positive feature of a liquid feed to a DMFC is that it eliminates the humidification subsystem, which is required for a PEMFC with gaseous reactants. Another advantage is that the DMFC does not require a heavy and bulky fuel processor. The compensating feature of DMFCs compared with PEMFCs is that they eliminate the fuel processor, and a lower performance of the electrochemical cell stack may still be acceptable for some applications, e.g., portable power sources [3, 4].

With every new generation of products, portable electronic devices are becoming more powerful. For example, today cell phones are not only used for making phone cells, but also for taking pictures and film sequences, for navigating and as mobile televisions. However these extra features consume additional energy. Since even the best battery technologies can no longer meet the energy demand of modern electronic products, scientists are searching for innovative, miniaturized power systems that can significantly prolong the operation time of portable. Fuel cells are expected to solve the mobile power supply problem. The advantage of this technology is that fuel cell systems are able to convert chemically stored energy directly into electricity and have a significantly higher energy density than storage batteries.

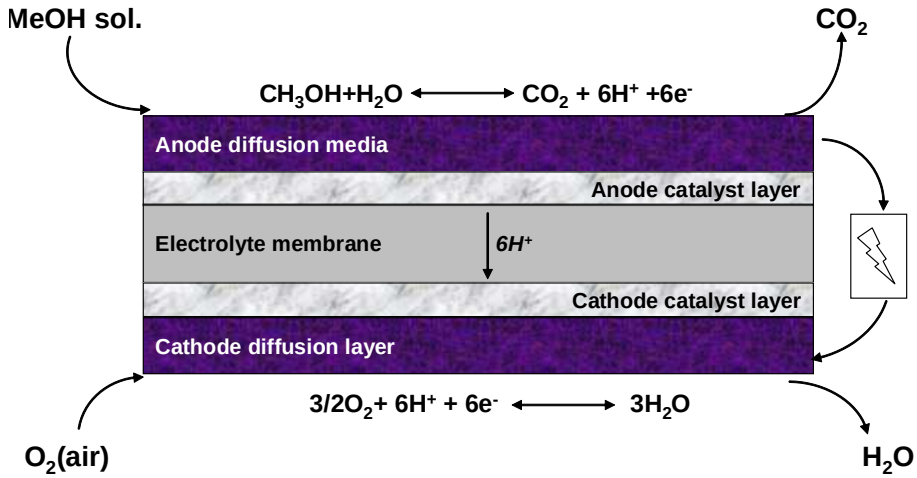

Figure1-2: A schematic of a DMFC employing an acidic solid polymer electrolyte membrane

There has been an increasing demand for the development of direct methanol fuel cells (DMFCs) [5-7] because of their high energy densities which are suitable for mobile electric devices and automobiles, the theoretical gravimetric energy density of MeOH is ten times higher than that of the rechargeable Li-ion batteries (6000 Wh/kg vs. 600 Wh/kg). Large efforts done now for the development of direct methanol fuel cells (DMFCs)[8–12]. However, the energy density of the DMFCs currently under development is still far from that expected due to the methanol crossover and the high over voltage at the electrodes [13-16].

Figure 1-3 shows a graph of the size of two types of direct methanol systems, 1-W average power and 5-W average power, and an advanced Li-ion rechargeable battery. It can be seen that, for devices of higher energy requirement like 25Wh, the DMFC becomes attractive because the DMFC systems show a smaller system size of a certain electrical energy stored i.e., the size of the DMFC will be smaller than that of the secondary battery after 5Wh in case of 1-W average power system while it will be smaller after 25Wh in case of 5-W average power system, and in both cases, the size of the DMFC system will be smaller with the further increase in the energy stored [17].

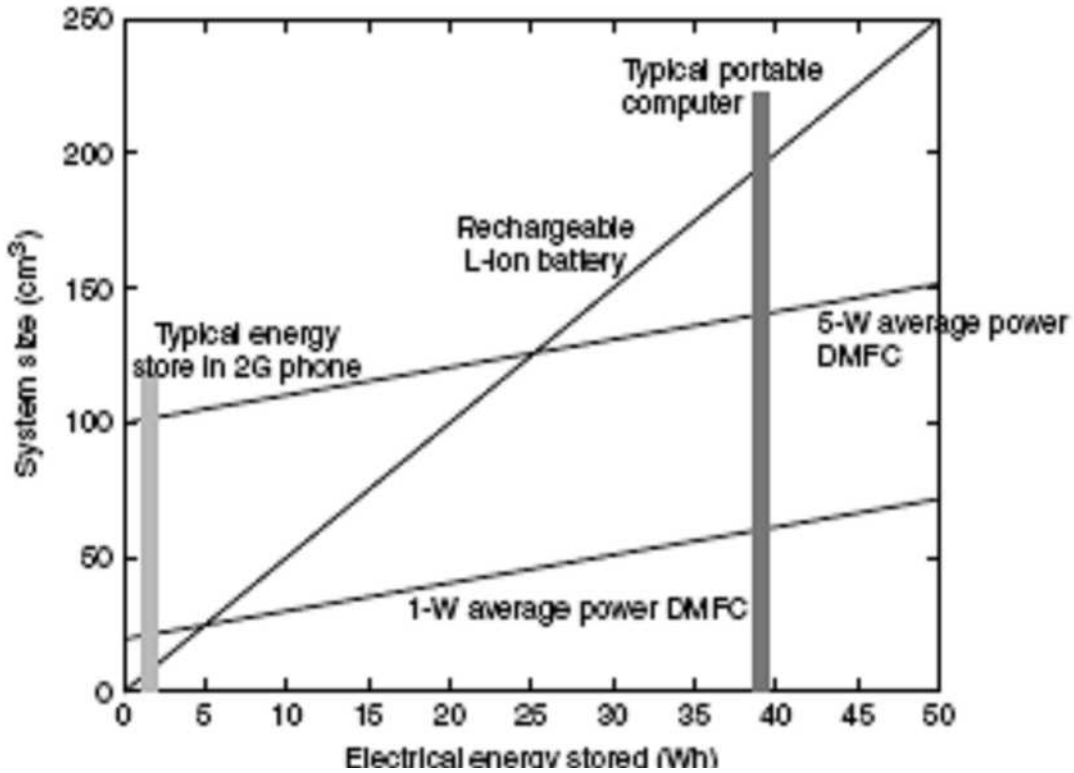

Figure 1-3: Graphs showing the change in volume of a Li – ion battery, and two hypothetical DMFCs, for different values of electrical energy stored. [17]

2.2. Fundamentals of DMFC

2.2.1. Cell components and polarization curve

A membrane-electrode assembly (MEA) was formed by sandwiching a perfluorosulfonic acid (PFSA) membrane between the anode and cathode electrodes. Upon hydration, the polymer electrolyte exhibits good proton conductivity.

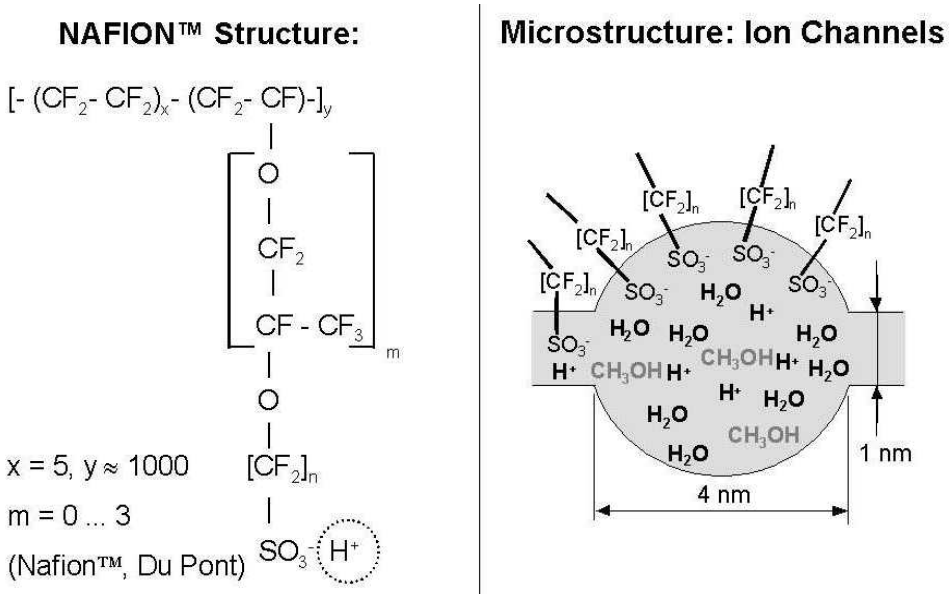

Figure 1-4: Polymer structure (left) and microscopic structure of wet Nafion [14]

2.2.1.1. Polymer Electrolyte Membrane (PEM)

PEM is the heart of the DMFC. Ideally it has to combine good proton conductivity with being an isolator for electron transport and being impermeable for all other compounds. Additionally it has to have a very high chemical and thermal stability. Operation at up to 120°C has been realized with commercial products like Nafion (by DuPont), Gore Select/PRIMEA (by Gore), Flemion (by Asahi Glass) and other quite similar fluorinated polymers carrying sulfonic acid groups. But even higher temperatures are desired when DMFCs are operated in the vapor phase. Some results with newly designed special high temperature membranes (e.g., based on acid-doped polybenzimidazole, PBI) indicate that above 150 - 200°C the kinetics of the methanol oxidation is not a limiting factor any more [18,19].

As a matter of fact, until very recently, Nafion was only one commercially available product on the free market fulfilling at least some of these requirements. It is a polymer with a fully fluorinated backbone carrying sulfonic acid groups (- SO_3H) for proton

conductivity as shown in figure 1-4. Thicknesses between 50 and 200 μm are available, but there are also new developments featuring a mechanical reinforcement to allow for thicknesses down to 20 μm [14]. Unfortunately, protons within Nafion (and the same is true for all other similar products) only become mobile when there is water within the material to solvate them and the counter ion (in Nafion SO_3^-), which is fixed to the polymer backbone. The material is strongly hygroscopic and soaks up large amounts of water (up to 25 weight %, which makes for a 10% thickness increase due to swelling). On a microscopic scale, Nafion is no homogeneous material (Fig. 1-4, right): There are water-filled channels with walls formed from the sulfonic acid groups, and totally aliphatic regions where only the polymeric backbones are present. The water-filled channels have diameters between one and roughly 4 nanometers, which is only a few molecule diameters of a water molecule. As this channel cross the whole material, water is easily transported through it, even a slight pressure difference is sufficient. As the proton transport resistance increases rapidly with decreasing water content within the material, high water content has to be maintained during fuel cell operation. In hydrogen-fed fuel cells, this places the demand to humidify the hydrogen to prevent the anode side of the membrane from drying out, as the water within the membrane is transported towards the cathode side by the protons (electro-osmosis, electro-osmotic drag). Also using thinner membranes helps to reduce the problem of the water management. But the problem gains another quality for the DMFC, as methanol is easily transported through Nafion. This phenomena called methanol crossover and has very bad effect on the performance of DMFC as will be shown later in section 2.5.

A further disadvantage of Nafion is its high price (500-1000 US$/$m^2$), which contributes severely to the overall costs of PEM fuel cell types. For cost reduction, generally membrane materials are under development that are chemically and thermally stable even without fluor contents, but instead featuring a highly aromatic backbone [20]. The acidic function is supplied by sulfonic acid groups, as in Nafion. Some of these materials showed lower methanol permeation than Nafion. Extensive studies in this direction have been published by Roziere et.al., [21], where polybenzimidazole (PBI), polyetherketone (PEK) and polyetheretherketone (PEEK) are the polymer backbones, respectively, which are functionalised in several different ways.

2.2.1.2. Electrodes

On either side of the PEM are electrodes, anode and cathode, each electrode composed of a) catalyst layer, b) micro porous layer, and c) backing layer. A cross-sectional SEM of a MEA segment consisting of a backing layer, a micro porous layer (MPL) and a catalyst layer is shown in Fig. 1-5, [22].

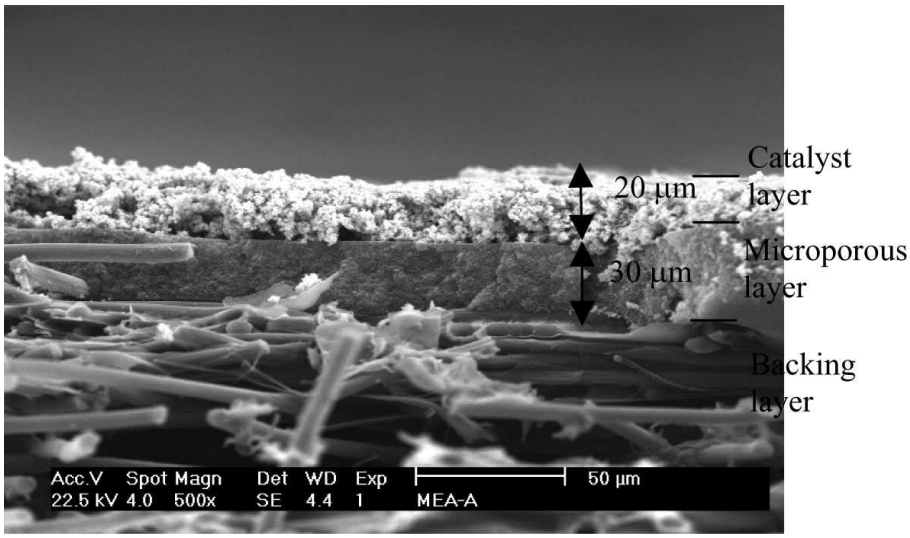

Figure 1-5: Cross-sectional SEM micrograph of backing layer, microporous layer, and catalyst layer. [22]

The electrodes of a fuel cell are where the electrochemical reactions take place. In order to increase the reaction rate, noble/precious metals are applied as catalysts in low-temperature fuel cells. Platinum is the most common material together with ruthenium, with particles as small as a few nanometers in diameter with high surface area, typically containing Pt-Ru on the anode side and Pt supported on carbon on the cathode side. Here the half-cell reactions described in eqns (1-3) and (1-4) are catalyzed. The microstructure of the catalyst layer is of paramount importance for the kinetics of an electrochemical reaction and species transport. Figure 1-6, [23] shows scanning electron microscopy (SEM) images of such microstructures of the DMFC anode and cathode, respectively, where high surface areas for electrochemical reactions are clearly visible. The MPL, with an average thickness of 30μm, overlays a carbon paper backing layer. The anode catalyst layer of about 20μm in thickness covers the MPL. In the anode, this MPL provides much resistance to methanol transport from the feed to the catalyst sites, thus reducing the amount of methanol crossover. In the cathode, the MPL helps alleviate cathode flooding by liquid water [24].

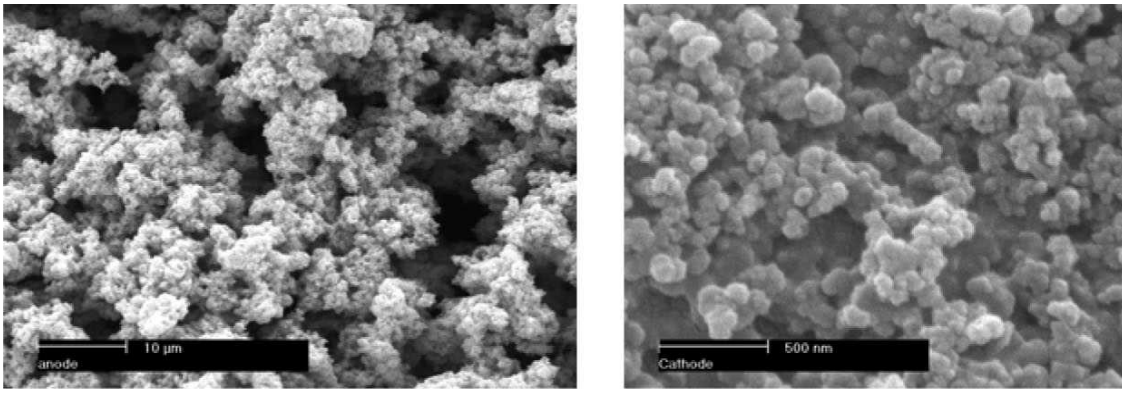

(a) anode (b) cathode

Figure 1-6: SEM images of electrodes. [23]

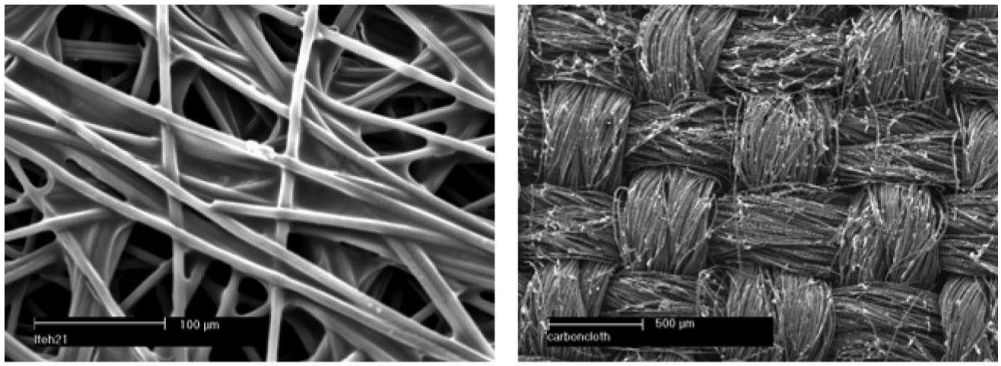

(a) (b)

Figure 1-7: SEM micrographs of (a) carbon paper and (b) carbon cloth [23]

On the outside of the MEA, backing layers made of non-woven carbon paper or woven carbon cloth as shown in Fig. 1-7, is placed to fulfill several functions. The primary purpose of a backing layer is to provide lateral current collection from the catalyst layer to the ribs as well as optimized gas distribution to the catalyst layer through diffusion. It must also facilitate the transport of water out of the catalyst layer. This latter function is usually accomplished by adding a coating of hydrophobic polymer, polytetrafluoroethylene (PTFE), to the backing layer. The hydrophobic character of the polymer allows the excess water in the cathode catalyst layer to be expelled from the cell by the gas flowing inside the channels, thereby alleviating flooding.

2.2.1.3. Polarization curve

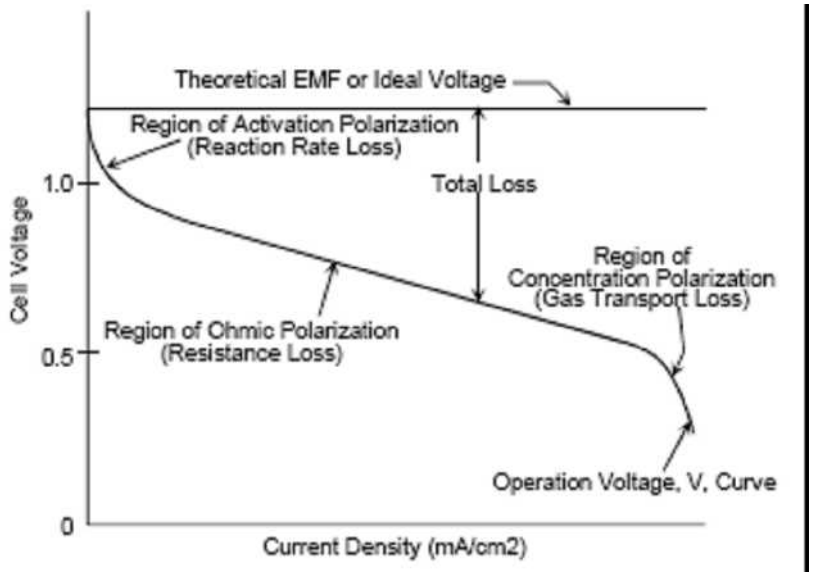

Figure 1-8: Ideal and Actual Fuel Cell Voltage/Current Characteristic [25]

Figure 1-8 displays a voltage vs. current density polarization curve of a typical DMFC. The thermodynamic equilibrium cell potential for a DMFC is approximately equal to 1.21V. However, the actual open circuit voltage in DMFCs is much lower than this thermodynamic value, largely due to fuel crossover [23].

Thermodynamic modeling is used to depict the equations so that only a limited number of tests are needed to define design constants within the equation. Adjustments can be applied to a reference performance at known operating conditions to achieve the performance at the desired operating conditions. Useful amounts of work (electrical energy) are obtained from a fuel cell only when a reasonably current is drawn, but the actual cell potential is decreased from its equilibrium potential because of irreversible losses as shown in Fig. 1-8. Several sources contribute to irreversible losses in a practical fuel cell. The losses, which are often called polarization, overpotential or overvoltage (η), originate primarily from three sources: (i) activation polarization (η_{act}), (ii) ohmic polarization (η_{ohm}), and (iii) concentration polarization (η_{conc}). These losses result in a cell voltage (V) for a fuel cell that is less than its ideal potential, E (V = E - Losses). Expressed graphically as a voltage/current density characteristic (Activation region and concentration region more representative of low-temperature cells): The activation polarization loss is dominant at low current density. At this point, electronic barriers have to be overcome

prior to current and ion flow. Activation losses show some increase as current increases. Ohmic polarization (loss) varies linearly with current, increasing over the whole range of current because cell resistance remains essentially constant. Gas transport losses occur over the entire range of current density, but these losses become prevalent at high limiting currents where it becomes difficult to provide enough reactants flow to the cell reaction sites [25].

Activation Polarization:

Activation polarization is present when the rate of an electrochemical reaction at an electrode surface is controlled by sluggish electrode kinetics. In other words, activation polarization is directly related to the rates of electrochemical reactions. There is a close similarity between electrochemical and chemical reactions in that both involve an activation barrier that must be overcome by the reacting species. In the case of an electrochemical reaction with η_{act} > 50-100 mV, η_{act} is described by the general form of the Tafel equation:

$$\eta_{act} = \frac{RT}{\alpha nF} \ln \frac{i}{i_0} \qquad \textbf{(1-6)}$$

where α is the electron transfer coefficient of the reaction at the electrode being addressed, F faraday constant, and i_o is the exchange current density.

Ohmic Polarization:

Ohmic losses occur because of resistance to the flow of ions in the electrolyte and resistance to flow of electrons through the electrode materials. The dominant ohmic losses, through the electrolyte, are reduced by decreasing the electrode separation and enhancing the ionic conductivity of the electrolyte. Because both the electrolyte and fuel cell electrodes obey Ohm's law, the ohmic losses can be expressed by the equation

$$\eta_{ohm} = iR \qquad \textbf{(1-7)}$$

Where i is the current flowing through the cell, and R is the total cell resistance, which includes electronic, ionic, and contact resistance.

Concentration Polarization:

As a reactant is consumed at the electrode by electrochemical reaction, there is a loss of potential due to the inability of the surrounding material to maintain the initial concentration of the bulk fluid. That is, a concentration gradient is formed. Several processes may contribute to concentration polarization: slow diffusion in the gas phase in the electrode pores, solution/dissolution of reactants/products into/out of the electrolyte, or diffusion of reactants/products through the electrolyte to/from the electrochemical reaction site. At practical current densities, slow transport of reactants/products to/from the electrochemical reaction site is a major contributor to concentration polarization:

$$\eta_{conc} = \frac{RT}{\alpha nF}\ln\left(1-\frac{i}{i_L}\right) \qquad \textbf{(1-8)}$$

where i_L is the limiting current

Summing of Electrode Polarization:

Activation and concentration polarization can exist at both the positive (cathode) and negative (anode) electrodes in fuel cells. The total polarization at these electrodes is the sum of η_{act} and η_{conc}, or

$$\eta_{anode} = \eta_{act,a} + \eta_{conc,a} \qquad \textbf{(1-9)}$$

$$\eta_{cathode} = \eta_{act,c} + \eta_{conc,c} \qquad \textbf{(1-10)}$$

The effect of polarization is to shift the potential of the electrode ($E_{electrode}$) to a new value ($V_{electrode}$):

$$V_{electrode} = E_{electrode} \pm /\eta_{electrode}/ \qquad \textbf{(1-11)}$$

For the anode,

$$V_{anode} = E_{anode} + /\eta_{anode}/ \qquad \textbf{(1-12)}$$

and for the cathode,

$$V_{cathode} = E_{cathode} - /\eta_{cathode}/ \qquad \textbf{(1-13)}$$

The net result of current flow in a fuel cell is to increase the anode potential and to decrease the cathode potential, thereby reducing the cell voltage.

Summing of Cell Voltage:

The cell voltage includes the contribution of the anode and cathode potentials and ohmic polarization:

$$\mathbf{V_{cell} = V_{cathode} - V_{anode} - iR} \qquad \mathbf{(1\text{-}14)}$$

When Eqs 1-12 and 1-13 are substituted in Eq. 1-14

$$\mathbf{V_{cell} = E_{cathode} - / \eta_{cathode} / - (E_{anode} + / \eta_{anode} /) - iR} \quad \mathbf{(1\text{-}15)}$$

Or

$$\mathbf{V_{cell} = \Delta E_e - / \eta_{cathode} / - / \eta_{anode} / - iR} \qquad \mathbf{(1\text{-}16)}$$

where $\Delta E_e = E_{cathode} - E_{anode}$. Equation 1-16 shows that current flow in a fuel cell results in a decrease in the cell voltage because of losses by electrode cell voltages and ohmic polarizations. The goal of fuel cell developers is to minimize the polarization so that V_{cell} approaches ΔE_e. This goal is approached by modifications to fuel cell design (improvement in electrode structures, better electrocatalysts, more conductive electrolyte, thinner cell components, etc.). For a given cell design, it is possible to improve the cell performance by modifying the operating conditions (e.g., higher gas pressure, higher temperature, change in gas composition to lower the gas impurity concentration). However, for any fuel cell, compromises exist between achieving higher performance by operating at higher temperature or pressure and the problems associated with the stability/durability of cell components encountered at the more severe conditions.

2.3. Thermodynamics of DMFC[23]

The thermodynamic equilibrium potential of a fuel cell can be calculated from:

$$\Delta E = -\frac{\Delta G}{nF} = -\frac{\Delta H - T\Delta S}{nF} \qquad \mathbf{(1\text{-}17)}$$

Table 1 lists thermodynamic data of common fuel cell reactions at 25 ◦C and 1 atm. For the liquid-feed DMFC, n = 6 and the thermodynamic cell potential is 1.21V, similar to that of the H_2/air PEMFC. The thermodynamic efficiency of a fuel cell is defined as the ratio of maximum possible electrical work to the total chemical energy, i.e.:

$$\eta_{rev} = -\frac{\Delta G}{\Delta H} = -\frac{nFE}{-\Delta H} \qquad \mathbf{(1\text{-}18)}$$

Table 1-1: thermodynamic data of cell reactions (per mole of fuel) [26]

Reaction	T(K)	Δg(KJ/Kg)	Δh(KJ/Kg)	Δs(KJ/KgK)	n	ΔE(V)	η_{rev}
PEMFC	298	-237	-285	-162	2	1.23	0.83
DMFC	298	-704	-727	-77	6	1.21	0.97

As shown in Table 1-1, the theoretical thermodynamic efficiency of DMFC reaches 97% at 25^0C. The practical energy efficiency, however, is much lower after accounting for voltage and fuel losses. The voltaic efficiency is defined as the ratio of the actual electric work to the maximum possible work, with the former given by:

$$W_{act} = -nFV_{cell} \qquad \textbf{(1-19)}$$

Where V_{cell} is the cell voltage at a current of I. Hence the voltaic efficiency can be written as:

$$\eta_{voltaic} = \frac{W_{act}}{W_{\max}} = \frac{-nFV_{cell}}{\Delta G} = \frac{-nFV_{cell}}{-nF\Delta E} = \frac{V_{cell}}{\Delta E} \qquad \textbf{(1-20)}$$

For example, if the cell is running at 0.4V, then the voltaic efficiency is only 33%. This low efficiency is caused by substantial over potentials existed in both the anode and cathode of a DMFC.

In a DMFC, there is also fuel efficiency due to methanol crossover defined as:

$$\eta_{fuel} = \frac{I}{I + I_{xover}} \qquad \textbf{(1-21)}$$

Where $I_{x\ over}$ is an equivalent current density caused by methanol crossover under the operating current density of I . The total energy efficiency of DMFC is therefore given by:

$$\eta = \eta_{rev}\eta_{voltaic}\eta_{fuel} \qquad \textbf{(1-22)}$$

Suppose that the fuel efficiency, η_{fuel}, in a DMFC is 80%, the total energy efficiency becomes η = 97% × 33% × 80% = 25.6% with cell voltage of 0.4V.

In comparison, for a PEMFC η = 83% × 0.7/1.23 = 40.5% with the cell voltage of 0.7V. The energy efficiency of the PEFC is relatively higher owing largely to its negligibly

small fuel crossover and overpotential for hydrogen oxidation on the anode. It is evident from eqn 1-21 that in order to achieve higher energy-conversion efficiency, one must control methanol crossover so as to maintain high fuel efficiency (e.g. >80%). In addition, it is desirable to operate DMFCs at higher voltages. Thus, high-voltage performance is a high priority for portable DMFC development. Waste heat produced in the DMFC can thus be expressed as:

$$Q = \frac{IV_{cell}}{\eta} - IV_{cell} = IV_{cell}(1/\eta - 1) \qquad \textbf{(1-23)}$$

By substituting the definition of the total energy efficiency, another expression of heat generation results:

$$Q = (-\Delta H)\frac{I + I_{xover}}{nF} - IV_{cell} \qquad \textbf{(1-24)}$$

Where the first term on the right hand side represents the chemical energy of methanol consumed for power generation and by crossover, while the second term stands for the electric energy generated [23].

2.4. Kinetics of DMFC

2.4.1. Methanol oxidation kinetics

The kinetic limitations of DMFCs have been well reviewed in detail from several different perspectives in recent years [27,28]. For effective utilization of methanol as a fuel, the catalyst must provide a good surface for the adsorption of methanol and its sequential breakdown to carbon dioxide/carbonate through loss of paired protons and electrons. Under acidic conditions, this has largely restricted practical catalysts to platinum and its alloys and bimetallics. Methanol will adsorb to platinum and platinum serves as an excellent electron transfer catalyst. The difficulty is that platinum passivates as carbon monoxide byproduct accumulates and adsorbs to the platinum surface. To oxidize carbon monoxide to carbon dioxide/carbonic acid, oxygenated species such as water must be adsorbed to the catalyst surface. Because platinum is not strongly hydrophilic, platinum bimetallics and alloys formed with more hydrophilic metals such as ruthenium are typically used to facilitate CO oxidation. Consider the mechanistic constraints for oxidation of methanol. As in eq. 1-3, the complete oxidation of methanol to carbon dioxide proceeds by a six proton, six-electron process.

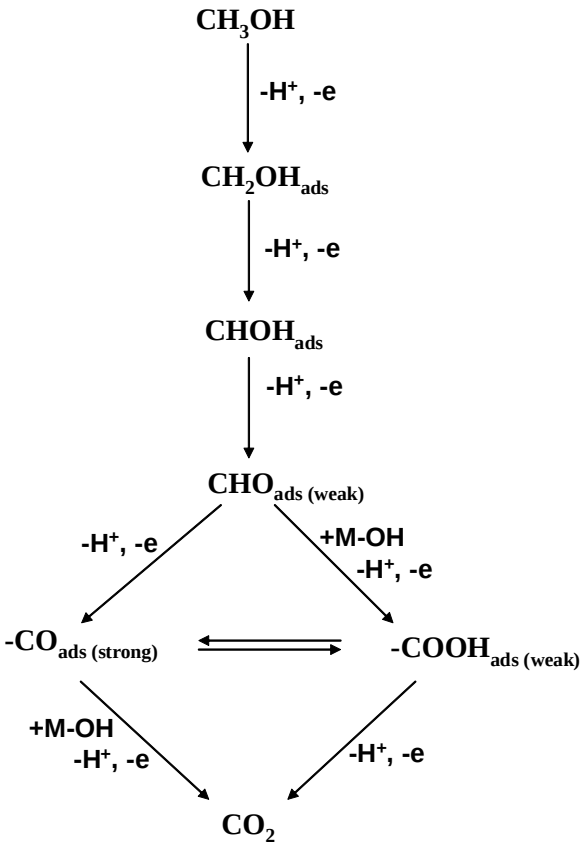

Figure 1-9: Schematic diagram showing the reaction pathways for methanol oxidation [29]

The mechanism presented in Fig. 1-9 outlines the basic route by which methanol is fully oxidized. The loss of paired protons and electrons is noted for each step. To account for all six electrons, recognize that the adsorption of water to the catalyst surface also generates an electron and proton. For a catalyst metal site, M:

$$M + H_2O \leftrightarrow M - OH + H^+ + e \qquad \textbf{(1-25)}$$

Methanol first is adsorbed by liberating one electron and one proton.

$$CH_3OH + Pt \leftrightarrow Pt - CH3OH_{ads} + H^+ + e \qquad \textbf{(1-26)}$$

This is followed by two steps to form the formyl intermediate, –CHO.

$$Pt - CH_2OH_{ads} + Pt \leftrightarrow Pt_2CHOH + H^+ + e \qquad \textbf{(1-27)}$$

$$Pt_2CHOH \leftrightarrow Pt + Pt - CHO + H^+ + e \qquad \textbf{(1-28)}$$

On clean platinum surfaces, these oxidations proceed smoothly to provide two electrons and two protons. Considered scheme is shown in Fig. 1-9. The weakly adsorbed –CHO is a point at which the oxidation mechanism breaks into two paths. One path yields adsorbed CO and the other adsorbed COOH. Adsorbed COOH is generated by reaction of –CHO and an adjacent M – OH to yield one proton and one electron and form weakly adsorbed –COOH. Adsorbed CO is generated by the direct oxidation of –CHO by one proton and one electron to form strongly adsorbed CO. Basic kinetic arguments would favor the strongly adsorbed CO over the weakly adsorbed –COOH because first, the oxidation of –CHO to –CO is direct and does not require an adjacent second species, M – OH, and second, because – CO is strongly bound and –COOH is weakly bound. It should be pointed out that there is an alternative branch point in the oxidation process in which adsorbed –CHOH undergoes a one-electron and a one-proton oxidation to form adsorbed –COH.

$$Pt_2CHOH + Pt \leftrightarrow Pt_3COH + H^+ + e \qquad \textbf{(1-29)}$$

The adsorbed –COH can then either undergo one-proton/one-electron oxidation to adsorbed – CO or react with an adjacent M – OH to form HCOOH in solution. Neither process leads to the efficient oxidation to carbon dioxide/carbonic acid. To the extent the platinum surface is passivated by CO, the reaction is terminated. Thus, the design of a system for the efficient and complete oxidation of methanol can be approached in two ways. The first approach is to circumvent the formation of adsorbed CO by favoring the formation of –COOH. Experimentally, this is done by enhancing the probability that –CHO is adjacent to an oxygen source, M – OH, by using bimetallics and alloys of platinum where M is more hydrophilic than platinum. There are questions of stability and cost associated with these catalysts although they have been shown to enhance conversion efficiency. But, based on the relative strengths of the adsorbates – CO and –COOH and the need for an additional catalyst site (M – OH), this approach poses some challenges. The second approach is to consider why – CO is so difficult to oxidize; that is, why does CO adsorb so strongly. Thermodynamically, the oxidation of CO to CO_2 in solution occurs at low potential.

$$CO_2 + 2H^+ + 2e \leftrightarrow CO + H_2O(1) in E^0 = -0.16V \qquad \textbf{(1-30)}$$

But, the oxidation of CO on platinum in acidic solution occurs at 600 to 700 mV positive of this value; Pt-Ru alloys are shown to oxidize CO at 200 to 300 mV lower overpotential

than Pt [30]. The oxidation of adsorbed CO is strongly disfavored. There are two ways to think about overcoming this large overpotential.

One is to design better catalysts. One common approach has been through the bifunctional mechanism where the bimetallic catalyst is designed to place *Pt* – CO adjacent to an oxygen source through M – OH. The other approach would rely on a paradigm shift in how the oxidation of –CO is viewed at a more fundamental level; better understanding could lead to better catalysts. Many factors significantly impact the catalytic efficiency of the conversion of methanol to carbon dioxide/carbonic acid. This includes surface structure, catalyst size, and catalyst crystal face as well as the history of the cell, the current coverage of CO, the pH, and the time since the start of the cell. [29]

2.4.2. Oxygen reduction kinetics [31]

At the cathode, which is commonly Pt, oxygen electro reduction occurs according to the overall reaction (in acid medium): (eq 1-4)

The kinetics of this reaction are relatively slow (i_o from 10^{-6} to 10^{-10} A cm^{-2}, referred to the geometric surface area, depending on the degree of dispersion of the platinum catalyst), which is the main cause of the high over potential η (η ≈ about 400 mV for a hydrogen oxygen PEMFC, working at 500 mA cm^{-2}).

The deviation from the equilibrium potential, even at low current densities, is a consequence of some related processes:

1. The production of H_2O_2, either as an intermediate in the four electron reduction of O_2 to water, or as a reaction product. In the latter case the thermodynamic equilibrium potential of the reaction, i.e.,

$$O_2 + 2H^+ + 2e^- \leftrightarrow H_2O_2 \qquad \textbf{(1-31)}$$

is 0.695 V/SHE, instead of 1.23 V/SHE for the overall oxygen reduction reaction. Usually in an acid medium, such as in a PEMFC, no H_2O_2 is formed at a platinum electrode at an operating potential, *Ec* , of 0.9 to 0.7 V.

2. A slow rate-determining step, i.e.,

$$O_2 + H^+ + e- \leftrightarrow O_2H_{ads} \qquad \textbf{(1-32)}$$

3. Observance of a mixed potential of about 1.0 V (instead of the equilibrium thermodynamic reversible potential E^o_c = 1.23 V vs. SHE) due to the formation of surface oxides at the platinum electrode, according to different electrode reactions:

$$Pt + H_2O \leftrightarrow PtO + 2H^+ + 2e^- \qquad \textbf{with } \boldsymbol{E_o} \textbf{ = 0.88 V} \qquad \textbf{(1-33)}$$

$$Pt + 2H_2O \leftrightarrow Pt(OH)_2 + 2H^+ + 2e^- \qquad \textbf{with } \boldsymbol{E_o} \textbf{ = 0.98 V} \qquad \textbf{(1-34)}$$

$$Pt(OH)_2 \leftrightarrow PtO_2 + 2H^+ + 2e^- \qquad \textbf{with } \boldsymbol{E_o} \textbf{ = 1.11 V} \qquad \textbf{(1-35)}$$

or even to the presence of minute traces of organic impurities undergoing an oxidation reaction, such as with methanol:

$$CH_3OH + H_2O \leftrightarrow CO_2 + 6H^+ + 6e^- \qquad \textbf{(1-36)}$$

In all these cases, the electrode potential E_m will be determined by a mixed reaction resulting from the reduction of oxygen and the oxidation of the platinum surface or of methanol at the same potential E_m. Since both reactions are quite irreversible, a Tafel behavior is practically always observed. Under these conditions, the current density (j_m) and mixed potential (E_m) are given by the equations:

$$j_m = j_{oa} e^{(E_m - E^o_a)/ba} = j_{oa} e^{-(E_m - E^o_c)/bc} \qquad \textbf{(1-37)}$$

and

$$E_m = \frac{b_c E^o_a + b_a E^o_c}{b_a + b_c} + \frac{b_a b_c}{b_a + b_c} \ln \frac{j_{oc}}{j_{oa}} \qquad \textbf{(1-38)}$$

where j_{oi} and b_i are the exchange current density and the Tafel slopes, respectively, for both half-cell reactions.

The exchange current density j_{oa} for methanol oxidation depends on the methanol concentration, i.e.:

$$j_{oa} = nFk^o_s [CH_3OH]^{\alpha_a} \qquad \textbf{(1-39)}$$

Where the value of the charge transfer coefficient α_a is very probably equal to 0.5. For the sake of simplicity, the standard rate constant k^o_s includes the concentration of the oxidized species (i.e., CO_2). Therefore a small crossover of methanol through the membrane, increasing, for example, the methanol concentration in the cathodic compartment by a

factor of 10^6, will result in a negative shift of the potential, ΔE_m , at the oxygen cathode, which is expressed by the following equation:

$$\Delta E_m = \frac{b_a b_c}{b_a + b_c} \ln \frac{j_{oc}}{j_{o'a}} \qquad \textbf{(1-40)}$$

with $j_{óa}$= 10^3 j_{oa} and $b_a \approx b_c \approx$ 120mV/decade for both the oxygen reduction (at high current densities) and the methanol oxidation reactions. For a higher membrane crossover rate, leading to a methanol concentration in the cathodic compartment on the order of 10^{-2} *M* for Nafion 117, after 5 hr of operation[32] the shift of the oxygen electrode potential will be $\Delta E_m \approx$ 120/2 log $l0^{-5} \approx$ .300 mV. Such cathode potential shifts are effectively observed in a working DMFC.

Therefore, one main drawback of the PEMFC configuration with a standard proton exchange membrane (such as Nafion) and a standard platinum gas diffusion cathode is the cathode depolarization caused by a mixed potential resulting from the methanol crossover through the membrane. There are two possibilities for overcoming these difficulties; the first is to conceive new electrocatalysts for oxygen reduction but which are highly inactive for methanol oxidation, and the second is to develop new membranes that are more methanol impermeable [3].

2.5. Methanol crossover

Apart from the problems of low electrocatalytic activity of the methanol electrode and poisoning of the electrocatalyst by adsorbed intermediates, an overwhelming problem is the migration of the methanol from the anode to the cathode via the proton-conducting membrane, MCO. The perfluorosulfonic acid membrane contains about 30% of water by weight, which is essential for achieving the desired conductivity. The proton conduction occurs by proton hopping process, Grottus mechanism; similar to what occurs in an aqueous acid electrolyte (e.g., H_2SO_4, $HCLO_4$) as well as the vehicle mechanism. Methanol is highly soluble in water over the entire range of composition from nearly 0% to nearly 100%. Generally methanol transported through the electrolyte membrane by means of (a) active transport together with the protons and their solvation shell water (electro osmotic drag) as well as (b) diffusion through the water-filled pores and (c) diffusion through the aliphatic (polymer backbone) regions in the Nafion itself. When methanol reach the cathode surface it was oxidized, eq. (1.41), on its surface as well as the

oxygen reduction in the same time which results in the mixed potential on the cathode surface.

$$CH_3OH + 3/2O_2 \rightarrow CO_2 + 2H_2O \qquad \textbf{(1-41)}$$

For comparison of different membrane materials, very often a methanol permeation equivalent is calculated, which is the Faradic current density of the methanol crossover flux through the membrane according to Faraday's law:

$$\mathbf{i_{crossover} = n\ F\ J_{CH3OH}} \qquad \textbf{(1-42)}$$

where n=6 is the number of transferred electrons for full oxidation of one methanol molecule, F=96485 C mol^{-1} is Faraday's constant and J_{CH3OH} is the molar methanol permeation flux density [mol s^{-1} cm^{-2}] with respect to the cross-sectional area of the cell. For Nafion 117, the methanol permeation equivalent reaches values from 100 up to several 100 mA/cm^2, while the total cell current densities are typically between 100 and 500 mA/cm^2. This emphasizes the dramatic losses due to the methanol crossover phenomenon. More detailed information about this can be found in [33-36].

There are three very detrimental effects of the methanol crossover through the membrane:

(1) The extent of crossover is so high (corresponding to a current density of 100 mA/cm^2 for a methanol-oxygen or methanol- air fuel cell operating at 300 mA/cm^2) that it can cause a loss of Coulombic efficiency by about 20 to 30%.

(2) The methanol, which reaches the cathode, depolarizes the oxygen electrode, causing a decrease in the open circuit potential from 0.7-0.6 V to about 0.5 V. Thus the maximum possible efficiency of the cell (assuming no zero activations, ohmic and mass transport overpotentials) is only 65%.

(3) The performance of the oxygen electrode is reduced, probably owing to the presence of small amounts of organic adsorbed intermediates, at half-cell potentials less than 0.8 V [3].

2.5.1. Techniques for reducing methanol crossover

There are four principle ways that DMFC designers use to reduce fuel crossover:

1. The anode catalyst is made as active as possible, within the bounds of reasonable cost. This results in the methanol reacting properly at the anode and not being available to diffuse through the electrolyte and on to the cathode.

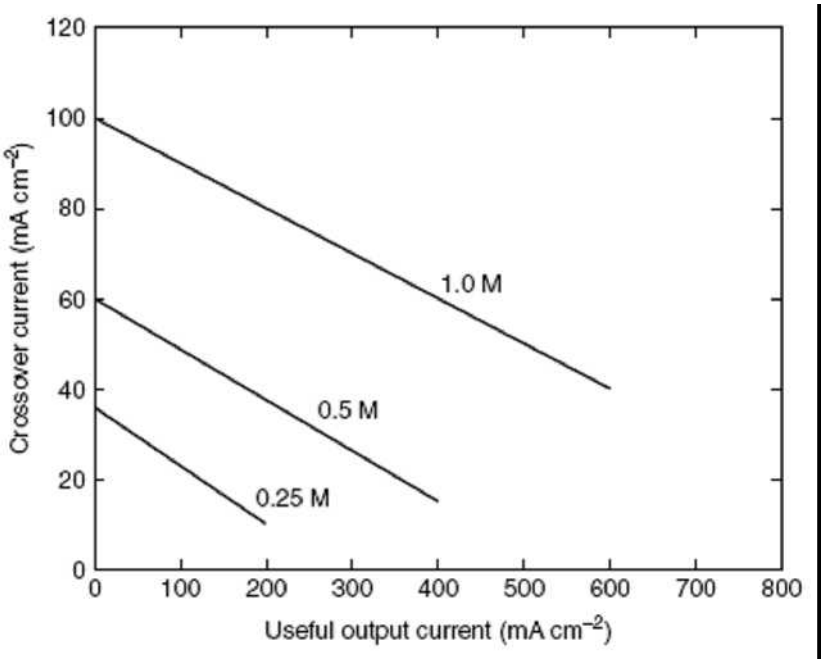

Figure 1-10: Graph showing how the crossover of methanol to the cathode changes with fuel concentration at the anode and with load current. [17]

2. The fuel feed to the anode is controlled, so that at times of low current there is no excess of methanol. Clearly, the lower the methanol concentration at the anode, the lower it will be in the electrolyte, and hence at the cathode. See Figure 1-10. The effect of methanol concentration on DMFC fuel cell performance has been extensively studied [35,37]. Mathematical models have also been developed. The conclusion is that the concentration should always be about 1M, though a more accurate optimum will need to be found for every type of cell under all conditions [38].

It should also be noted that fuel crossover reduces as the current from the cell increases. This is linked to points 1 and 2 above – the fuel reacts promptly at the anode and is not made available to crossover. In Ren, Zelanay et al., 2000,[39] it is shown how the crossover equivalent current falls with methanol concentration and with increasing current. These results are summarized in Fig. 1-10.

3. The use of selective (non-platinum) catalysts on the air cathode. These will stop the fuel reacting on the cathode and so eliminate the voltage drop due to the ‘mixed-potential’. However, there are problems with this approach. The first is that all catalysts that do not

promote the fuel oxidation tend only to very slowly promote the reaction of oxygen with the H^+ ions. Thus, the activation losses on the cathode are made even worse than normal, and there is no increase in performance. Another problem is that although the mixed-potential problem may be solved, the fuel is still crossing over, and while it may not be reacting on the cathode, it will probably just evaporate instead. Thus, it will still be wasted. So, although it may be possible in the future to find selective cathode catalysts that ameliorate the fuel crossover problem, this approach does not offer a complete solution.

4. Nafion membrane still has unacceptable level of methanol crossover. On going efforts to develop PEMs appropriate for DMFCs with lower MCO fall roughly into two categories:

1- Tailoring the properties of Nafion.

Strategies for tailoring the properties of Nafion membranes include surface modification of the membrane with a barrier less permeable to methanol that still allows facile proton conduction, addition of intercalates into the membrane to react with methanol to reduce crossover, and blending Nafion with other polymers to form hybrid membranes.

Palladium metal is of particular interest for researchers as it is impermeable to methanol but not proton [40,41]. A variety of methods to apply the Pd layer to Nafion have been assessed and the effectiveness of the modification in reducing methanol crossover evaluated. Ma et al. looked at the effectiveness of reducing methanol crossover by sputtering a Pt/Pd-Ag/Pt layer onto Nafion [42]. It was found that while the layers were not crack-free, the Pd alloy-coated Nafion had increased performance over uncoated Nafion.

Hejze et al. evaluated the performance of electrolessly deposited Pd-coated Nafion 117 to that of unmodified Nafion 117 membrane [41]. Here, Pd layers were coated onto fully hydrated Nafion substrates and the performance as a separator evaluated in a specialized cell for methanol concentrations <10%. Over the course of 10 hours, methanol crossover through the Pd-coated membrane was found to be much lower than for the unmodified Nafion control. Palladinized Nafion PEMs were found to be less permeable to methanol and uptake more water than unmodified Nafion. A DMFC made with the palladinized Nafion PEM generated roughly 40% higher maximum current density than the Nafion control cell.

Kim et al. used supercritical carbon dioxide (sCO_2) to graft polystyrene onto Nafion 115 as sCO_2 produces low thermal stress and has a plasticizing effect when used as a swelling agent in polymers [43]. Following impregnation, the membrane was sulfonated and its properties compared to unmodified Nafion. Impregnated membranes have higher ion exchange capacity and lower permeability to methanol. DMFCs made with impregnated membranes generate more current at 350 mV (~140 mA cm^{-2}) than a Nafion 115 control cell (~113 mA cm^{-2}).

Kang et al. deposited thin (0.1 μm), clay-nanocomposite films onto Nafion 117 using layer-by-layer assembly [44]. The purpose was to reduce methanol crossover using exfoliated (leaf-like) clay nanosheets that are efficient components in barrier membranes for gas and water vapor. Permeability of methanol and ionic conductivity of the treated Nafion are measured and compared to a Nafion control. The control membrane has a methanol permeability of 1.91 × 10–6 cm^2 s^{-1} and in-plane conductivity of 0.122 S cm^{-1}. The Nafion modified with a 20-bilayer nanocomposite, has roughly half the methanol permeability as the control Nafion, 7.58 × 10–7 cm^2 s^{-1} and nearly the same in-plane ionic conductivity, 0.124 S cm^{-1}.

Chan et al. modified Nafion 115 membranes using *in situ* acid-catalyzed polymerization of furfuryl alcohol (PFA) to introduce highly cross-linked and methanol impermeable domains into the Nafion matrix. Modified and untreated Nafion PEMs were prepared and characterized [45]. It was found that methanol flux through the membranes, measured potentiostatically, changed as a function of the wt% of PFA in the membranes. Under all conditions, the DMFCs made with PFA PEMs generated significantly more power than the control DMFC. Peak power densities for DMFCs made with the PFA membranes were 2 to 3× larger than the unmodified Nafion DMFC.

One strategy to enhance water retention in PEMFCs is to incorporate inorganic particulates into the PEMs of fuel cells [46-48]. Nafion membranes impregnated in this fashion act as a barrier to methanol crossover and can be used in high temperature (~150°C) direct alcohol fuel cells and H_2/air fuel cells [49]. Aricò et al. evaluated the surface properties of basic and neutral alumina, ZrO_2, SiO_2, and SiO_2-phosphotungstic acid (SiO_2-PWA) using X-ray photoelectron spectroscopy (XPS), Brunauer Emmett and Teller (BET) surface area, and acid base characterizations. Composite membranes were prepared by recasting Nafion with the inorganic fillers. The resulting membranes were

incorporated into DMFCs [49]. All of the membranes showed similar methanol crossover behavior of $4 \pm 1 \times 10^{-6}$ mol min^{-1} cm^{-2} at 145°C and 0.5 A cm^{-2}. The electrochemical performance and conductivity of the composite membranes tracks the acidity of the intercalates and follow the series: SiO_2-PWA > SiO_2 > ZrO_2 > n-Al_2O_3 > b- Al_2O_3. That is, the membranes with the best performance were the most acidic. Here "n" stands for neutral and "b" for basic. The DMFC made with the hybrid SiO_2-PWA/Nafion membrane produced 400 mW cm^{-2} at 900 mV using pressurized O_2 and a cell temperature of 145°C. Bauer and Willert-Porada characterized Zr-phosphate-Nafion membranes as candidate materials for use in DMFCs [50]. The inorganic filler reduced methanol permeability and the phosphate layer had preferred permeability to water over methanol. The preliminary results suggest Zr-phosphate can be used to tailor such Nafion properties.

2- Developing entirely new PEM materials

New materials are being developed for use as separators/ionic conductors in DMFCs. These materials generally fall into one of two categories, fluorinated and nonfluorinated. Here some current developments in both areas are presented. In an effort to develop an inexpensive and effective separator for DMFCs and fuel cells operated on other fuels, Melman et al. developed a nano porous proton conducting membrane (NP-PCM) [51]. The NP-PCM is made of polyvinylidene fluoride (PVDF) and SiO_2. Characteristics of the NP-PCM separator that bests Nafion include: pore sizes roughly 50% that of Nafion; methanol crossover cut in half; as much as 4× greater ionic conductivity; and a membrane insensitive to heavy metal corrosion products that allow for less expensive hardware and catalysts. One disadvantage of this type of membrane is the high cost . A review of nonfluorinated PEMs for use in DMFCs was prepared by Rozière and Jones [52]. The number of nonfluorinated polymer materials for application in higher-temperature fuel cells (i.e., > 80°C) is limited by thermal instability. Thermally stable polymers tend to have either polyaromatic or polyheterocyclic repeat units. Examples of these include polybenzimidazole (PBI), poly(ether ketone)s (PEK), poly(phenyl quinoxaline (PPQ), polysulfone (PSU), and poly(ether sulfone) (PES). The chemical structures of some common nonfluorinated polymers are shown in Fig. 1-11. These polymers are thermally stable but are poor ionic conductors until modified.

Silva et al. evaluates inorganic-organic hybrid membranes made from sulfonated poly(ether ether ketone) (sPEEK) [53,54]. The sPEEK membranes have a sulfonation

degree of 87% and zirconium oxide content that varies between 2.5 and 12.5 wt%. The organic/inorganic hybrid sPEEK/ZrO_2 membranes exhibit good proton conductivity and the addition of ZrO_2 particles can tailor the electrochemical performance of the membranes. This makes the organic/inorganic hybrid sPEEK/ZrO_2 membranes a possible alternative to perfluorinated membranes. It was found the proton transport resistance increased as the wt% ZrO_2 in the membrane increased and that proton conductivity followed the opposite trend. Water uptake decreases as the inorganic component increases.

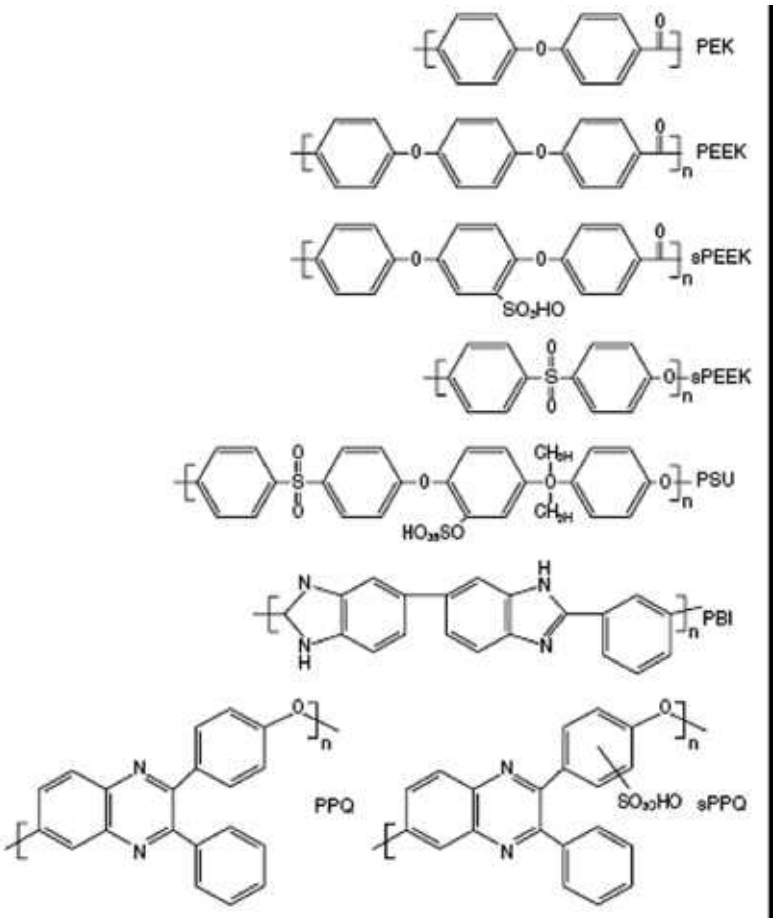

Figure 1-11: Chemical structures of some of the more common nonfluorinated polymers being tested as PEMs. Structures redrawn from [52].

Another nonfluorinated material of promise is poly(vinyl alcohol) (PVA). The material is chemically and thermally robust and quite inexpensive relative to Nafion. In a recent article by Khan et al., the synthesis and characterization of PVA-based membrane is described [55]. Membranes were based on PVA and its ionic blends with sodium alginate (SA) and chitosan (CS). All of the PVA-based membranes were found to have lower methanol permeability than Nafion. The PVA-CS membrane had the lowest permeability at 6.9 × 10–8 cm^2 s^{-1} as compared to Nafion 117 with a permeability of 2.76 × 10–7 cm^2

s^{-1}. Contrasting the desirable characteristic of lower methanol permeability than Nafion 117, the proton conductivities of the PVA-based membranes are significantly lower (~0.01 S cm^{-1}) than that for Nafion 117 (0.1 S cm^{-1}).

2.6. Motivation and scope of this study:

Passive DMFCs, that suck methanol from a reservoir by an osmotic action and breathe air from its surrounding by natural convection and diffusion, have been demonstrated, and the performance was investigated by some researchers under different conditions [8-12, 56-61]. The reports on the passive DMFCs revealed some different performance behaviors compared to that of active DMFCs. For example, a methanol concentration like 5M, which is higher than that for an active DMFC, was sometimes assigned as the optimum condition for the i-V performance [58,62,63]. An air-breathing DMFC with a thinner membrane exhibited a better i-V performance at low current density [16]. The power density calculated on the basis of the unit area of the electrode for a stack was much better than that of the single cell [57]. A passive vertically oriented DMFC always produced a better performance than that horizontally oriented [64]. These behaviors were attributed to the methanol crossover that induced an increase in the cell temperature due to the exothermic reaction between the permeated methanol and the oxygen at the cathode, so that the polarization was reduced, and hence, a high performance was achieved [16, 57]. These do not suggest that the methanol crossover played a desirable role in the passive DMFC. It should be noted that the methanol crossover causes a loss of the methanol and significantly reduced the energy density and the efficiency of the DMFC. In the passive DMFCs, the methanol crossover and the temperature of the cell were not controlled, which sometimes leads to fatal damage to the cell.

Although of the large efforts which have been done to reduce the MCO as shown in section 2.5, very little work considered the methanol transport control through the backing layer [24, 56, 65].

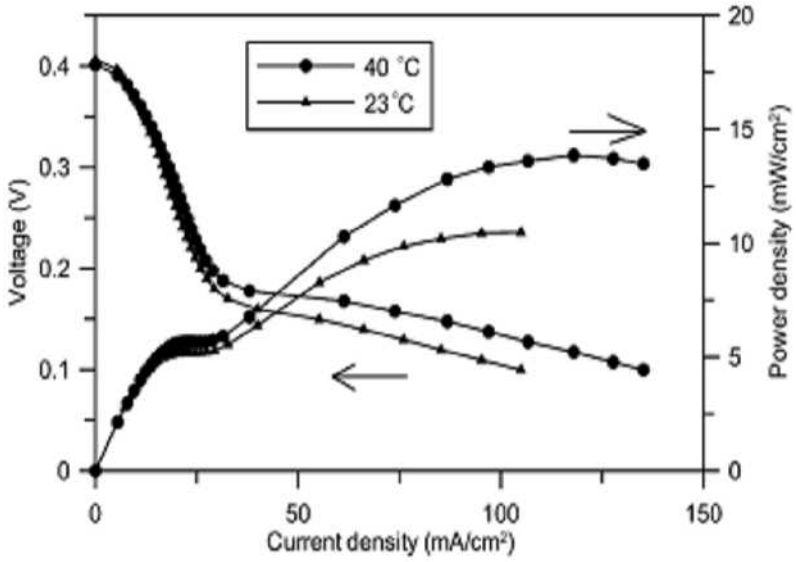

Figure 1-12: Polarization and power density curves at different temperatures using 8M methanol solution with the air flow rate of 88 ml/min and methanol flow rate of 0.283 ml/min at atmospheric pressure [65].

Lu et.al., fabricated a membrane-electrode assembly (MEA) to mitigate methanol crossover. This MEA features a modified anode backing structure in which a compact microporous layer is added to create an additional barrier to methanol transport thereby reducing the rate of methanol crossing over the polymer membrane [24, 65]. This MEA with the microporous layer showed a reasonable performance under 8 M methanol solution at room temperature. As shown in Fig. 1-12. Using 8M concentrated methanol solution, the fuel tank volume decreases by roughly eight-fold compared to the 1M dilute solution containing the same amount of pure methanol. Although power density will decrease under concentrated solutions due to methanol crossing over the polymer membrane, the reduction using 8M solution (10.5 mW/cm^2 at 23 ◦C) is only 27% as compared to that using 1M solution (14.3 mW/cm^2 at 23 ^oC).

Others tried blocking methanol permeation by making a denser catalyst layer at the anode, Ren et.al. [39].

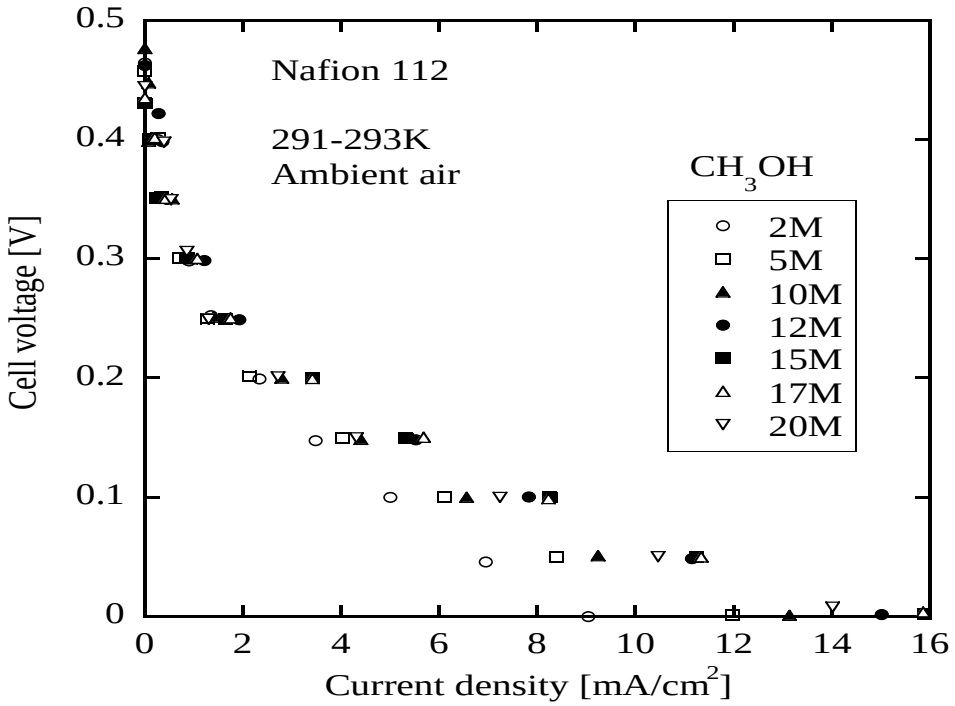

Figure 1-13: current – voltage curves of the test cell using a porous carbon support at different methanol concentrations [56].

Unfortunately, although of these big efforts to reduce MCO, the DMFC usually shows the highest performance at low concentrations of methanol from 2 to 3M [66, 67] under the active conditions and about 5M [68–70] under the passive conditions. The modified or new membranes showed the highest performance at a methanol concentration range from 0.4M to 2M as shown the recent review by V. Neburchilov et.al., [71]. Controlling of the methanol transport across the backing layer showed optimum performance at 4M, and maximum concentration is 8M at lower performance. These achievements are far away from the production of passive DMFC operated efficiently with neat methanol, 100wt%. In our laboratory we have confirmed that a novel DMFC that uses a porous carbon plate as support generates power by sucking the methanol solution through the porous body by osmotic action and breathing air by natural diffusion and convection revealed a higher performance at methanol concentration as high as 17M, as shown in Fig. 1-13 suggesting that the porous carbon plate provided a function of controlling the methanol crossover. Although of the promising results of this cell structure, the highest methanol still less than neat and low performance. At this stage the mechanism of this novel structure not clears yet.

Purpose of this study:

Based on the novel electrode structure proposed in our laboratory, the objective of this study is the production of high energy density passive DMFC operated with neat methanol efficiently with high power density. While our purpose is the operation with neat methanol, water must be supplied to the anode surface for the complete electrochemical reaction at the anode surface as shown in eqn 1-3. Water can be supplied from the anode surface but this will decrease the energy density of the cell therefore we considered the supplying of water to the anode surface from the cathode. At the cathode water was produced from the oxidation of the permeated methanol as well as the reduction of oxygen as shown in eqs (1-41) and (1-4) respectively, this water can easily transported across the Nafion membrane under the concentration gradient between anode and cathode. By understanding the mechanism of this novel electrode structure, the factors affecting the methanol crossover could be controlled so neat methanol could be efficiently used producing high energy density DMFC.

Structure of the thesis:

To realize our purpose, firstly we have to understand the basic factors affecting the performance of this novel electrode structure. A theoretical consideration for the mechanism of controlling MCO through this electrode structure has been made and its validity has been checked experimentally under open circuit conditions, chapter 2.

Under closed circuit condition, CO_2 would evolve at the anode side and it was expected to fill the pores of the porous plate. The application of this electrode structure under closed circuit condition would be different from the conventional one; we investigated its performance and compared it with the conventional one with respect to, efficiency, methanol and water fluxes. We have confirmed high efficient operation and high reduction of MCO compared to the conventional one. In the same time the mechanism of water supply from cathode to anode, water back diffusion, was confirmed so neat methanol could be operated, chapter 3.

It is a very common problem in the conventional passive DMFC that the long term performance largely decreased within very short time whether due to the methanol depletion at the anode or the flooding at the cathode. In this electrode structure high methanol concentration, neat, could be used and no flooding at cathode. We checked the long term behavior of this novel electrode structure and how it will be affected by the

different fuel, methanol and oxygen, supplying modes and comparing it with the conventional one. Results showed superior properties of this DMFC, where stably operated under completely passive condition in contrast of the conventional one, chapter 4.

Under closed circuit conditions we have understood that not only the PCP controlled the methanol transport but also the CO_2 gas layer which formed between the anode and the porous plate. We need to clarify the importance of the existence of this gas barrier as well as its pressure on the obstructing the methanol transport from the fuel reservoir to the anode surface. We discovered that the existence of the gas barrier was essential for the obstructing of methanol transport, chapter 5.

Although operation with neat methanol was confirmed, chapter 3, efficiency relatively low. The factors affecting the performance of this novel electrode structure such as porous plate structure and thickness as well as gas barrier thickness were studied under closed circuit condition. By controlling these factors high energy density DMFC operated efficiently with neat methanol was obtained, chapter 6.

The scheme of the thesis is summarized as show in Fig. 1-14.

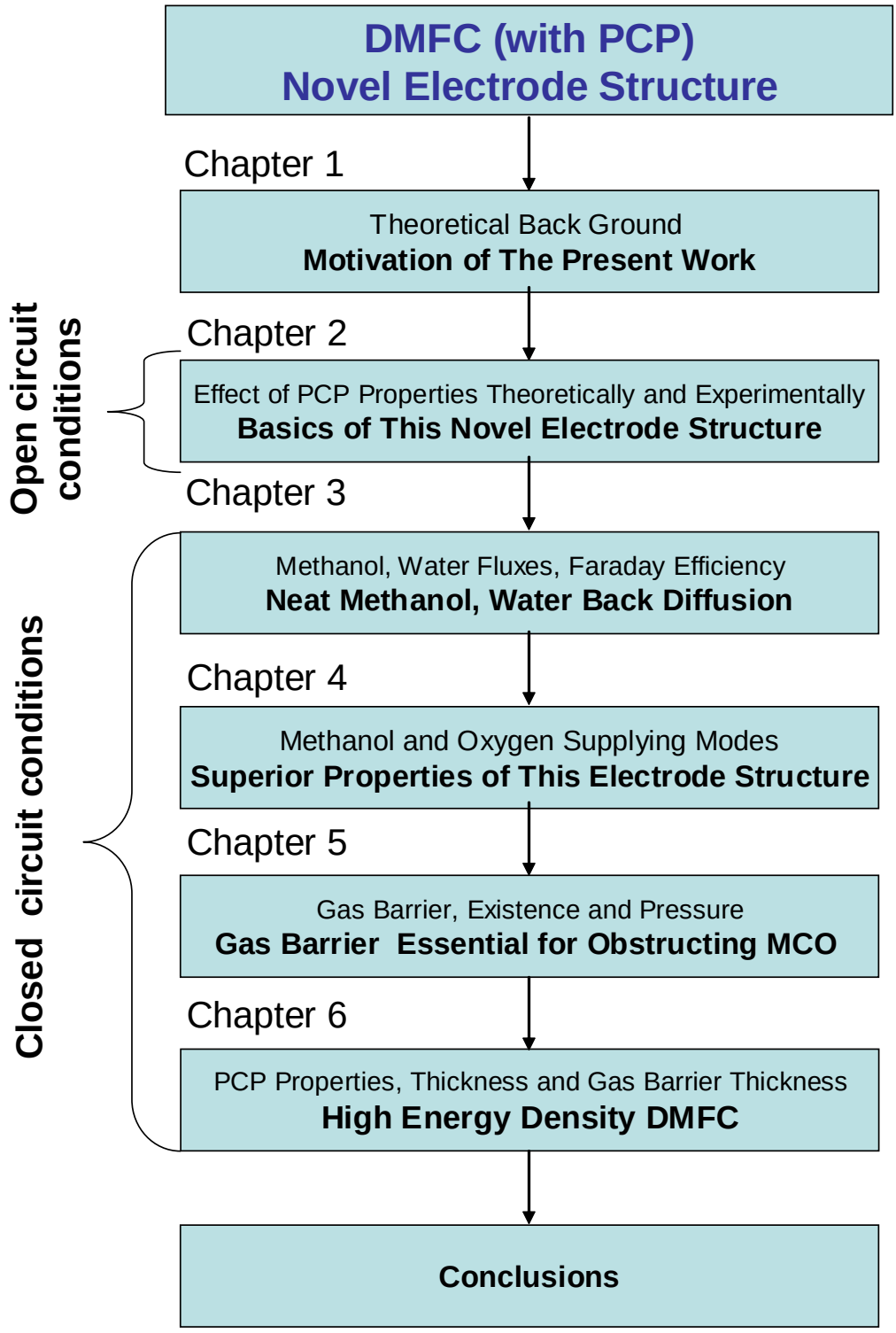

Figure 1-14: A scheme and structure for the thesis

3. References

1. G. Hoogers, Fuel cell technology handbook, CRC, (2003) chapter 1.
2. A.S. Arico, A.K. Shukla, K.M. El-khatib, P. Creti and V. Antonucci, *J. Appl. Electrochem.,* **29** (1999) 671.
3. J. O. Bockris, B. E. Conway and R. E. White, modern aspects of electrochemistry No.34 (2001).
4. R. Dillon, S. Srinivasan, A.S. Arico, V. Antonucci, *J. Power sources* **127** (2004) 112.
5. H. Chang, J.R. Kim, J.H. Cho, H.K. Kim, K.H. Choi, *Solid State Ionics* **148** (2002) 601–606.
6. A. Blum, T. Duvdevani, M. Philosoph, N. Rudoy, E. Peled, *J. Power Sources* **117** (2003) 22–25.
7. D. Kim, E.A. Cho, S.A. Hong, I.H. Oh, H.Y. Ha, *J. Power Sources* **30** (2004) 172–177.
8. Z. Guo, Y. Cao, *J. Power Sources* **132** (2004) 86–91.
9. T. Shimizu, T. Momma, M. Mohamedi, T. Osaka, S. Sarangapani, *J. Power Sources* **137** (2004) 277–283.
10. H. Qiao, M. Kunimatsu, T. Okada, *J. Power Sources* **139** (2005) 30.
11. Q. Ye, T.S. Zhao, *J. Power Sources* **147** (2005) 196–202.
12. B. Kho, I. Oh, S. Hong, H.Y. Ha, *Electrochim. Acta* **50** (2004) 781.
13. A.S. Arico, S. Srinivasan, V. Antonucci, *Fuel Cells* **1** (2001) 133–161.
14. T. Schultz, S. Zhou, k. Sundmacher, *Chem. Eng. Technol*. **24** (2001) 1223–1233.
15. J.G. Liu, T.S. Zhao, R. Chen, C.W. Wong, *Electrochem. Commun.* **7** (2005) 288.
16. J.G. Liu, T.S. Zhao, Z.X. Liang, R. Chen, *J. Power Sources* **153** (2006) 61–67.
17. J. Larminie, A. Dicks, Fuel cell systems explained, second edition (2003).
18. J.S. Wainright, J.T. Wang, D. Weng, R.F. Savinell, M. Litt, *J. Electrochem. Soc.* **142** No. 7(1995) L121.

19. D. Weng, J.S. Wainright, U. Landau, R.F. Savinell, *J. Electrochem. Soc.* **143** No. 4 (1996) 1260-1263.

20. N. Carretta, V. Tricoli, F. Picchioni, *J. Membrane Sci.* **166** (2000) 189-197.

21. D.J. Jones, J. Roziere, *J. Membrane Sci.* **185** (2001) 41-58.

22. C. Lim, C.Y. Wang, *J. Power Sources,* **113** (2003) 145–150.

23. G. Lu, C.Y. Wang, Transport phenomena in fuel cells, Two-phase microfluidics, heat and mass transport in direct methanol fuel cells (2005) chapter 9.

24. G.Q. Lu, C.Y. Wang, *J. Power Sources,* **144** (2005) 141–145.

25. J.H. Hirschenhofer, D.B. Stauffer, R.R. Engleman, M.G. Klett, Fuel cell hand book by fourth edition, (1998) chapter 2.

26. E. Barendrecht, Fuel cell systems, eds L.J.M.J. Blomen & M.N. Mugerwa, New York, (1993) p. 75.

27. C. Lamy, J.M. Léger, Advanced Electrode Materials for the Direct Methanol Fuel Cell, in Interfacial Electrochemistry Theory, Experiment, and Applications, Wreckowski, Ed., Marcel Dekker, Inc., New York, (1999)p. 885–894.

28. W. Vielstich, CO, Formic Acid, and Methanol Oxidation in Acid Electrolytes—Mechanisms and Electrocatalysis, in Encyclopedia of Electrochemistry, Volume 2: Interfacial Kinetics and Mass Transport, Bard, A.J., Stratmann, M., Calvo, E.J., Eds.

29. S. Minteer, Alcholic fuels, (2006) by Taylor & Francis Group, LLC CRC Press is an imprint of Taylor & Francis Group, Current Status of Direct Methanol Fuel-Cell Technology, chapter 9.

30. H.A. Gasteiger, N. Markovic, P. N. Ross Jr., E.J. Cairns, *Electrochimica Acta,* **39** (1994) 1825–1832.

31. J. O. Bockris, S. U. M. Khan, *Surface Electrochemistry, A Molecular Approach,* Plenum Press, New York, (1993).

32. C. Lamy, J. M. Léger, in Proc. 1st International Symposium on New Materials for Fuel Cell Systems, Ed. by O. Savadogo, P. R. Roberge, T. N. Veziroglu, Ecole Polytechnique, Montreal, (1995) 296-309.

33. A. Heinzel, V.M. Barragan, *J. Power Sources* **84** (1999) 70-74.

34. J. Cruickshank, K. Scott, *J. Power Sources* **70** (1998) 40-47.

35. K. Scott, W.M. Taama, P. Argyropoulos, K. Sundmacher, *J. Power Sources* **83** (1999) 204-216.

36. S. Kato, K. Nagahama, H. Noritomi, H. Asai, *J. Membrane Sci.***72** No. 1 (1992) 31-41.

37. H. Dohle, H. Schmitz, T. Bewer, J. Mergel, D. Stolten, *J. Power Sources* **106** (2002) 313–322.

38. H. Dohle, J. Divisek, R. Jung, J. *Power Sources* **86** (2000) 469–477.

39. X. Ren, P. Zelanay, S. Thomas, J. Davey, S. Gottesfeld, *J. Power Sources* **86** (2000) 111–116.

40. Y.J. Kim, W.C. Choi, S.I. Woo, W.H. Hong, *Electrochimica Acta* **49** (2004) 3227–3234.

41. T. Hejze, B.R. Gollas, R.K. Sauerbrey, M. Schmied, F. Hofer, J.O. Besenhard, *J. Power Sources*, **140**, (2005) 21–27.

42. Z.Q. Ma, P. Cheng, T.S. Zhao, *J. Membrane Science* **215** (2003) 327–336.

43. J. Sauk, J. Byun, H. Kim, *J. Power Sources* **132**, 5(2004) 9–63.

44. D.W. Kim, H.-S. Choi, C. Lee, A. Blumstein, Y. Kang, *Electrochimica Acta* **50** (2004) 659–662.

45. J. Liu, H. Wang, S. Cheng, K.-Y. Chan, *J. Membrane Science*, **246** (2005) 95–101.

46. M. Watanabe, H. Uchida, Y. Seki, M. Emori, *J. Electrochem. Soc.* **143** (1996) 3847–3852.

47. M. Watanabe, H. Uchida, M. Emori, *J. Physical Chemistry B*, **102** (1998) 3129–3137,.

48. M. Watanabe, H. Uchida, Y. Ueno, H. Hagihara, *J. Electrochemic. Soc.* **150** (2003) A57–A62.

49. A.S. Arico, V. Baglio, A.D. Blasi, E. Modica, P.L. Antonucci, V. Antonucci, *J. Power Sources*, **128** (2004) 113–118.

50. F. Bauer, M. Willert-Porada, *J. Membrane Sci.* **233** (2004) 141–149.

51. E. Peled, T. Duvdevani, A. Aharon, A. Melman, , Direct-Oxidation Fuel Cells Based on Nanoporous Proton- Conducting Membrane (NP-PCM), In *Direct Methanol Fuel Cells: Proceedings of the International Symposium*, S. R. Narayanan, S.R., Gottesfeld, S. and Zawodzinski, T., Eds.

52. J. Roziere, D.J. Jones, Non-Fluorinated Polymer Materials for Proton Exchange Membrane Fuel Cells, *Annual Review of Materials Research*. **33** (2003) 503–555.

53. V.S. Silva, B. Rumann, H. Silva, Y.A. Gallego, A. Mendes, L.M. Madeira, S.P. Nunes, *J. Power Sources*, **140** (2005) 34–40.

54. V.S. Silva, J. Schirmer, R. Reissner, B. Rumann, H. Silva, A. Mendes, L.M. Madeira, S.P. Nunes, *J. Power Sources*, **140** (2005) 41–49.

55. B. Smitha, S. Sridhar, A.A. Khan, *J. Applied Polymer Science*, **95** (2005) 1154–1163.

56. N. Nakagawa, K. Kamata, A. Nakazawa, M. Ali Abdelkareem, K. Sekimoto, *Electrochemistry* **74** No.3 (2006) 221-225.

57. J. Liu, G. Sun, F. Zhao, G. Wang, G. Zhao, L. Chen, B. Yi, Q. Xin, *J. Power Sources*, **133**, (2004)175-180.

58. R. Chen, T.S. Zhao, *J. Power Sources*, **152** (2005)122-130.

59. J. Liu, T. Zhao, R. Chen, C. W. Wong, *Fuel Cells Bulletin*, February, (2005) 12-17.

60. B. Kho, I. Oh, S. Hong, H.Y. Ha, *Fuel Cells Bulletin*, September, (2004) 11-14.

61. C. Y. Chen, P. Yang, *J. Power Sources* **123** (2003) 37-41.

62. S.R. Yoon, C.H. Hwang, W.I. Cho, I-H. Oh, S-A. Hong, H.Y. Ha, *J. Power Sources* **106** (2002) 215–223.

63. B. Bae, B.K. Kho, T. Lim, I. Oh, S. Hong, H.Y. Ha, *J. Power Sources* **158** (2006) 1256–1261.

64. R. Chen, T. S. Zaho, J. G. Liu, *J. Power Sources* **157** (2006) 351–357.

65. G.Q. Lu, C.Y. Wang, T.J. Yen, X. Zhang, *Electrochimica Acta* **49** (2004) 821–828.

66. A. S. Arico, P. Creti, P. L. Antonucci, V. Antonucci, *Electrochemical and Solid-State Letters*, **1** (1998) 66-68.

67. C. Yang, S. Srinivasan, A. S. Arico, P. Creti, V. Baglio, V. Antonucci, *Electrochemical and Solid-State Letters*, **4** (2001)A31-A34.

68. N. Jia, M.C. Lefevre, J. Halfyard, S. Qi, P .G. Pickup, *Electrochemical and Solid-State Letters*, **3** (2000) 529-531.

69. I.J. Hobson, H. Ozu, M. Yamaguchi, M. Muramatsu, S. Hayase, *Journal of Materials Chemistry*, **12**, (2002) 1650-1656.

70. W.C. Choi, J.D. Kim, S.I. Woo, *Journal of Power Sources*, **96** , (2001) 411-414.

71. V. Neburchilov, J. Martin, H. Wang, J. Zhang, *J. Power Sources*, **169** (2007) 221-238.

CHAPTER 2

Control of Methanol Transport and Separation in a DMFC with a Porous Support under open circuit conditions

1. Introduction

There has been an increasing demand for the development of direct methanol fuel cells (DMFCs) [1-3] because of their high energy densities which are suitable for mobile electric devices and automobiles. However, the energy density of the DMFCs currently under development is still far from that expected due to the methanol crossover and the high overvoltage at the electrodes [4, 5]. Due to the methanol crossover, the DMFC usually shows the highest performance at low concentrations of methanol from 2M to 3M [6, 7] under the active conditions. To overcome the methanol crossover, a large number of studies [8-12] were carried out for developing a new proton-conducting membrane with a low methanol permeability and high proton conductivity. Modification of the existing membranes like Nafion has also been conducted by making it a composite membrane [13-15] with inorganic or organic materials, surface modification by physical treatment [16] or by coating the surface with a thin film [17-19]. Only a few papers considered the reducing ability in methanol crossover by mass transport control in the backing layer [20, 21].

Passive DMFCs, that suck methanol from a reservoir by an osmotic action and breath air from its surrounding by natural convection and diffusion, have been demonstrated, and the performance was investigated by some researchers under different conditions [20, 22-32]. The reports on the passive DMFCs revealed some different performance behaviors compared to that of active DMFCs. For example, a methanol concentration like 5M, which is higher than that for an active DMFC, was sometimes assigned as the optimum condition for the i-V performance [18, 27, 33]. An air-breathing DMFC with a thinner membrane exhibited a better i-V performance at low current density [34]. A passive vertically oriented DMFC always produced a better performance than that horizontally oriented [35]. These behaviors were attributed to the methanol crossover that induced an increase in the cell temperature due to the exothermic reaction between the permeated methanol and the oxygen at the cathode, so that the polarization was reduced, and hence, a high performance was achieved [23, 34, 35]. These do not suggest that the methanol crossover played a desirable role in the passive DMFC. It should be noted that the methanol crossover causes a loss of the methanol and significantly reduced the energy

density and the efficiency of the DMFC. In the passive DMFCs, the methanol crossover and the temperature of the cell were not controlled, which sometimes leads to fatal damage to the cell.

We demonstrated, in a recent report [20], that a passive DMFC with a porous carbon plate as a support reduced the methanol crossover and constantly controlled the cell temperature. In the experiment, two different types of porous carbon plates were used, and their methanol crossover reductions were different suggesting that the properties of the porous plate affected the methanol crossover. The mechanism of reducing the MCO was explained by the diffusion control of the methanol through the porous plate. This chapter is primarily focused on a theoretical consideration for the reduction of the methanol crossover through the MEA with a porous plate. The behavior of the transport and separation of methanol through this type of passive DMFC under open circuit conditions was then investigated. Experiments were conducted to show the unique properties of this cell by measurement of the MCO using different porous materials, i.e., porous carbon and porous alumina, with different properties, e.g., pore structures, water absorptivity, at different methanol concentrations and different temperatures.

2. Theoretical consideration of the mass transfer through MEA

When an MEA with a polymer electrolyte membrane like Nafion is in contact with a methanol solution and air at both surfaces, the crossover of methanol and also water occurs. The mass flow rate of the solution M_T, a mixture of methanol and water, through the MEA would be controlled by the rate of removal of the solution from the cathode surface into the cathode gas due to vaporization under open circuit conditions, in some cases. The driving force of the vaporization is the difference in vapor pressure of the solution between the cathode surface and the flowing gas and the rate of vaporization, v_l, can be expressed as follows:

$$\mathbf{v_l = k\,(p_v - p_a)} \qquad \textbf{(2-1)}$$

$$\mathbf{= k\,(p_0\,\exp(-L_a/(RT)) - p_a)} \qquad \textbf{(2-2)}$$

where k is a constant, p_v is the vapor pressure of the solution at the meniscus of the porous cathode, p_a is the vapor pressure of the cathode gas, p_0 is the vapor pressure of the bulk solution, and L_a is the latent heat of vaporization of the solution. Equation (2-2) was derived from the Clausuis-Clapeyron relation.

The solution that exists at the cathode was a mixture of methanol and water, and the total flux across the membrane J_T consists of a methanol flux J_M and a water flux J_W.

$$\boldsymbol{J_T = J_M + J_W} \qquad \textbf{(2-3)}$$

and also, as the total flux is controlled by the rate of vaporization, and hence,

$$\boldsymbol{J_T = M_T / A = v_l / A} \qquad \textbf{(2-4)}$$

where A is the area of the membrane. The methanol flux can be related to the water flux based on the general relationship in flux between a solute and a solvent that permeate through a membrane as follows:

$$\boldsymbol{J_M = (1 - \sigma)\, C_m^*\, J_W - D_{mM}\, (dC_m/dx)} \qquad \textbf{(2-5)}$$

$$\boldsymbol{= J_{CM} + J_{DM}}$$

The first term of eq.(2-5) is the convection flux of methanol J_{CM} with the water flux and the second term shows the diffusion flux of methanol J_{DM}, where σ is the reflection coefficient, and C_m* is the average concentration of methanol in the membrane and D_{mM} is the diffusion coefficient of methanol in the membrane, and C_m is methanol concentration at position x in the membrane from the surface.

Methanol that usually permeated to the cathode is oxidized by oxygen into water with the help of a catalyst, and the methanol concentration at the cathode surface remained low. Under this situation, the diffusion flux, J_{DM} is increased by the increase of difference in the methanol concentration between both surfaces of the membrane. This raised the methanol flux J_M, while the total flux was constant, i.e., reducing the flux of water, because the total flux was controlled by the rate of water vaporization as shown by eq. (2-3) and (2-4). As a result, methanol preferentially permeated through the membrane, and this caused a significant loss in energy density and energy efficiency of the DMFC.

2.1. Methanol diffusion through a porous plate

Let us now consider a case where a porous plate, which absorbs water into the body by osmotic action, is used as a support of the MEA on the anode side. When the flow rate of the solution through the MEA driven by the evaporation of water at the cathode is not very high, the porous plate is not a resistance for the transport of the total solution through the porous plate and MEA, if the porous plate absorbs sufficient water. In addition, the flux of methanol through the membrane can be controlled by the diffusion resistance of the

porous plate. This mechanism can reduce the diffusion flux of methanol through the membrane J_{DM} by reducing the methanol concentration at the anode surface resulting in reducing the difference in the methanol concentration between the surfaces of the membrane. The diffusion flux of methanol controlled by the porous plate can be given by Fick's law as follows:

$$J_{DM} = -D_{eff,M} \ (\Delta C_M \ / \Delta X) \qquad (2\text{-}6)$$

Where $D_{eff,M}$ is the effective diffusion coefficient of methanol through the porous plate, and ΔC_M is the difference in the concentrations of methanol between both sides of the porous plate with thickness ΔX.

The effective diffusion coefficient $D_{eff,\,M}$ depends on the properties of the porous plate where the coefficient is proportional to the porosity of cross section ε_s and inversely proportional to the tortosity τ of the porous plate as follows:

$$D_{eff,M} = k \, D_M \, \varepsilon_s / \tau \qquad (2\text{-}7)$$

where D_M is the diffusion coefficient of methanol in water and k is a constant related to the affinity between methanol and the surface of the porous material.

When some pores are filled with the methanol-water solution due to the hydrophilic properties of the porous plate and the diffusion through the flooded pore dominates the mass transport, eq. (2-7) can be modified as follows:

$$D_{eff,M} = k' \, D_M \, (\alpha_s \, \varepsilon)^{2/3} / \tau \qquad (2\text{-}8)$$

where α_s is the absorptivity of the solution to the porous plate defined by the volume fraction of flooded pore to that of the total pore, and ε is the porosity in volume. The power 2/3 in the equation expresses the transfer in the cross-sectional value instead of the volumetric value.

For a methanol-water solution, the absorptivity of solution α_s can be empirically related to that of water α_w due to the change in the surface tension

$$\alpha_s = k_1 + k_2 \, \alpha_w \qquad (2\text{-}9)$$

Where k_1 and k_2 are constants depending on the methanol concentration and type of porous material.

Based on the above mechanism, the methanol flux through the MEA and the acceleration effect on it can be reduced by the porous plate. In the following sections, the mechanism will be experimentally confirmed.

3. Experimental

3.1 Measurements of the pore structure and the water absorptivity of the porous plates

The porous plates used as the MEA support in this study included seven different types of porous carbon plates supplied from Mitsubishi Pencil Co., Ltd., and one Al_2O_3 porous plate from Nikkato Co., Ltd., used as a membrane in the electrolysis. The properties and pore structure of this porous plate are listed in Table 2-1. The porous carbon plates were categorized into two types, the CS type that was made of graphitic carbon and amorphous carbon and the CY type that was made of amorphous carbon. The Al_2O_3 porous plate, denoted as CER, was prepared as a reference to check if the carbon material is significantly important for controlling the MCO.

The microstructure of the porous plates was measured using a mercury porosimeter, Pascal 140 + 440 (Thermo Finnigan, Inc.). The water absorptivity, α_w, was defined as the fraction of the pore volume that filled with water when the plate was dipped into water for a long enough time. In the table, the properties and pore structure of a conventional carbon paper, C-paper, is also listed for comparison. It was clear that the porous carbon plates had a smaller average-pore diameter and porosity than that of the carbon paper.

Table 2-1 Properties of the carbon paper and the porous carbon plates used.

			Pore structure measured by the mercury porosimeter		
Anode backing	δ [mm]	α_w [-]	V_p [cm^3/g]	$d_{p,ave}$ [μm]	ε [-]
C-paper	0.17	0.82	1.51	50.6	0.81
CS1	2.0	0.0	0.137	2.0	0.244
CS2	2.0	0.15	0.521	2.0	0.487
CS3	2.0	0.55	0.248	2.0	0.33
CS4	2.0	0.9	-	2.0	0.49
CS5	2.0	0.83	0.265	7.8	0.43
CY1	2.0	0.5	-	20	0.59
CY2	2.0	0.7	0.775	43.8	0.588
CER	2.0	0.87	0.129	0.4	0.322

The water absorptivity α_w of the porous plates cut into a 10mm wide, 50mm long and 2mm thick strip measured by fully immersing the stick in water until its weight became constant. From the volume of the initial pore, V_0, and the volume of the absorbed water, V_w, the absorptivity was calculated as follows:

$$\alpha_w = V_w/V_0 \qquad \textbf{(2-10)}$$

3.2 MEA preparation

3.2.1Conventional MEA

The conventional MEA, which uses carbon paper as the anode-backing layer, was prepared in the following manner. Catalyst ink containing Pt-Ru (54 wt%, Pt/Ru=1.5)/C catalyst, a 5 wt% Nafion solution (Wako, Inc.) and glycerol in the weight ratio of 1:3:3 was applied on the carbon paper (TGP-H-060, Toray, Inc.) to give a catalyst loading of 3-4 mg/cm^2 and then used as the anode after being dried in a vacuum oven for 3h. A ready-made electrode, EC-20-10 (ElectroChem, Inc.) with Pt (1.0 mg/cm^2)/C was used as the cathode. Nafion 112 was used as the electrolyte membrane. It was pretreated to activate the proton conduction as follows: dipping it into 3 vol% H_2O_2, de-ionized water, 2.5 mol/dm^3 H_2SO_4 and de-ionized water in that order and boiling each solution for 1 hour during each step. Finally, the MEA was fabricated by sandwiching the membrane between the anode and the cathode and hot pressing them at 403K and 9 MPa for 3 minutes. The conventional MEA was labeled as MEA_C.

3.2.2 MEA with the porous plate

The porous plate was cut into a 10 mm wide, 50 mm long and 2 mm thick strip and was used as the support of the cell, i.e., used as an anode backing instead of the carbon paper for the conventional MEA. In a preliminary experiment, we confirmed that the mass transport through the MEA with a porous plate was unrelated between the case where the porous plate was mated with the membrane by hot pressing and the case where the porous plate was just placed on the conventional MEA. Hence, we put the porous plate on the anode surface of the conventional MEA and fixed them by pressing them in the cell holder. Therefore, the porous plate acted as a barrier to mass transport between the methanol reservoir and the anode surface. These MEAs with the porous plate was denoted as MEA/CSi or MEA/CYi depending on the type of porous plate.

3.3 Methanol and water flux measurements

Figure 2-1 shows the experimental setup used to measure the mass transport through the MEA with or without the porous plate. The MEA with or without the porous plate was placed on a holder as shown in the figure. The cell chamber was separated by the MEA into the methanol reservoir and the oxygen flow chamber, and it arranged such that the reservoir top and the oxygen chamber bottom remained in constant contact between the solution and MEA. Into the oxygen chamber, the oxygen gas flowed at 500 ml min^{-1} from a cylinder. On the other hand, the CO_2 produced in the oxygen chamber by the oxidation of methanol permeated from the reservoir with the help of the Pt catalyst in the gas exhaust was measured using the IR CO_2 meter. In a preliminary experiment, we found, under certain conditions of this study, that 85% to 90% of the permeated methanol was converted to CO_2 and 10% to 15% of the permeated methanol was not completely oxidized. Hence, the CO_2 production rate was used to determine a trend in the time profile of the methanol crossover rate. We also measured the weight loss of the entire cell holder at a certain time interval and the methanol concentration of the liquid that remained in the reservoir after the experiment. The total flux was calculated from the weight loss, and the methanol flux was calculated from the amount of the methanol consumed from the reservoir during the experiment. The water flux was also calculated by subtracting the methanol flux from the total flux. These fluxes were the time average value in the 4h experiment.

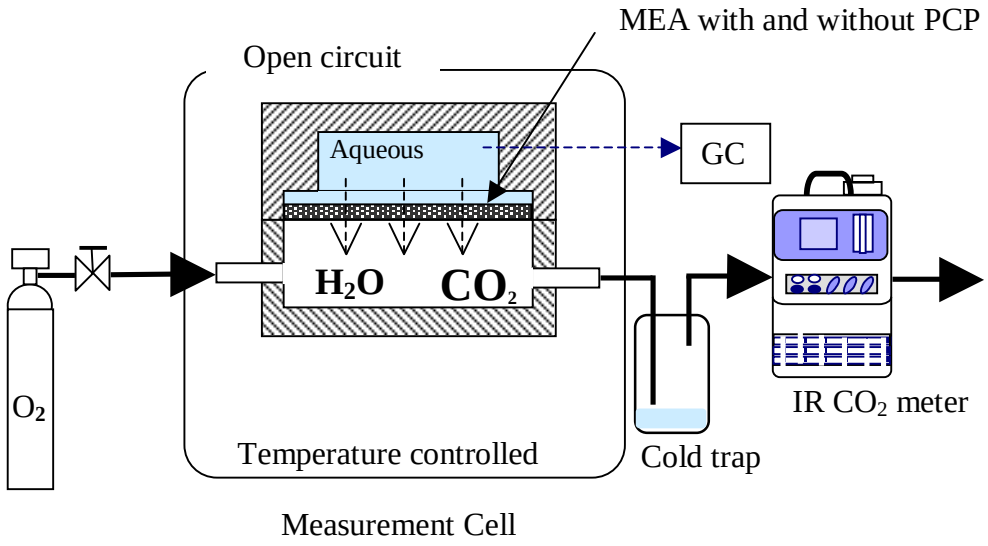

Figure 2-1 Apparatus used for measuring MCO under open circuit conditions.

3.4 Controlling and measuring the temperature of the cell

The entire cell holder was placed it in a furnace and the surrounding temperature was adjusted at the desired temperature by the furnace. The holder was kept for sufficient time until the entire holder reached to the desired temperature before the measurement. The surrounding temperatures employed in this study were 297K, 310K and 323K.

In some experiments, the temperature of the cell was directly measured using a thermocouple placed on the cathode surface.

4. Results and discussion

4.1 CO_2 production rate and loss of the total solution

Figure 2-2 (a) shows the CO_2 production rate measured for MEA_C, MEA/CS2, MEA/CY2 and MEA/CER at the methanol concentration of 2M, at 297K. The CO_2 production rate for the conventional MEA, MEA_C, was greater than that for the MEAs with the porous plate, especially at the initial time. At 25 min, the CO_2 production rate for the MEA_C was 3 to 5 times greater than that for the MEAs with the porous plate. The production rate for the MEAs with the porous plate was different from each other according to the type of porous plate. It should be noted that CO_2 production rate when using the porous plate was nearly constant during the measurement, whereas the rate for the conventional MEA was initially high and decreased with time. Although the CO_2 production rate did not accurately agree with the rate of the methanol crossover due to the –10% to –15% error in the mass balance, it roughly indicated that the rate of MCO for each MEA. Hence, it was clear that the porous plate significantly reduced the methanol crossover and constantly stabilized the crossover rate for a long time, and also, the degree of reduction in the methanol crossover depended on the properties of the porous plate.

Figure 2-2 (b) shows the weight loss of the cell holder with time for the cases shown in Fig. 2-2 (a). The weight loss was due to the crossover of methanol and water from the reservoir to the oxygen chamber followed by the vaporization that transferred the solution out of the chamber with the oxygen flow. The methanol solution loss increased with the increasing time in all cases. Here, it should be noted that the order of the rate of the loss did not agree with the order of the CO_2 production rate shown in Fig. 2-2 (a). This suggested that the rate of the methanol crossover did not coincide with the rate of the water permeation.

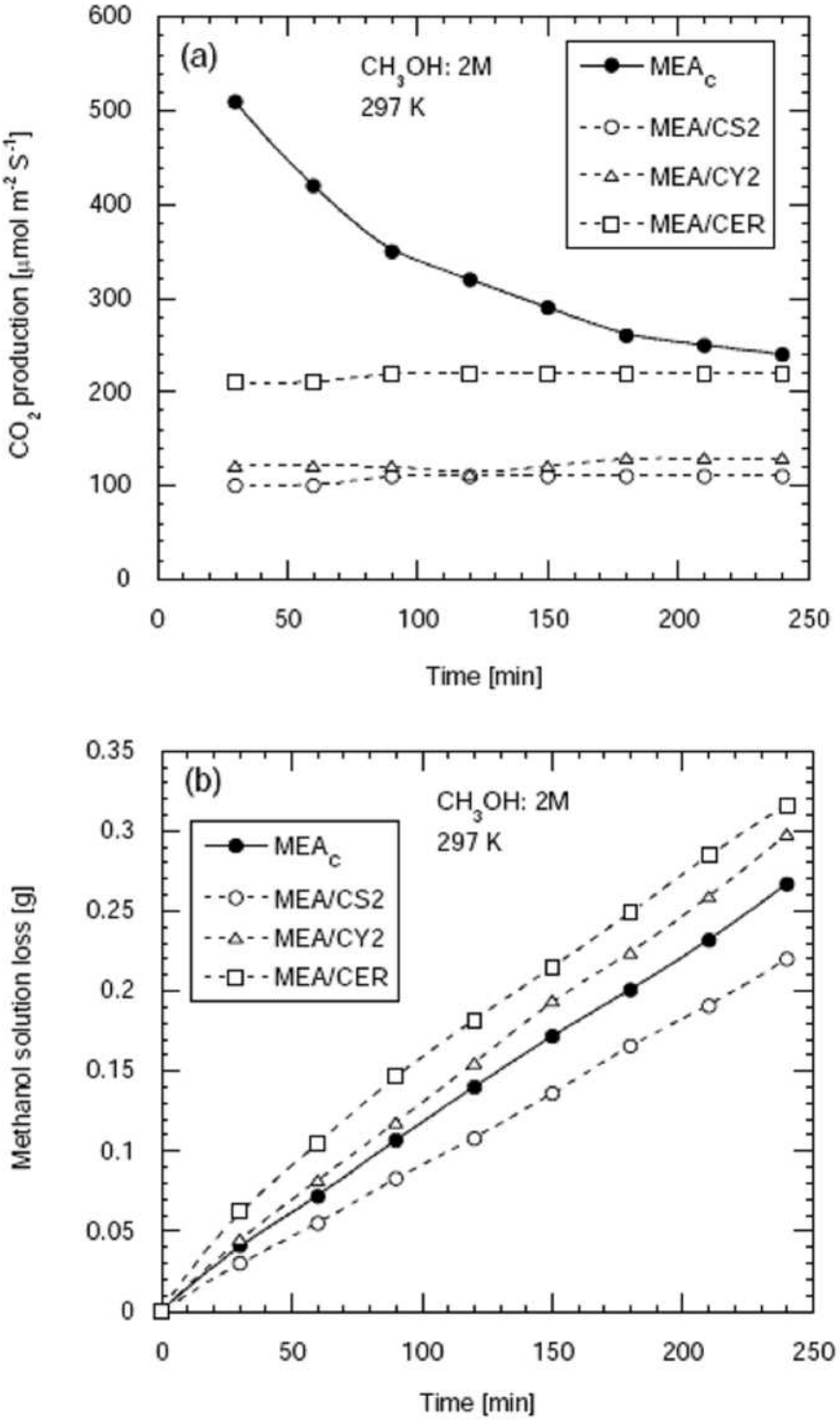

Figure 2-2 Variations in (a) CO_2 production rate, and (b) methanol solution loss with different porous materials at 2M.

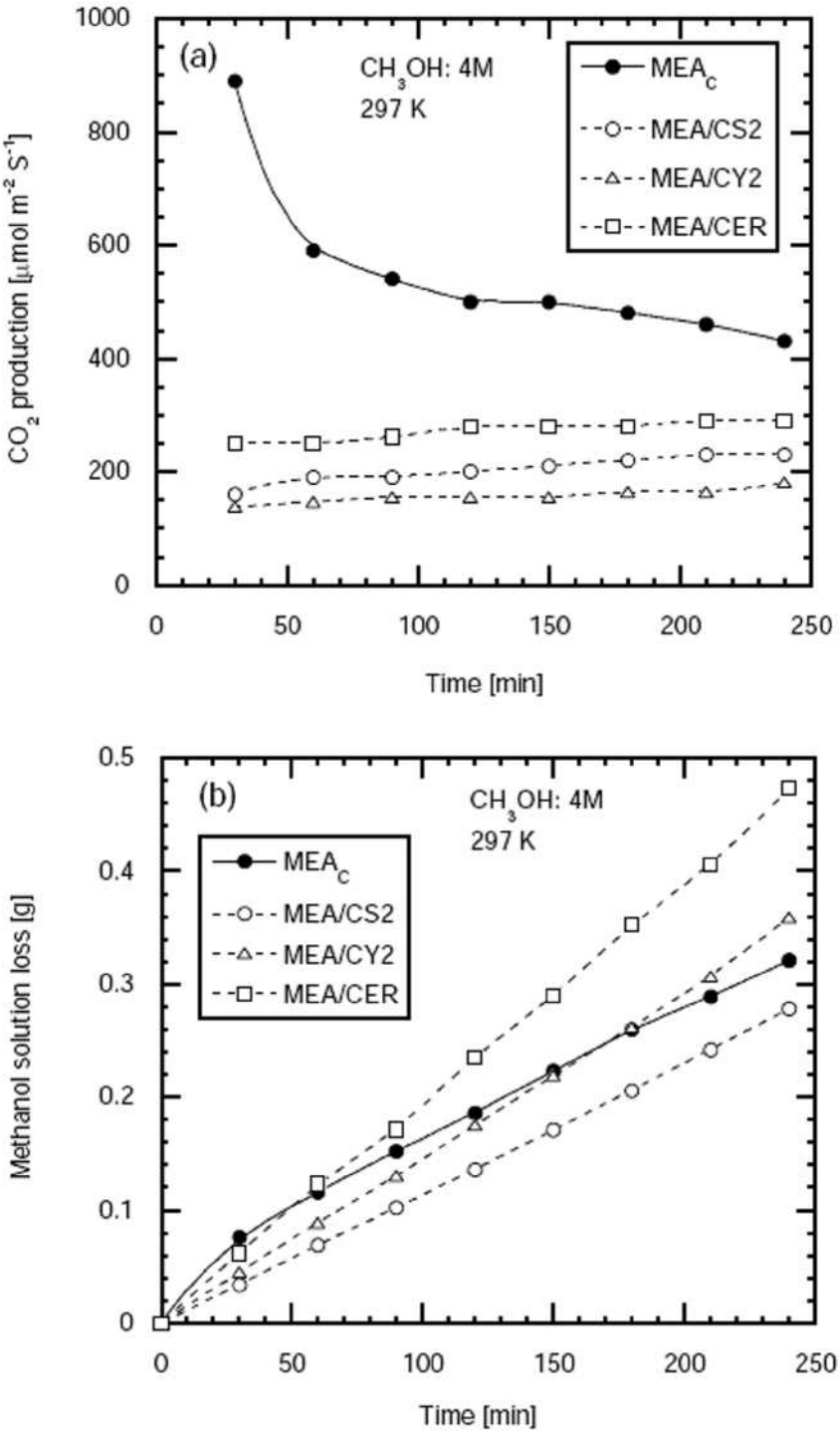

Figure 2-3 Variations in (a) CO_2 production rate, and (b) methanol solution loss with different porous materials at 4M.

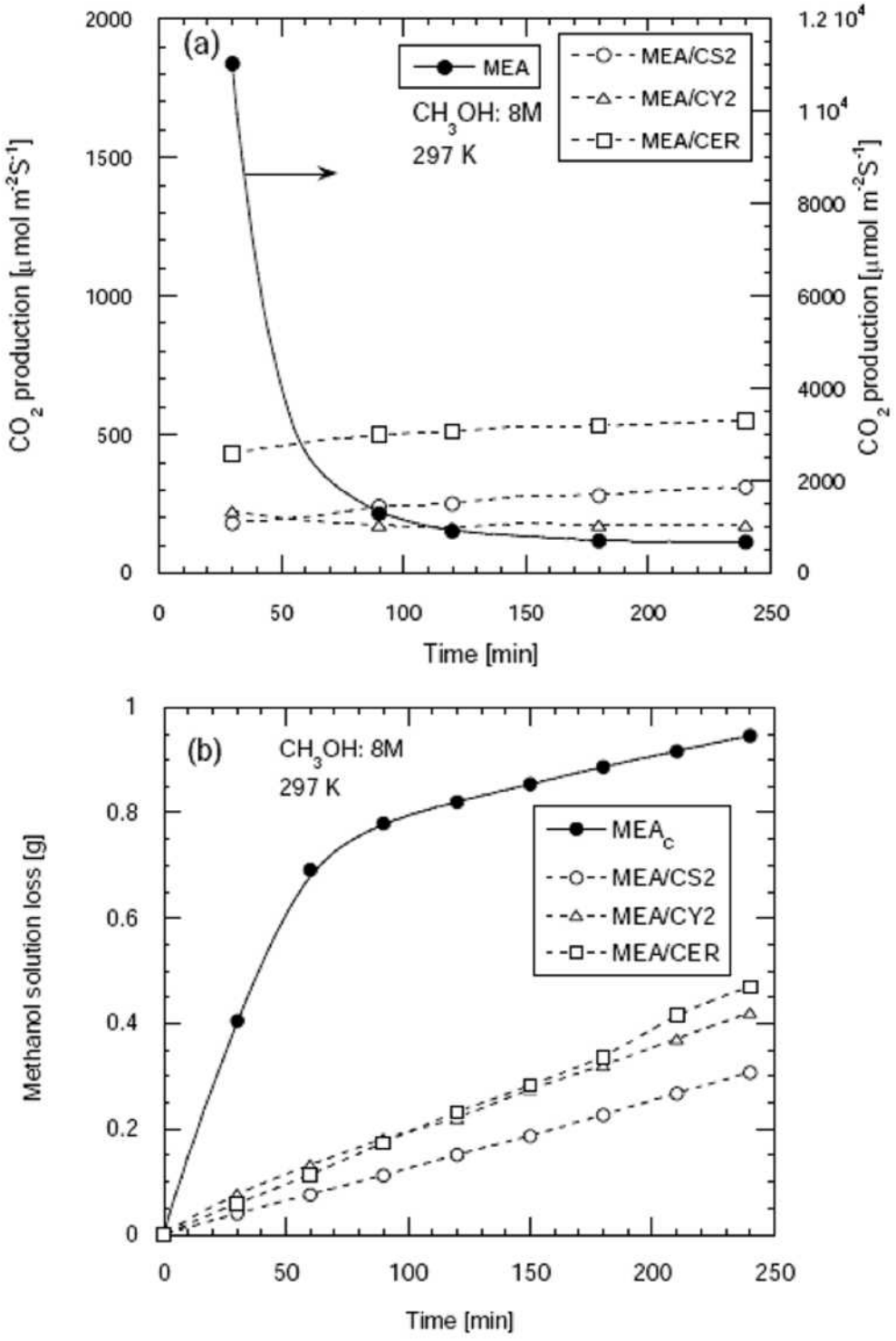

Figure 2-4 Variations in (a) CO_2 production rate, and (b) methanol solution loss with different porous materials at 8M.

Figures 2-3 and 2-4 show the CO_2 production rate and the weight loss at 4M and 8M, respectively. At 4M, as shown in Figs. 2-3 (a) and (b), nearly the same trend as that shown in Fig. 2-2 was obtained, but both the CO_2 production rate and the loss of the methanol solution increased with the increase the methanol concentration from 2M to 4M and 8M. With the increasing concentration of methanol in the reservoir, the methanol flux increased according to eq. (2-6). The difference in the methanol concentration of the solution between both surfaces of the porous plate increased with the increasing concentration in the reservoir.

When the methanol concentration was as high as 8M, the methanol crossover for the conventional MEA, MEA_C, was significantly increased from that at 4M and 2M. The production rate of CO_2 for the MEA_C was thirty to sixty times higher compared to that of the MEA with the porous plates as shown in Fig. 2-4 (a). This was caused by an increase in the temperature of the MEA as shown in the next section. On the other hand, in the case of the MEAs with the porous pate, the rate of the methanol crossover remained low and constant with time.

4.2 Effect of using the porous plate on cell temperature

Figures 2-5(a), (b) and (c) show the temperature of the cell in the measurement of the CO_2 production rate for each MEA, i.e., MEA_C, MEA/CS2 and MEA/CER, at 2M, 4M and 8M, respectively. In case of the MEA_C, the temperature increased from 297K to 306K, 317K and 383K, during 5 to 15 min at 2M, 4M and 8M, respectively, then decreased with time. Whereas, in the case of MEA/CS2 and MEA/CER, the temperatures slightly increased and the change at the end of the measurement was 2K and 6K, respectively, regardless of the methanol concentration. These temperature profiles were consistent with the variations in the production rate of CO_2 shown in Figs. 2-2 to 2-4. The consistency between them was reasonable, because the increase in temperature was caused by the oxidation of the methanol that permeated to the cathode. It should be noted that the temperature at 8M for the conventional MEA reached 383K that is close to the glass transition temperature of Nafion. Such a high temperature resulted from the methanol crossover being out of control, and it may cause significant damage to the microstructure of the MEA. This pointed out that such a high methanol concentration can't be used during practical operation of DMFC with the conventional MEA. As a result of the uncontrollable methanol crossover, the loss of methanol fed to the reservoir significantly increased.

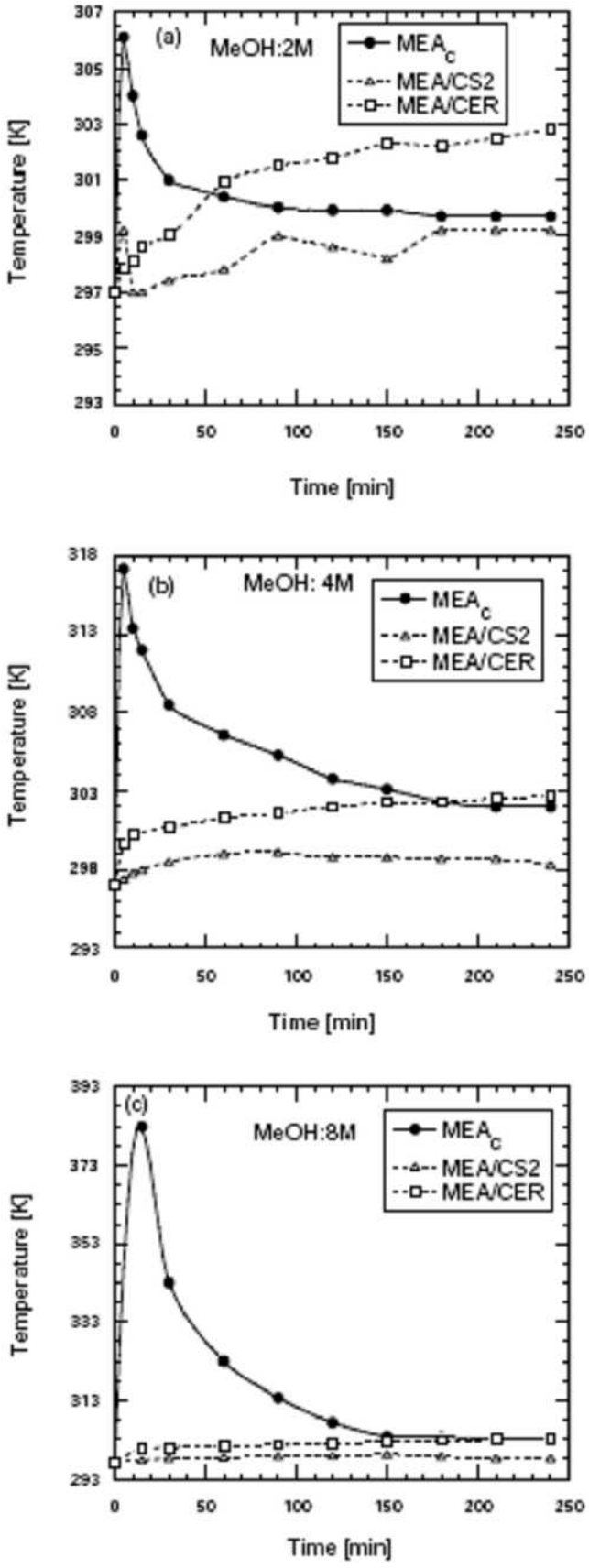

Figure 2-5 Effect of using different porous plates on cathode temperature at different methanol concentrations of (a) 2M, (b) 4M, and (c) 8M.

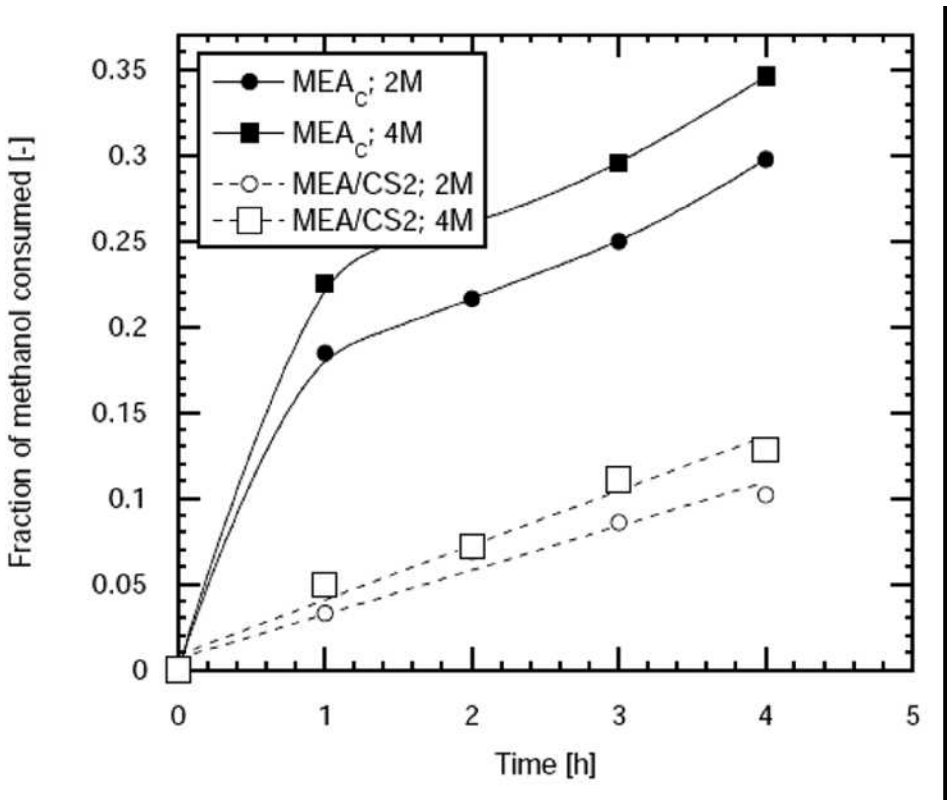

Figure 2-6 Effect of using porous plate on methanol consumption at different methanol concentrations of 2M and 4M.

Figure 2-6 shows the fraction of the methanol consumed in the reservoir for every 1h interval for the MEA_C and MEA/CS2 at 2M and 4M. It was clearly shown that the consumption of methanol for the MEA_C was several times higher than that for MEA/CS2 in the first one hour where the uncontrollable methanol crossover occurred as shown in Figs. 2-2, 2-3 and 2-5. In case of the MEA_C, a large fraction of methanol was lost during the initial time due to the initial high methanol concentration and decreased with increasing time because of a decrease in the methanol concentration during the time. However, in the case of using the porous plate, the methanol crossover was controlled by the resistance for mass transfer by the porous plate, and it resulted in a small and linear increase in the consumed fraction with increasing time. As shown above, it was clear that the MEA with the porous plate provided an important function of controlling the methanol crossover rate.

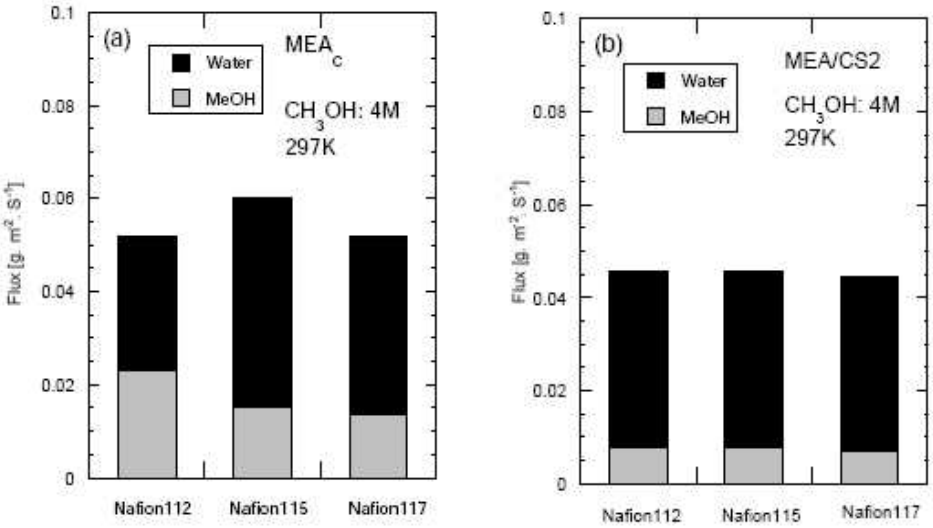

Figure 2-7 Effect of membrane thickness on the methanol and water fluxes for the conventional MEA and MEA with a porous plate.

4.3 Effect of different properties of porous plate on methanol crossover

Figure 2-7 shows the effect of the membrane thickness on the methanol flux and the water flux measured for the MEA with (b) and without (a) a porous plate. When a porous plate was not used as the support, Fig. 2-7 (a), the methanol flux decreased in the order of Nafion 112, 115 and 117, i.e., in the order with the increasing thickness of the membrane, suggesting that the mass transport through the membrane controlled the methanol flux. On the other hand, the methanol flux and also the water flux for the MEA with the porous plate were not affected by the membrane, suggesting that these fluxes were not controlled by the membrane, but by the porous plate when the porous plate was used.

Figure 2-8 shows the methanol flux and water flux measured for the different MEAs with and without a porous plate at 2M, 4M and 8M. It was clearly shown that the methanol flux was reduced at the MEAs with a porous plate compared to that at the MEA_C. It was also found that the methanol flux almost proportionally increased with the increasing methanol concentration as suggested by eq. (2-6), except for the MEA_C case at 8M. The exceptional case, MEA_C at 8M, must be affected by the significant increase in temperature at the initial time as described above. Not only the methanol flux, but also the water flux was dependent on the properties of the porous plate. Therefore, we investigated the property that affected the methanol flux for the porous plates used.

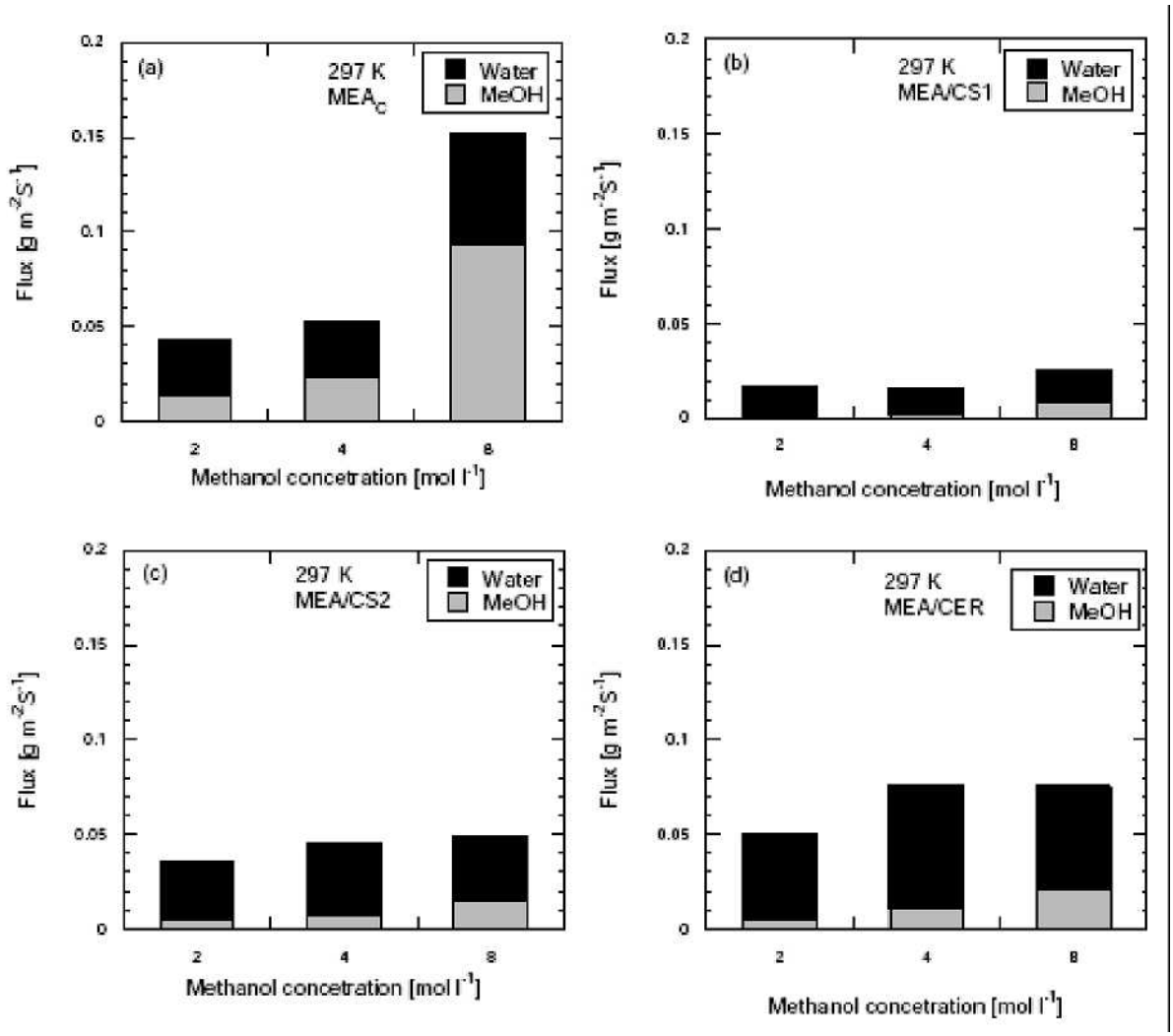

Figure 2-8 Methanol and water fluxes for MEAs with and without porous materials; (a) MEA$_C$, (b) MEA/CS1, (c) MEA/CS2, and (d) MEA/CER.

Figure 2-9 shows the relationship between the methanol flux and the product of the porosity, ε, and the water absorptivity, α_w, for all of the MEAs with the porous plate shown in Table 2-1. A strong correlation could be observed between the methanol flux and the product, $\varepsilon\alpha_w$, as shown in the figure, but not between the methanol flux and the porosity, suggesting that the methanol transport was controlled by the diffusion through the flood pore with the solution as assumed in eq. (2-8). The curves drawn in the figure were the results of a curve fitting for the data with the function; $a + b\,(\varepsilon\alpha_w)^{2/3}$, where a and b were constants, based on eq. (2-8). The methanol flux increased with the increasing $\varepsilon\alpha_w$ and the methanol concentration. On the other hand, the methanol flux obtained for MEA$_C$ was 0.0125gm^{-2}s^{-1}, 0.0230gm^{-2}s^{-1} and 0.0927gm^{-2}s^{-1} at 2M, 4M and 8M, respectively. The reduction in the methanol flux for the MEA with the porous plate having $\varepsilon\alpha_w$=0 and

$\varepsilon\alpha_w$=0.2 was calculated as around 1/10 and 1/5, respectively, to that for the conventional MEA at the methanol concentrations used in this study.

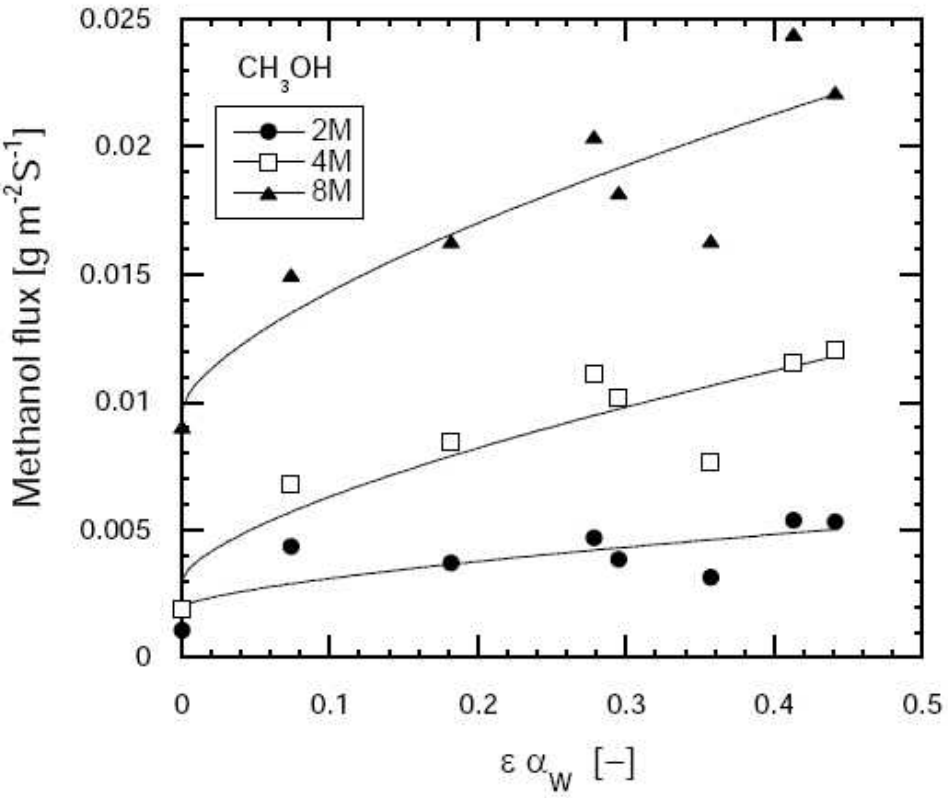

Figure 2-9 Effect of $\varepsilon\alpha_w$ on the methanol flux.

Figure 2-10 shows the relationship between $\varepsilon\alpha_w$ and the water flux at different methanol concentrations. The water flux increased with the increasing $\varepsilon\alpha_w$ up to a definite value then it slightly decreased. It would be controlled by the evaporation rate of the solution at the cathode as assumed in the theoretical section. For the conventional MEA without a porous plate, the $MEA_{C,}$ the obtained water flux was 0.0303$gm^{-2}s^{-1}$, 0.0278$gm^{-2}s^{-1}$ and 0.0593 $gm^{-2}s^{-1}$ at 2M, 4M and 8M, respectively. The high water flux at 8M would be caused by the high temperature shown in Fig. 2-4 (a). Where as, similar and relatively low water fluxes for MEA_C at 2M and 4M, compared to 0.045 $gm^{-2}s^{-1}$ for the MEA with the porous plate, would result from the total flux controlled by the evaporation of the solution transported to the cathode as assumed in the theoretical section.

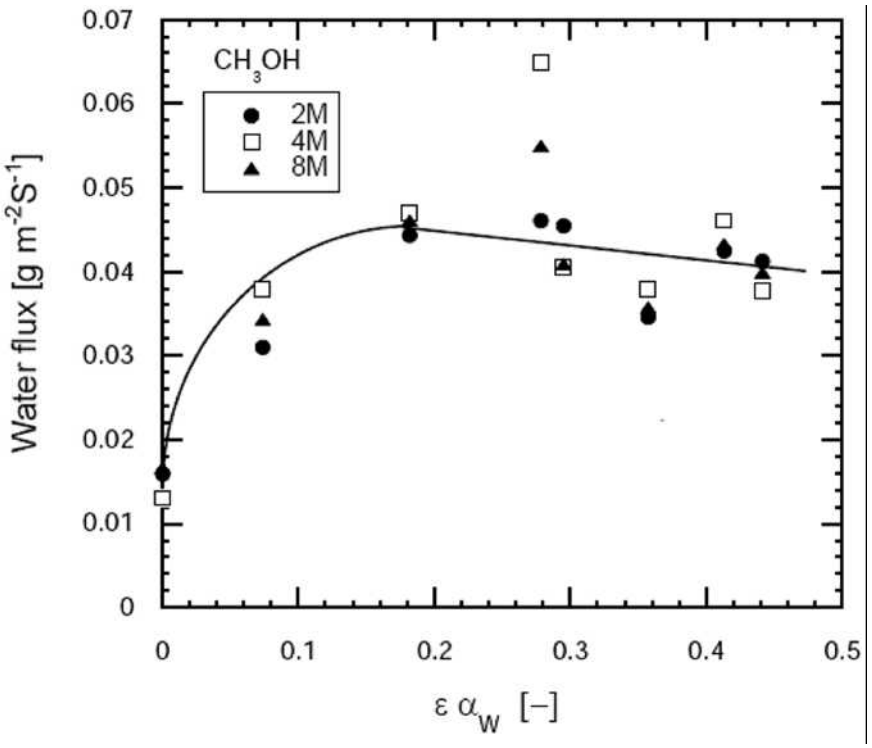

Figure 2-10 Effect of $\varepsilon\alpha_w$ on the water flux.

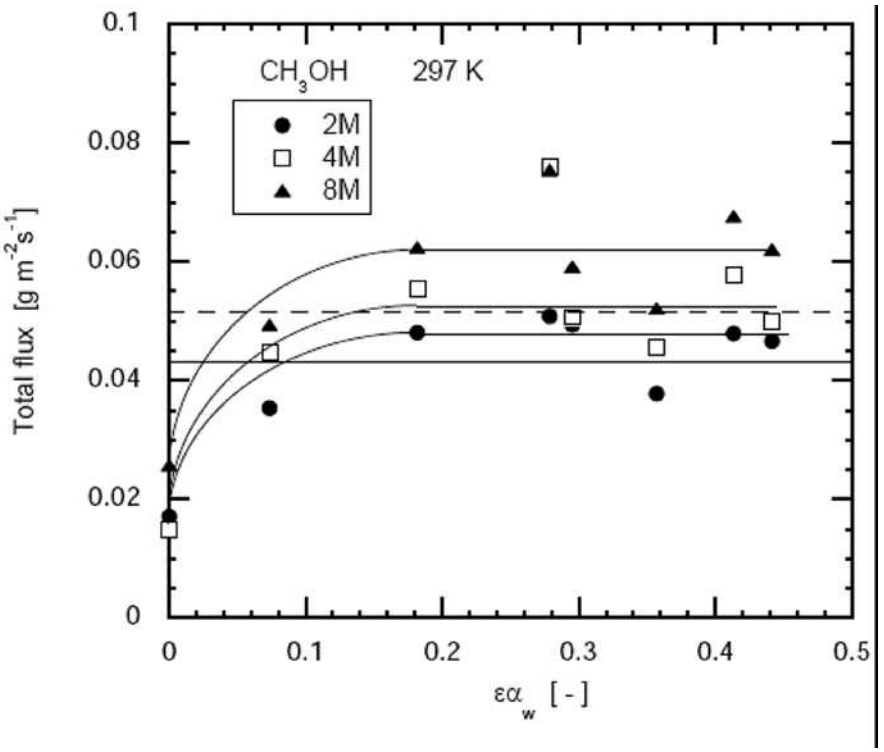

Figure 2-11 Effect of $\varepsilon\alpha_w$ on the total flux.

The total flux that was the sum of the methanol flux and the water flux for the different MEAs with the porous plate are plotted in Figure 2-11, showing the total fluxes at 2M and 4M for the MEA_C as the dotted lines. When $\varepsilon\alpha_w$ was over 0.2, the total flux became constant for the MEAs with the porous plate and it was also similar to that for the MEA without the porous plate. This supported the assumption that the total flux was controlled by the rate of evaporation of the permeated solution at the cathode as described in the theoretical section. It is known that the evaporation rate of water from a surface of a porous material become constant over a certain water content, because the lateral diffusion within a boundary layer allows the vapor pressure to equilibrate [36]. Due to this phenomenon, the water flux would be constant at an $\varepsilon\alpha_w$ over 0.2. During fuel cell operation, the water content in the membrane is very important, because the ionic conductivity of the membrane is directly related to the water content and temperature. On the other hand, excessive water at the cathode may cause flooding, i.e., liquid water accumulated at the cathode prevents oxygen access to the reaction sites. The water content in the membrane should be properly controlled during fuel cell operation.

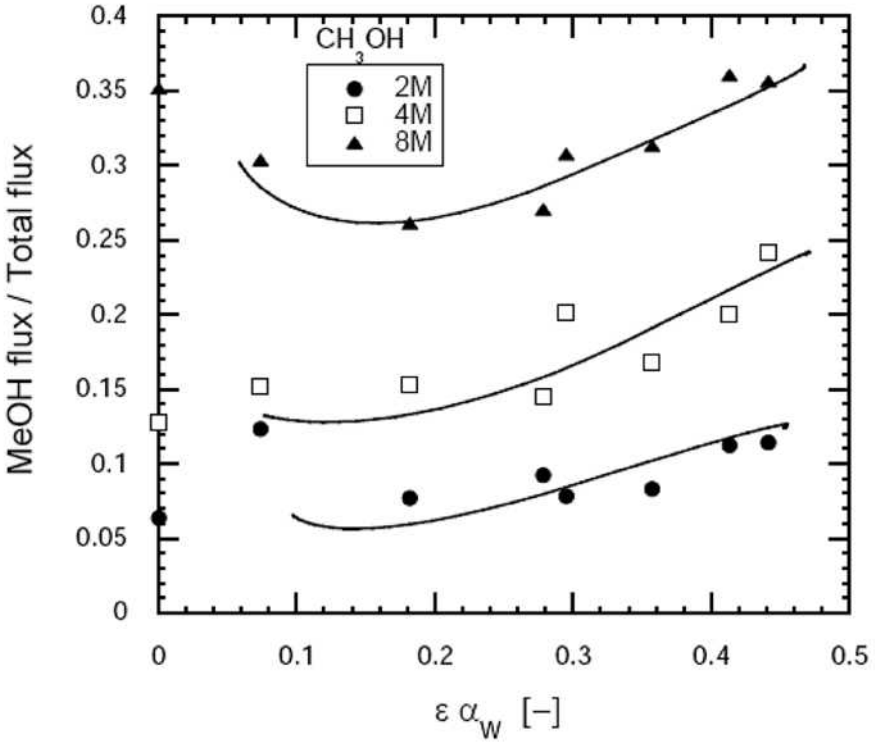

Figure 2-12 Effect of $\varepsilon\alpha_w$ on the separation.

Figure 2-12 shows the relationship between the value of $\varepsilon\alpha_w$ and the degree of methanol separation defined by the methanol flux divided by the total flux. When the degree of separation was low, it means that the porous plate strongly controlled the methanol flux compared to the water flux. This figure showed that there was an optimum value for $\varepsilon\alpha_W$ at around $\varepsilon\alpha_W = 0.2$ where the degree of separation shows a minimum at a high methanol concentration. The degree of separation calculated for the conventional MEA was 0.292, 0.453 and 0.670 at 2M, 4M and 8M, respectively. It clearly showed that the degree of separation for the MEA with the porous plate was much smaller, 1/2 to 1/6, than that for the conventional MEA.

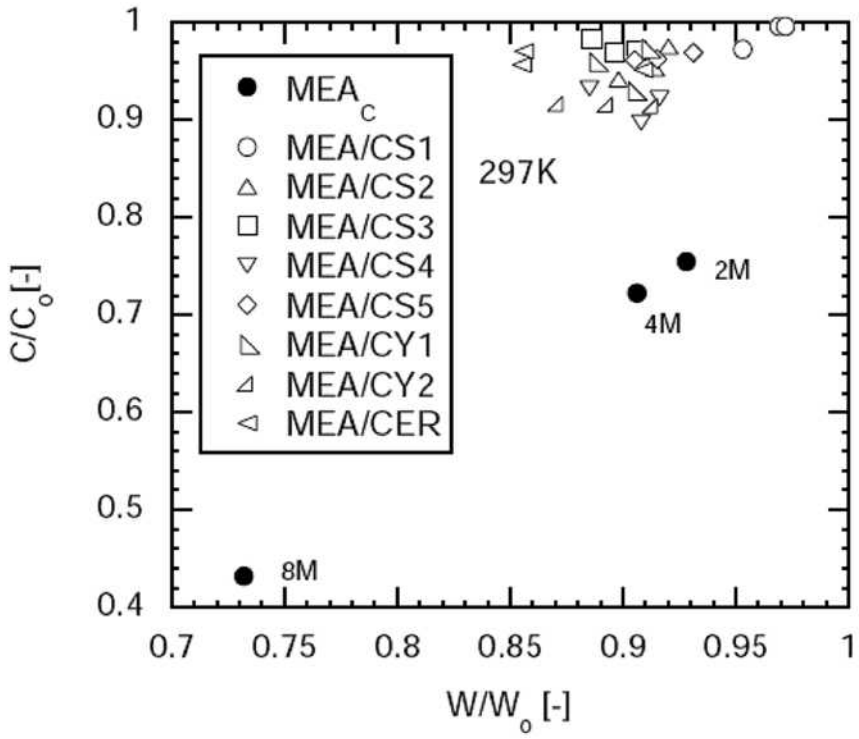

Figure 2-13 Relationship between the decrease in the weight and that in the methanol concentration for the solution remaining in the reservoir during the 4h crossover experiment.

Figure 2-13 shows the relationship between the change in the methanol concentration, C/C_0, and the loss of the solution, W/W_0, at different MEAs, where C and W are the methanol concentration and the weight of the solution, respectively, remaining in the reservoir after the 4h crossover experiment, and C_0 and W_0 are the initial values. The plots for MEA_C are located at the lower positions in C/C_0 and also W/W_0 compared to the plots for the MEAs with the porous plate, whereas, the plots for the MEAs with the porous

plate, including that at 2M, 4M and 8M, located in the domain with C/C_0>0.9 and W/W_0 >0.85 in the figure.

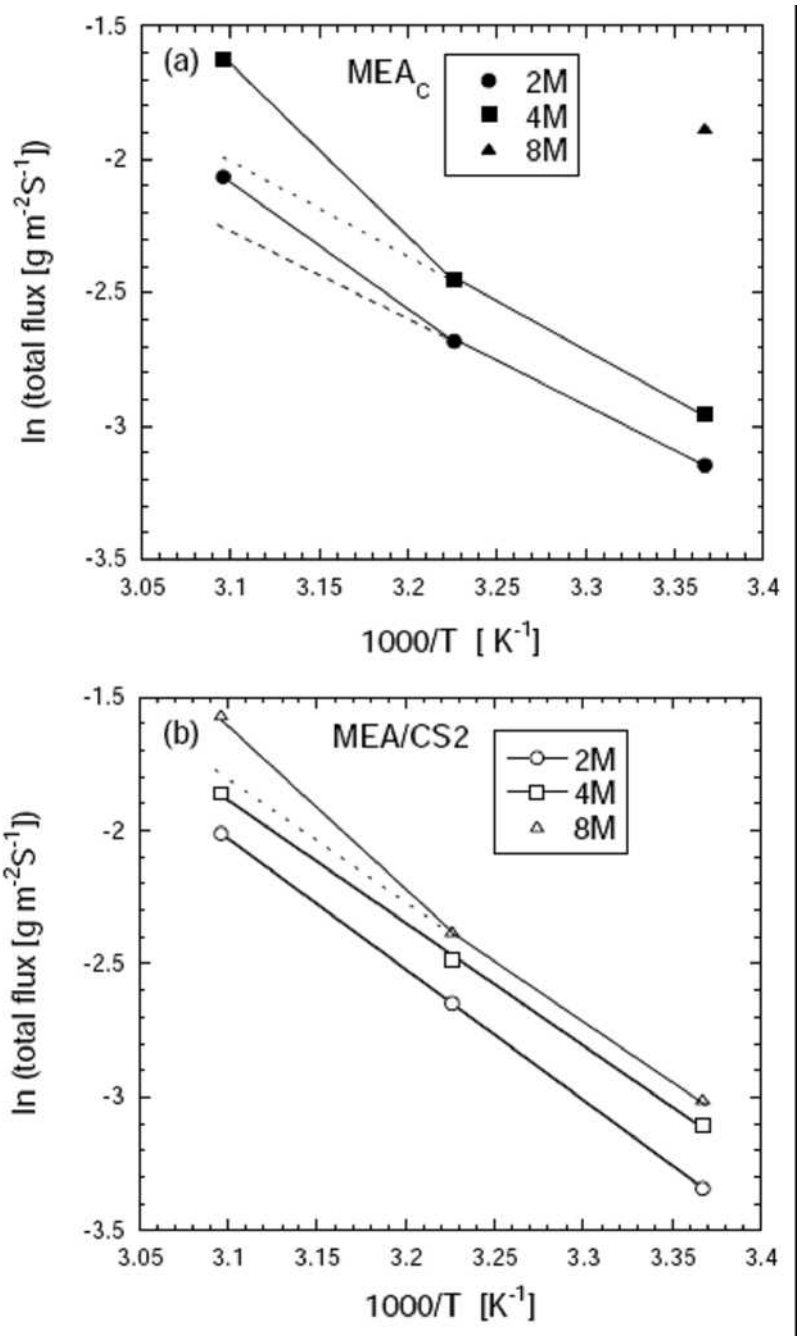

Figure 2-14 Arrehenuis plot for total flux in case of (a) MEA$_C$, and (b) MEA/CS2

This means that the methanol is preferentially transported through the conventional MEA, and it was controlled by the porous plate. As shown in eq. (2-5), the methanol flux J_M was accelerated by the increase of the diffusion flux through the membrane J_{DM} due to the large difference in the methanol concentration between the anode and cathode for the conventional MEA. The value of J_{DM} was reduced for the MEA with the porous plate by

reducing methanol concentration at the anode surface resulting in a reduced driving force for J_{MD} by the diffusion resistance of the porous plate. Hence, C/C_0 was never greater than 1 in all cases.

4.4. Effect of surrounding temperature on MCO

Figure 2-14 shows the effect of the surrounding temperature ranging between 297K and 323K on the total flux for the MEA_C and MEA/CS2. The total flux increased with the increasing temperature showing the minus slope on the Arrhenius plot for both cases of the MEA_C and MEA/CS2. The plots showed a straight line within the temperature range measured at 2M and 4M for MEA/CS2, as shown in Fig. 2-14 (b). The activation energy calculated for both cases was 39kJ/mol which almost agreed with the latent heat of vaporization of water, 44kJ/mol. This suggested that the total flux was controlled by the evaporation rate of water at the cathode as mentioned in the theoretical consideration with eqs. (2-2) and (2-4), noting that the vapor pressure of the cathode gas, p_a, in the equation was negligibly small in this measurement. At 323K and 8M for MEA/CS2, the total flux was plotted above the straight line that was for the plots at low temperatures. This would be because the actual temperature of the cell was higher than that of the surrounding one due to the effect of the high methanol crossover at this condition. A similar tendency was observed for the conventional MEA, MEA_C, at 2M and 4M as shown in Fig. 2-14 (a). In the case of MEA_C, the effect of the methanol crossover on the actual temperature of the cell was significant even at the low concentration of 2M. Hence, the relationship between the total flux and the surrounding temperature did not reflect the actual relationship between the flux and the cell temperature. The experiments for the higher temperatures, 310K and 323K, at 8M were not conducted because it was uncontrollable.

Figure 2-15 shows the effect of temperature on the methanol flux for both the MEA_C and MEA/CS2. The activation energies at different methanol concentrations for MEA/CS2 were 42.7kJ/mol, 44.7kJ/mol and 38.2kJ/mol at 2M, 4M and 8M, respectively. These values were much higher than that calculated for the diffusion. This confirmed that the methanol transport through the MEA was by diffusion and convection flow from the anode to the cathode as given in eq. (2-5), and the convective flow was accelerated by the increase in the surrounding temperature as mentioned above. Based on this consideration, the blocking of the methanol transport by the porous plate based on the diffusion resistance mechanism would be reduced under the condition of high temperature and high

methanol concentration, because the methanol flux by the diffusion would be relatively low to that due to the convective flow driven by the evaporation of water at the cathode.

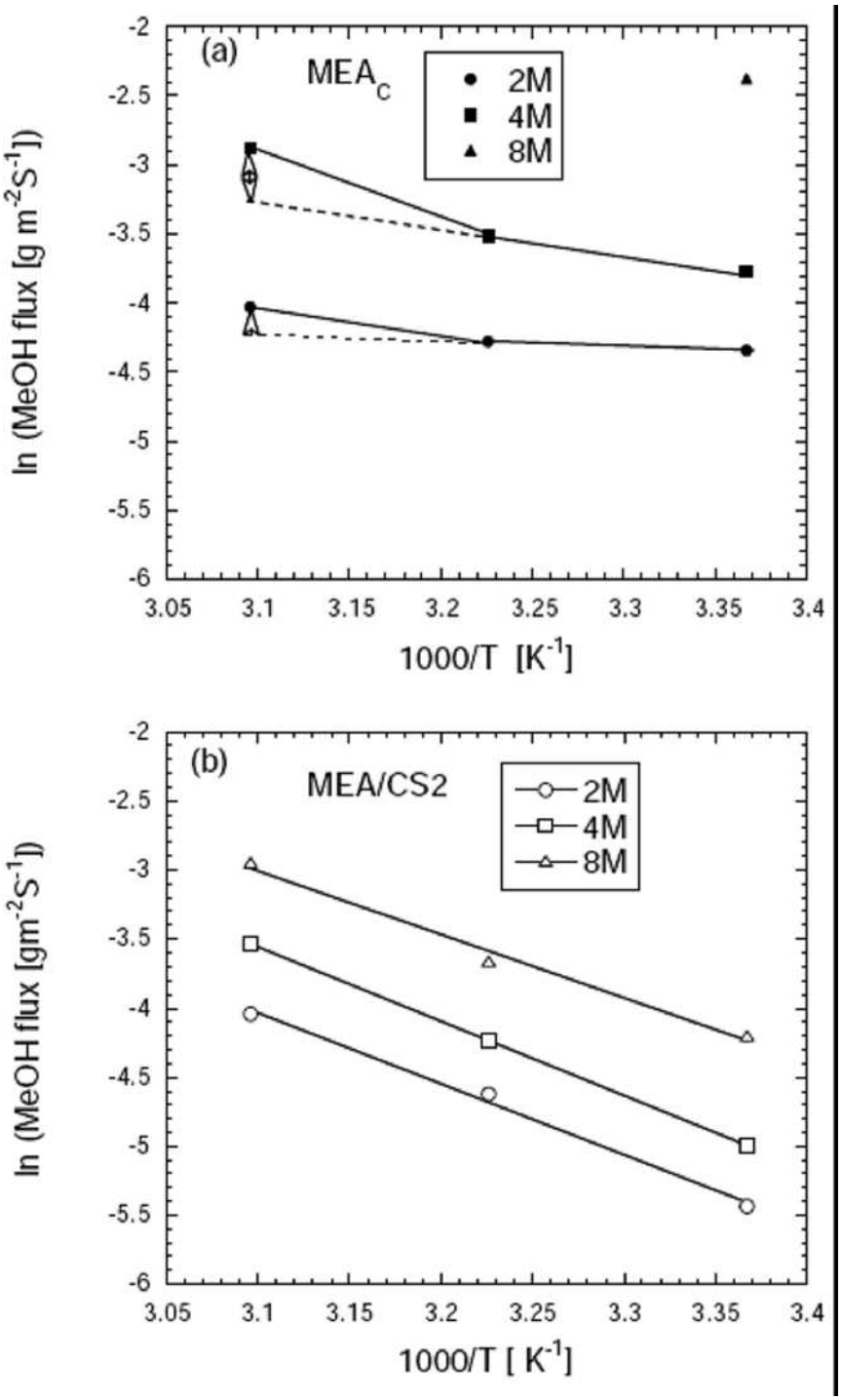

Figure 2-15 Arrehenuis plot for methanol flux in case of (a) MEA_C, and (b) MEA/CS2

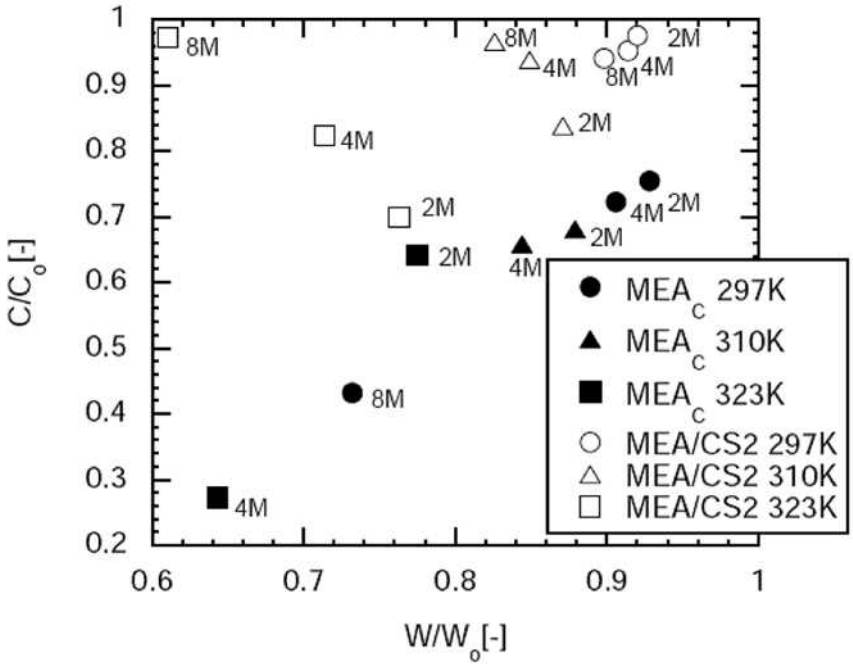

Figure 2-16 Relationship between the decrease in the weight and that in the methanol concentration for the solution remaining in the reservoir during the 4h crossover experiment.Comparison between MEA_C and MEA/CS2 at different temperatures and methanol concentrations.

Figure 2-16 shows the relationship between the separation and the loss for the cases measured at different surrounding temperatures for the MEA_C and MEA/CS2. The separation of methanol by the porous plate was still effective at these temperatures, although the loss of the total solution relatively increased as the temperature increased for the cases with MEA/CS2.

5. Conclusions

Methanol crossover in a passive DMFC using a porous plate as a support had been studied under open circuit conditions using different porous plates with different structures and different water absorptivities at different methanol concentrations and temperatures. The following conclusions were drawn.

The porous plates controlled and reduced the methanol crossover. As the material of the porous plate, both the porous carbon plate and the porous Al_2O_3 plate were useful. The mechanism of reducing the methanol crossover could be explained by the controlling the diffusion of methanol through the porous plate which reduced the methanol flux. As the properties of the porous plate that affect the methanol flux, the porosity, water absorptivity

and others involved in eq. (2-8), were predicted, which were confirmed by experiment. The methanol flux and water flux could be expressed as a function of the products of the porosity and the water absorptivity, $\varepsilon\alpha_W$. The methanol flux increased with the increasing $\varepsilon\alpha_W$ and the methanol concentration. The water flux increased with the increasing $\varepsilon\alpha_W$ to a certain value of $\varepsilon\alpha_W$ and then slightly decreased, and was not affected by the methanol concentration. As a result of reducing the methanol crossover, the temperature of the cell was constantly controlled without causing an uncontrollable temperature increase that was observed for the conventional MEA. Also, a considerable amount of methanol loss due to the uncontrollable temperature increase was neglected for the MEAs with the porous plate. The total flux for the MEAs with the porous plate measured at different surrounding temperatures showed an activation energy similar to that of the latent heat of vaporization of water, suggesting that the evaporation rate controlled the total flux.

6. References

1. H. Chang, J.R. Kim, J.H. Cho, H.K. Kim, K.H. Choi, *Solid State Ionics*, **148** (2002) 601-606.
2. A. Blum, T. Duvdevani, M. Philosoph, N. Rudoy, E. Peled, *Journal of Power Sources*, **117** (2003) 22-25.
3. D. Kim, E.A. Cho, S.A. Hong, I.H. Oh, H.Y. Ha, *Journal of Power Sources*, **30** (2004) 172-177.
4. A.S. Arico, S. Srinivasan, V. Antonucci, *Fuel Cells*, **1** (2001) 133-161.
5. T.Schultz, Su Zhou, K. Sundmacher, *Chem. Eng. Technol*. **24** (2001) 1223-1233.
6. S. Surampudi, S.R. Narayanan, E. Vamos, H. Frank, G. Halpert, A.LaConti, J. Kosek, G.K. Surya Prakash, G.A. Olah, *Journal of Power Sources*, **47** (1994) 377-385.
7. M.K. Ravikumar, A.K. Shukla, *J. Electrochem. Soc*., **143** (1996) 2601-2606.
8. J.T. Wang, S. Wasmus, R.F. Savinell, *J. Electrochem. Soc*., **143** (1996) 1233-1239.
9. E. Peled, T. Duvdevani, A. Aharon, A. Melman, *Electrochemical and Solid-State Letters*, **3** (2000) 525-528.
10. M.V Fedkin, X. Zhou, M. A. Hofmann, E. Chalkova, J. A. Weston, H.R. Allcock, S.N. Lvov, *Materials Letters*, **52** (2002) 192-196.
11. T. Yamaguchi, M. Ibe, B.N. Nair, S. Nakao, *J. Electrochem. Soc.*, **149** (2002) A1448-A1453.
12. M.L. Ponce, L. Prado, B. Ruffmann, K. Richau, R. Mohr, S.P. Nunes, *J. of Membrane Science*, **217** (2003) 5-15.
13. A. S. Arico, P. Creti, P. L. Antonucci, V. Antonucci, *Electrochemical and Solid-State Letters*, **1** (1998) 66-68.
14. C. Yang, S. Srinivasan, A. S. Arico, P. Creti, V. Baglio, V. Antonucci, *Electrochemical and Solid-State Letters*, **4** (2001) A31-A34.
15. N. Jia, M.C. Lefevre, J. Halfyard, S. Qi, P .G. Pickup, *Electrochemical and Solid-*

State Letters, **3** (2000) 529-531.

16. I.J. Hobson, H. Ozu, M. Yamaguchi, M. Muramatsu, S. Hayase, *Journal of Materials Chemistry*, **12** (2002) 1650-1656.
17. W.C. Choi, J.D. Kim, S.I. Woo, *Journal of Power Sources*, **96** (2001) 411-414.
18. S. R. Yoon, G. H. Hwang, W. I. Cho, I. - H. Oh, S. - A. Hong, H. Y. Ha, *Journal of Power Sources*, **106** (2002) 215-223.
19. Y.K. Xiu, K. Kamata, T. Ono, K. Kobayashi, T. Nakazato, N. Nakagawa, *Electrochemistry*, **73** (2005) 67-70.
20. N. Nakagawa, K. Kamata, A. Nakazawa, M. Ali Abdelkareem, K. Sekimoto, *Electrochemistry* **74** (2006) 221-225.
21. G. Q.Lu, C. Y. Wang, T. J.Yen, X. Zhang, *Electrochimica Acta*, **49** (2004) 821.
22. Z. Guo, Y. Cao, *J. Power Sources*, **132** (2004) 86-91.
23. J. Liu, G. Sun, F. Zhao, G. Wang, G. Zhao, L. Chen, B. Yi, Q. Xin, *J. Power Sources*, **133** (2004) 175-180.
24. T. Shimizu, T. Momma, M. Mohamedi, T. Osaka, S. Sarangapani, *J. Power Sources*, **137** (2004) 277-283.
25. H. Qiao, M. Kunimatsu, T. Okada, *J. Power Sources*, **139** (2005) 30.
26. Q. Ye, T.S. Zhao, *J. Power Sources*, **147** (2005) 196-202.
27. R. Chen, T.S. Zhao, *J. Power Sources*, **152** (2005) 122-130.
28. J. Liu, T. Zhao, R. Chen, C. W. Wong, *Fuel Cells Bulletin*, February, 12-17 (2005).
29. B. Kho, I. Oh, S. Hong, H.Y. Ha, *Fuel Cells Bulletin*, September, 11-14 (2004).
30. J.G. Liu, T.S. Zhao, R. Chen, C.W. Wong, *Electrochemistry Communications*, **7** (2005) 288.
31. B. Kho, I. Oh, S. Hong, H. Y. Ha, *Electrochimica Acta*, **50** (2004) 781.
32. C. Y. Chen, P. Yang, *J. Power Sources*, **123** (2003) 37-41.

33. B. Bae, B.K. Kho, T. Lim, I. Oh, S. Hong, H.Y. Ha, *J. Power Sources* **158** (2006) 1256–1261.

34. J.G. Liu, T.S. Zhao, Z.X. Liang, R. Chen, *J. Power Sources* **153** (2006) 61–67.

35. R. Chen, T. S. Zaho, J. G. Liu, *J. Power Sources*, **157** (2006) 351–357.

36. M. Suzuki, S. Maeda, *J. Chem. Eng. Japan*, **1** (1968) 26-31.

CHAPTER 3

DMFC Employing a Porous Plate for an Efficient Operation at High Methanol Concentrations

1. Introduction

Compared with hydrogen, methanol, as a liquid non-fossil fuel for fuel cells, offers many advantages such as high energy density more than 6000 Wh/kg at 25^{o}C, easily transported and stored as well as low cost. From this point of view, DMFCs are suitable for mobile electric devices and automobiles. Large efforts done now for the development of direct methanol fuel cells (DMFCs) [1–8]. Although of these large efforts, the energy density of the DMFCs currently under development is still far from that expected due to the methanol crossover and the high over voltage at the electrodes [9-12]. Methanol crossover means the transport of methanol from the anode to the cathode where it was oxidized on the cathode catalyst surface as well as the reduction of oxygen. Due to the methanol crossover, the DMFC usually shows the highest performance at low concentrations of methanol from 2 to 3M [13, 14] under the active conditions and about 5M [15–17] under the passive conditions. To overcome the methanol crossover, a large number of studies [18–22] were carried out for developing a new proton-conducting membrane with a low methanol permeability and high proton conductivity. Modification of the existing membranes like Nafion has also been conducted by making it a composite membrane [23–25] with inorganic or organic materials, surface modification by physical treatment [26] or by coating the surface with a thin film [27–29]. Only a few papers considered the reducing ability in methanol crossover by mass transport control in the backing layer [30-32].

Another problem, especially encountered for the passive DMFCs with air breathing and decreased the DMFC power output, is the flooding at the cathode [33, 34]. The accumulation of water at the cathode has a strong impact on the performance where the water blocks the openings of the cathode. The water at the cathode includes water produced by oxygen reduction reaction, ORR, and that transported with proton from the anode as well as that generated by the oxidation of methanol permeated through the membrane. Then, the water has to be smoothly removed from the cathode, or it should be controlled [35, 36].

We have demonstrated in chapter (2) that under open circuit conditions a passive DMFC with a porous plate as a support significantly reduced the methanol crossover and constantly regulated the cell temperature. The mechanism of reducing MCO was successfully explained by the diffusion control of the methanol through the porous plate. The transport and separation of methanol and water through MEA with a porous plate under open circuit conditions were dependent on the properties of the porous material, i.e., thickness, porosity and water absorptivity of the porous material. It is expected that the DMFC employing the porous plate can be efficiently operated with high methanol concentrations and effective to achieve a high energy density of DMFC systems.

In this chapter, we investigated how the employment of a porous plate to a DMFC affects the performance under closed circuit conditions. A porous carbon plate was placed at the anode side and used to control the mass transfer from the methanol reservoir to anode. i-V and i-t performances at different methanol concentrations ranging from 1M to 24.7M (neat methanol), were measured for the DMFC with and without porous plate and compared the performance with each other. Also, in the i-t experiment, methanol flux and water flux through the MEA and Faraday efficiency were evaluated at different methanol concentrations. In the same time, the effect of the distance between anode surface and porous plate on the performance was investigated. And the mechanism of the cell performance with the porous plate was discussed based on the consideration of the mass transfer for the anode.

2. Experimental

2.1. MEA preparation

The conventional MEA, which uses carbon cloth (35% Teflonized, ElectroChem, Inc.) as the anode and cathode backing layers, was prepared in the following manner. Pt black (HiSPEC 1000, Johnson Matthey Fuel Cells, Co. Ltd.) and Pt-Ru black (HiSPEC 6000, Johnson Matthey Fuel Cells, Co. Ltd.) were used as catalyst for the cathode and anode, respectively. The catalyst ink was prepared by dispersing an appropriate amount of the catalyst in a solution of de-ionized water, isopropyl alcohol, and 5wt% Nafion solution (Wako, Inc.). Then, the ink was coated on the carbon cloth to make electrodes. The catalyst loading was 10mg/cm^2 in each electrode, and the ionomer loading to the catalyst was 10 wt% for the cathode and 15 wt% to the anode. Nafion 112 was used as the

electrolyte membrane. Then, the MEA was fabricated by sandwiching the membrane between the anode and the cathode and hot pressing them at 408K and 5 MPa for 3 min.

2.2 Porous plate

A porous carbon plate, denoted as PCP hereafter, with 2.0mm thickness made of a composite of amorphous and graphite carbons, supplied from Mitsubishi Pencil Co., Ltd., was used in this study. The microstructure of the PCP measured by using a mercury porosimeter, (Pascal 140 + 440, Thermo Finnigan, Inc.), revealed that it had 0.543 in total cumulative pore volume and 42.3μm in average pore diameter and 0.417 in total porosity. The PCP was hydrophobic and its water absorptivity defined in chapter (1) was nearly zero.

Table 3-1: Properties of the porous carbon plate

Anode backing	δ (mm)	αw	Pore structure measured by the mercury porosimeter		
			Vp (cm3 g−1)	dp,ave (μm)	ε
PCP	2.0	zero	0.5428	42.33	41.6702

δ: thickness; αw: water absorptivity defined; Vp: total cumulative volume; dp: pore diameter; ε: total porosity.

2.3 Passive DMFC with or without PCP

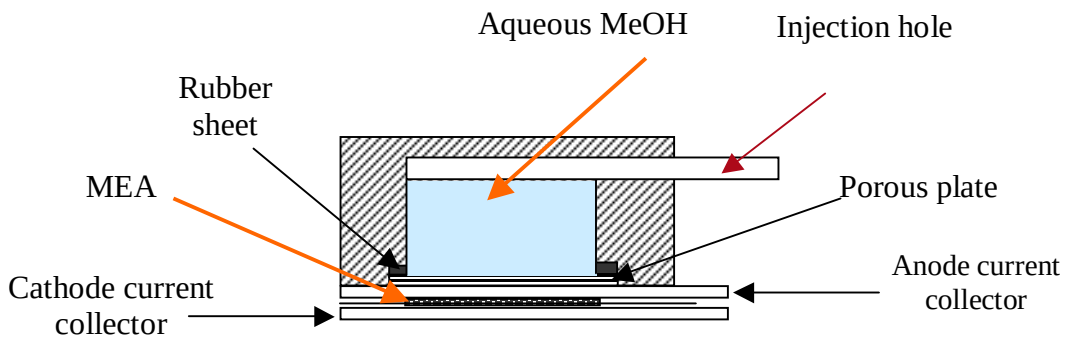

Figure 3-1: Schematic diagram of passive DMFC with or without porous plate

MEA with or without the porous plate was set in a plastic holder as shown in Figure 3-1. In the anode compartment, a methanol reservoir, 7 dm^3, was arranged. The MEA was

sandwiched between two current collectors, which were stainless steel plates of 2mm thickness with open holes for the passages of fuel and oxidant. The open ratio of the area for the active electrode was 73%. As a result of this configuration, methanol had to pass through the porous plate then through the openings of the anode current collector. Under closed circuit conditions, the openings of the anode current collector was filled with CO_2 gas which is enclosed between the porous plate and the anode. Therefore, a layer of CO_2 gas was formed between the porous plate and the anode, and the gas layer obstruct methanol transport from the reservoir to the anode. On the other hand, in the case of no PCP, CO_2 was easily escaped through the opening of the anode current collector into the methanol solution as bubbles without preparing the CO_2 gas layer, and the solution directly attached to the anode. On the other hand, oxygen, from the surrounding air, was diffused into the cathode catalyst layer through the openings of the cathode current collector.

2.4 Measurement of the cell performance

In this study, all the experiments were conducted in a complete passive mode at ambient conditions (293K and 1atm), methanol solution with different concentration was fed into the reservoir by a syringe through the injection hole, and left in the cell from few minutes to 1h according to methanol concentration. We avoided the MEA from direct contact with the solution for long time, when the methanol concentration was high. Current-voltage, i-V, characteristics were measured by linear sweep voltanmetry from the open circuit voltage, OCV, to zero with scan rate 1mV/sec. After that, time progress of the current density, i-t characteristics, at 0.1V was measured for 5h to 12h. These measurements were conducted by using a electrochemical measurement system (HAG-5010, Hokuto Denko, Co., Ltd.). The temperature of the cell was also measured using a thermocouple placed between the surface of anode current collector and the porous plate.

At the end of the i-t experiments for a certain methanol concentration, the weight loss of the entire cell holder was measured and the methanol concentration of the remained solution in the reservoir was also measured by a gas chromatography. From the results, methanol and water fluxes during the i-t experiment were evaluated as shown below. And then, the remained solution was removed from the reservoir, and a new solution with another concentration was injected in the cell. And hence, the same measurements were conducted for the new solution.

2.5 Evaluation of the methanol and water flux

The weight loss of the reservoir during the i-t experiment, ΔM_{LT}, which was obtained by subtracting the final weight of the remained solution in the reservoir after the experiment, W_a, from that of the initial weight, W_0, can be expressed as follows,

$$\Delta M_{LT} = W_0 - W_a = \Delta M_{PM} + \Delta M_{PW} + \Delta M_{RM} + \Delta M_{RW} + \Delta M_V \qquad \textbf{(3-1)}$$

where, ΔM_{PM} and ΔM_{PW} is the weight loss of methanol and that of water permeated from anode to cathode, respectively, ΔM_{RM} and ΔM_{RW} is weight loss of methanol and that of water consumed by the anode reaction, respectively, and finally, ΔM_V is weight loss due to the evaporation of the solution and CO_2 gas exhaust through the injection tube opened for environment.

Here, ΔM_V was experimentally confirmed that it was less 1% of ΔM_{LT} and negligible. Both of ΔM_{RM} and ΔM_{RW} were calculated by integrating the area of the i-t curve assuming the complete oxidation of methanol,

$$\mathbf{CH_3OH + H_2O \rightarrow 6H^+ + CO_2 + 6e} \qquad \textbf{(3-2)}$$

As follows,

$$\mathbf{\Delta M_{RM} = 32A \int_0^t i_{(t)}\, dt /(6\, F)} \qquad \textbf{(3-3)}$$

$$\mathbf{\Delta M_{RW} = 18A \int_0^t i_{(t)}\, dt /(6\, F)} \qquad \textbf{(3-4)}$$

Where, A is apparent electrode area, t is time in i-t experiment, F is the Faraday constant.

On the other hand, weight loss of methanol from the reservoir ΔM_{LM} and that of water ΔM_{LW} were calculated as follows,

$$\mathbf{\Delta M_{LM} = 32\,(C_0V_0 - C_aV_a)} \qquad \textbf{(3-5)}$$

$$\mathbf{\Delta M_{LW} = \Delta M_{LT} - \Delta M_{LM}} \qquad \textbf{(3-6)}$$

Where C_0 and V_0 is the concentration and volume of methanol solution in the reservoir at the start of the experiment, respectively, and C_a and V_a is those after the experiment, respectively.

Hence, methanol flux J_M and water flux $J_{W,}$ those permeated through MEA from anode to cathode, were calculated as

$$J_M = (\Delta M_{LM} - \Delta M_{RM})/(A\ t) \quad (3\text{-}7)$$

$$J_W = (\Delta M_{LW} - \Delta M_{RW})/(A\ t) \quad (3\text{-}8)$$

And the Faraday efficiency η_F could be calculated as

$$\eta_F = \Delta M_{RM} / \Delta M_{LM} \quad (3\text{-}9)$$

3. Results and discussion

3.1. Current – voltage characteristics of the passive DMFC operated at different methanol concentrations with or without the porous plate

Figures 3-2a and b show the performances of the cell voltage, V, and power density, P, as a function of the current density, i, respectively, of the passive DMFC without porous plate, i.e., a conventional MEA denoted hereafter as MEA_C, operated with various methanol concentrations from 1.0M to 5.0M. As shown in Fig. 3-2a, the cell voltage in the high current densities over 50 mA/cm^2 showed maximum at 2M and decreased as further increasing the methanol concentration mainly due to the methanol crossover. The maximum power density was about $24mW/cm^2$ as shown in Fig. 3-2b. The cell voltages and power densities at high current densities and high methanol concentrations fluctuated and were unstable as shown in the figures, suggesting the flooding occurred at the cathode and it affected the performance.

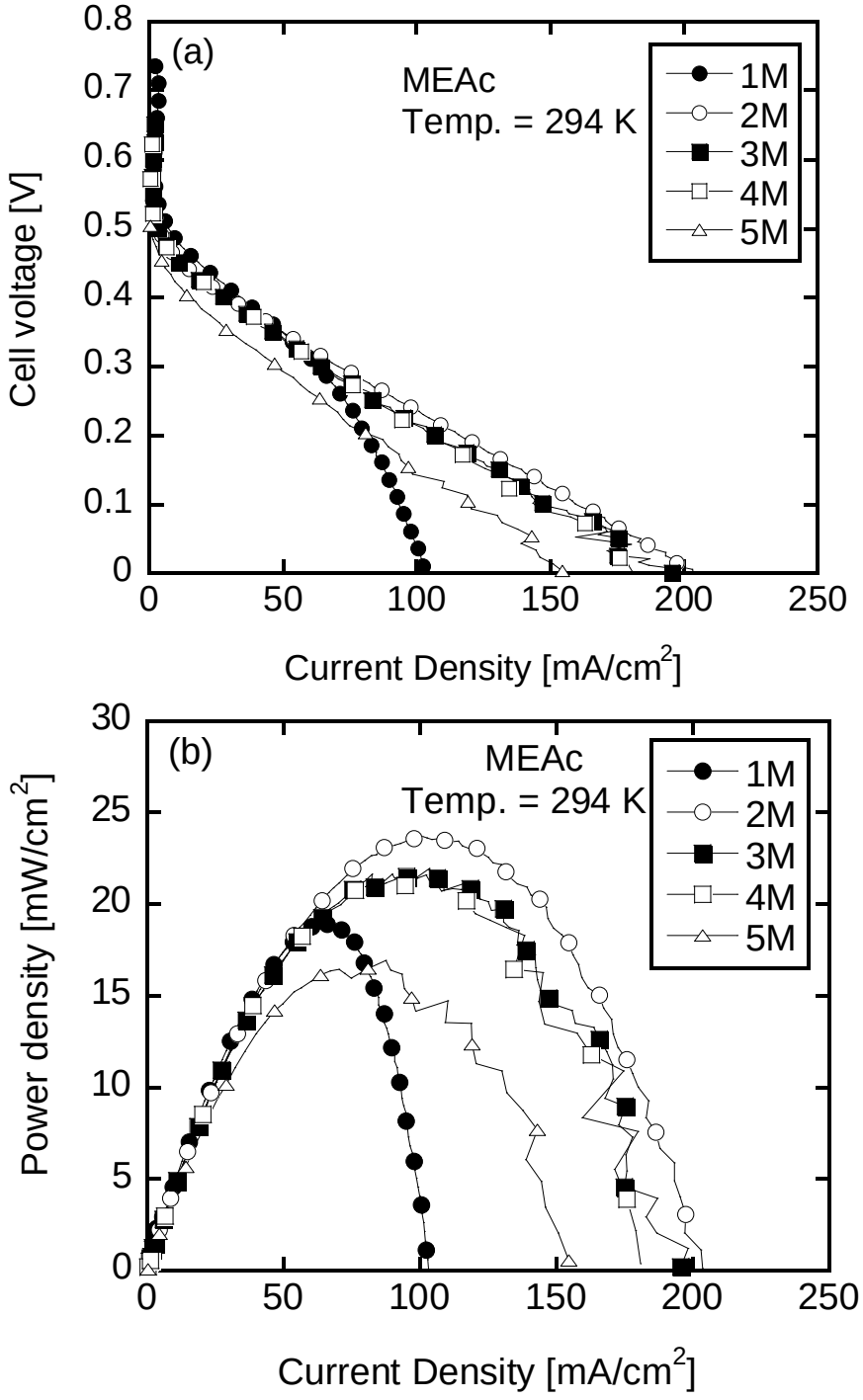

Figure 3-2: Effect of methanol concentration on the performance of the passive DMFC without porous plate, MEAc.

(a) Polarization curve (b) Power density curve

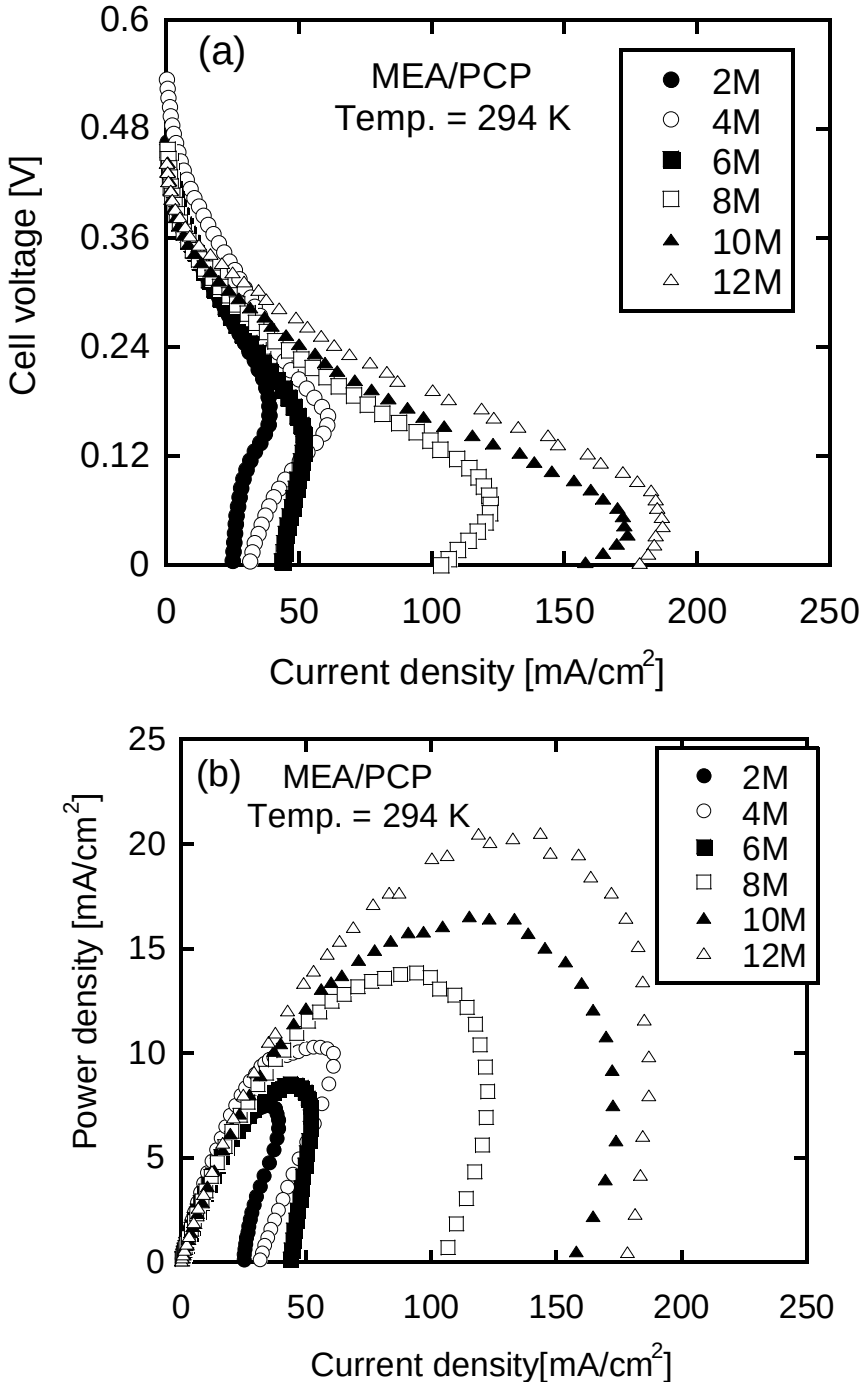

Figure 3-3: The performance of the passive DMFC with the porous plate, MEA/PCP, within low methanol concentration range from 2M to 12M

(a) Polarization curve **(b) Power density curve**

Figures 3-3a and b show the i-V and i-P performances, respectively, for the passive DMFC with PCP, dented hereafter as MEA/PCP, operated with the methanol concentrations from 2M to 12M. In the high current densities over 50mA/cm^2, the performances increased with the increase of the methanol concentration. In the low cell

voltages, the current did not increased with decreasing the cell voltage at each methanol concentration, clearly showing limiting current occurred due to the shortage of methanol supply at the anode side. The limiting current was caused by the restriction of methanol transfer rate from the reservoir to the anode by the porous plate [30, 31] even at high methanol concentration like 12M in this experiment.

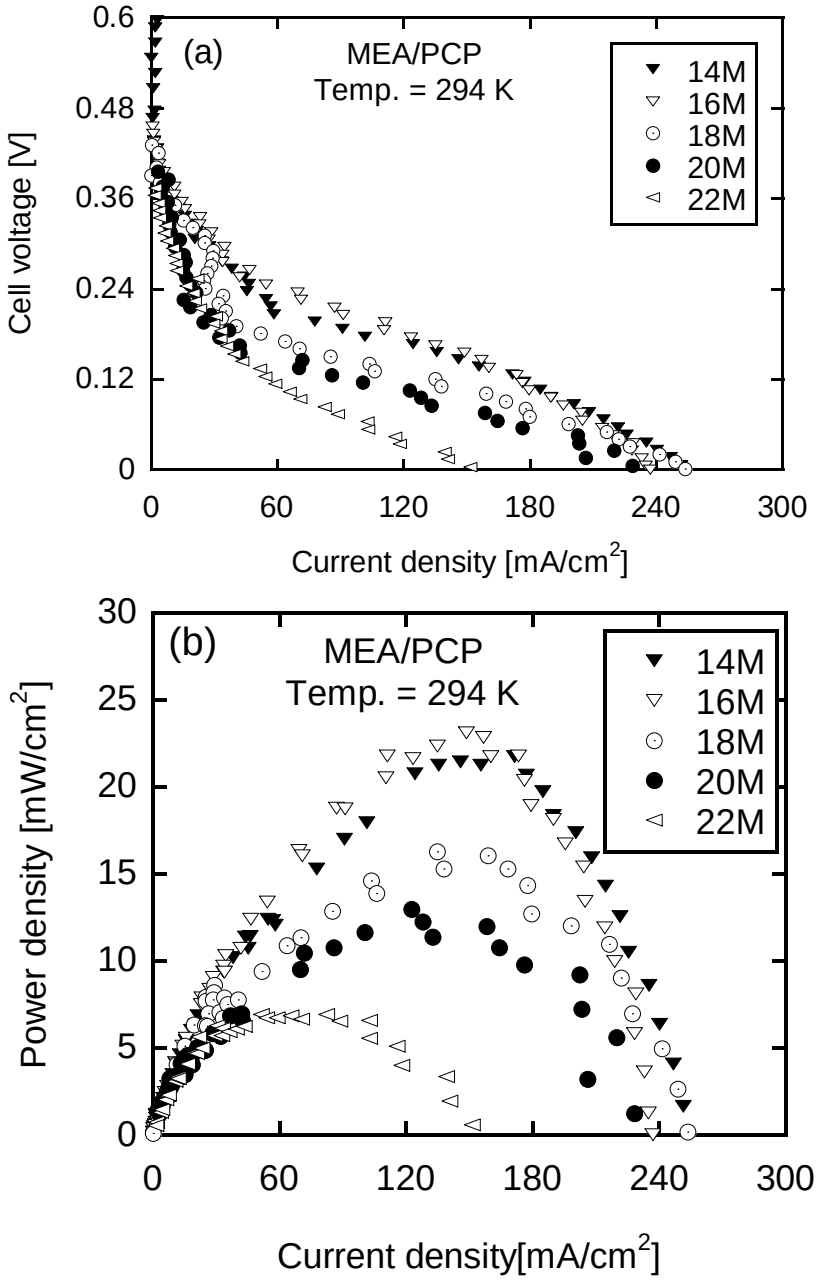

Figure 3-4: The performance of the passive DMFC with the porous plate , MEA/PCP, within high methanol concentration range from 14M to neat methanol

(a) Polarization curve **(b) Power density curve**

Figures 3-4a and b show the performances for the MEA/PCP operated at high methanol concentrations over 14M. As shown in the Fig. 3-4a, the limiting current was not observed in the i-V curves as a result of increasing the concentration. The decrease of the cell voltage at almost every current densities with increasing the methanol concentration over 16M would be due to the effect of the methanol crossover. Power density at 16M reached 24mW/cm^2 as shown in Fig. 3-4b. However, it should be noted that DMFC with PCP could be operated with the high methanol concentration like 16M by keeping its maximum power density with that of the DMFC without PCP at 2M.

3.2 Time progress of the current at a constant cell voltage

Figure 3-5 shows time progress of the current density, i-t curves, at 0.1V for the DMFC without PCP, MEA$_C$, with different methanol concentrations from 1.0M to 8.0M. From this figure, it was clear that the current density was initially high, then rapidly decreased to less than one third of its initial value within 1h. The current density further decreased with time, and, sooner or later, reached nearly zero at last for all of the methanol concentrations. The time at which the current density reached nearly zero depended on the methanol concentration. The lower the concentration, the shorter the time.

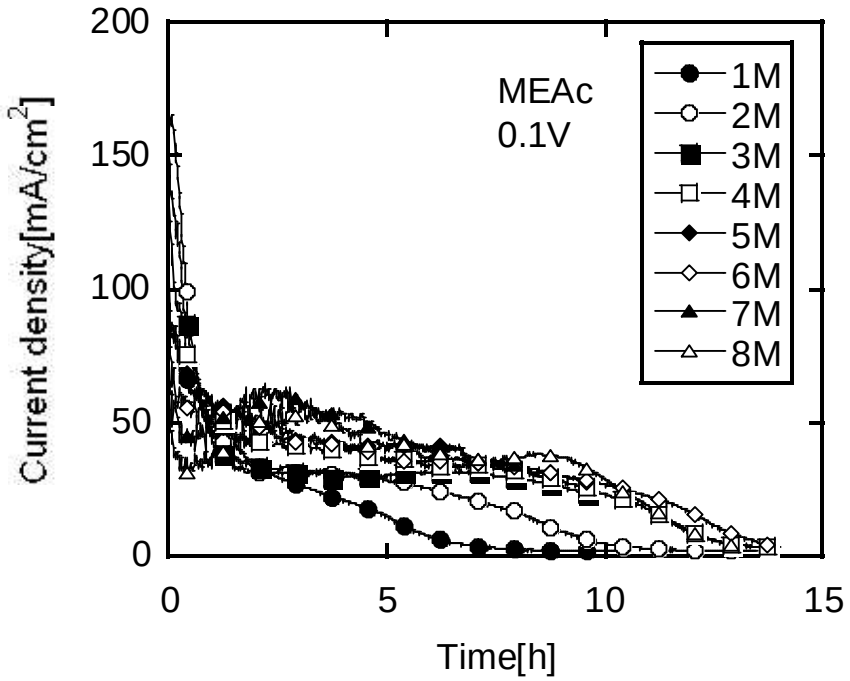

Figure 3-5: Current profile during continuous operation of passive DMFC without porous plate, MEAc, under cell voltage 0.1V.

The rapid reduction in current density at the initial would be related to the rapid depletion of the methanol at the anode due to a high rate of MCO at the high methanol concentration like 8M, or low initial methanol at low methanol concentrations. Fluctuation in current density was observed at high methanol concentrations over 3M and it became strong as increasing the concentration up to 8M. It would be due to the effect of the flooding, because we confirmed a formation of water film and droplets on the cathode surface by an eye observation in these conditions.

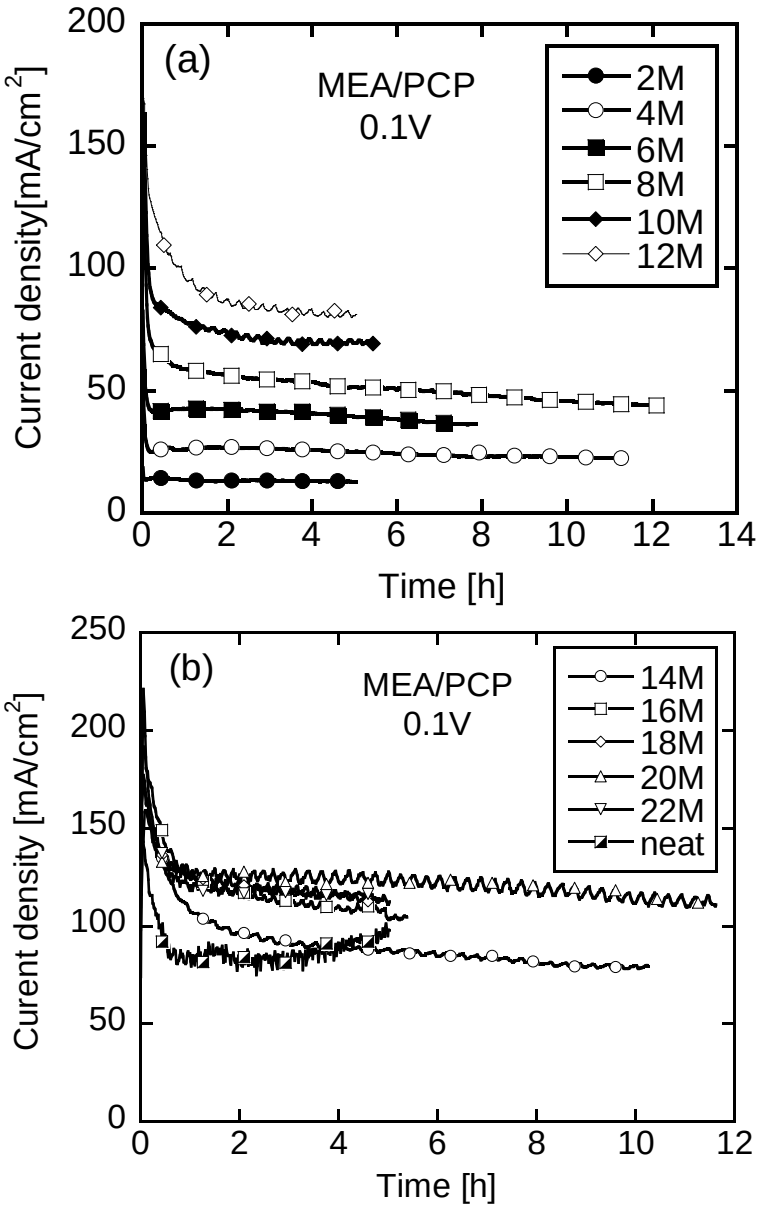

Figure 3-6: Current profile during continuous operation of passive DMFC with porous plate, MEA/PCP, under cell voltage 0.1V.

Figures 3-6a and b show the variations in current density at 0.1V for MEA/PCP, with methanol concentrations from 2M to 12M, and high methanol concentrations from 14M to neat methanol, respectively. The current density initially somewhat decreased then it became nearly constant with time within 2h in contrast to that for MEA_C. This was related to the employment of the PCP, which constantly regulated the methanol transfer rate from the reservoir to the anode and prevented the excess loss of methanol by MCO. The regulation could be understood from the constant current density which was almost proportionally increased with increasing the methanol concentration in the range from 2M to 16M as shown in Figs. 3-6a and b. The constant current density further increased with increasing methanol concentration until reached maximum, about 130mA/cm^2, at 20M, and then decreased with the further increase in methanol concentration as shown in figure 2-6b. The decrease in the constant current density over 20M would be due to MCO as well as a depletion of water in the solution. Equi-molar of methanol and water react with each other at the anode based on eq. (3-2). Hence, operation at high concentrations over 17M (= 50mol%), especially neat methanol, must requires water supply to the anode from the stoichiometric consideration. Optimum concentration, 20M, that was higher than that in the case of the i-V curve, 16M as shown in Fig. 3-4b, was related to the relaxation time for the mass transfer in this experiment, because the current density at 16M was highest within the initial 1h from the start. The fluctuations appeared on the high current densities over 70mA/cm^2, except for the case with the neat methanol, was periodic and may be related to the CO_2 removal from the anode. Neither water film nor water droplets were found at the cathode surface, in the experiment for MEA/PCP even at neat methanol, suggesting that the electrode was free from flooding. Although the current density was relatively small, it was demonstrated that the neat methanol could be used as shown in Fig. 3-6b. The current density was initially low then slightly increased with time. This slight increase in the performance would be caused the water supply from the cathode to the anode by the back diffusion as mentioned later.

3.3. Influence of methanol concentration on the cell temperature

Figure 3-7 shows the changes in cell temperature corresponded to the i-t experiment, Fig. 3-5, for MEA_C. The cell temperature initially increased to a certain level then decreased showing a peak of the temperature in the profile. As the methanol concentration increased, the level of the peak increased. When the concentration was as high as 8M, the temperature increased from 298K to 315K and then decreased. It has already been pointed out that the cell temperature of a passive DMFC is generally related to the magnitude of MCO [11, 16] and also the increase of temperature by MCO reflexively accelerate MCO [31]. A depletion of methanol at the anode would decrease MCO and then temperature after the peak.

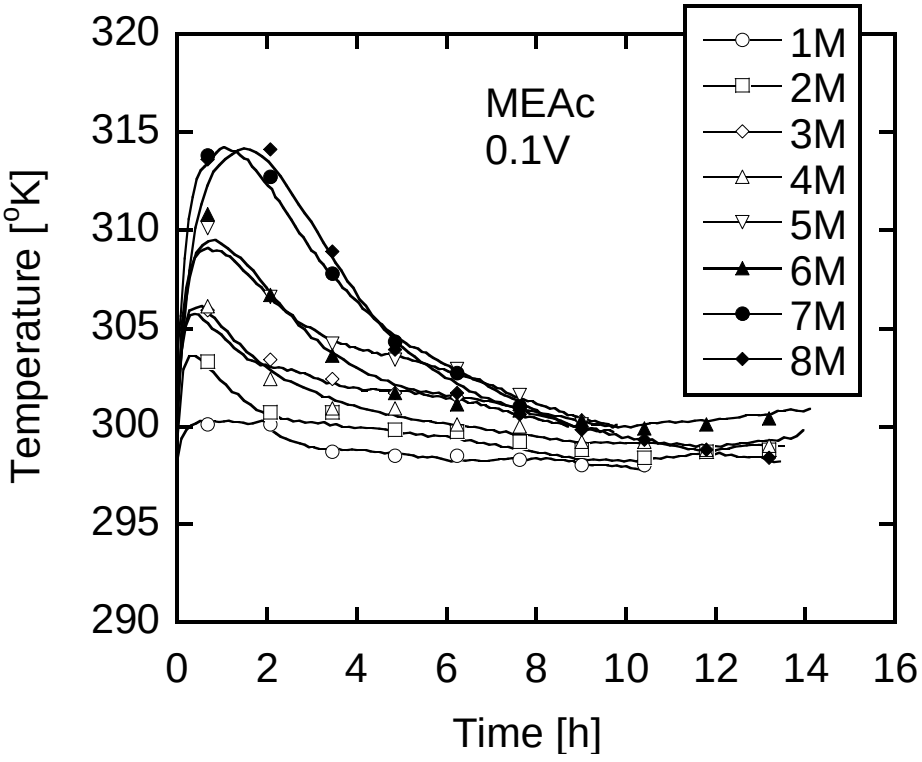

Figure 3-7: Variations in operating cell temperature of passive DMFC without porous plate, MEAc, under cell voltage 0.1V

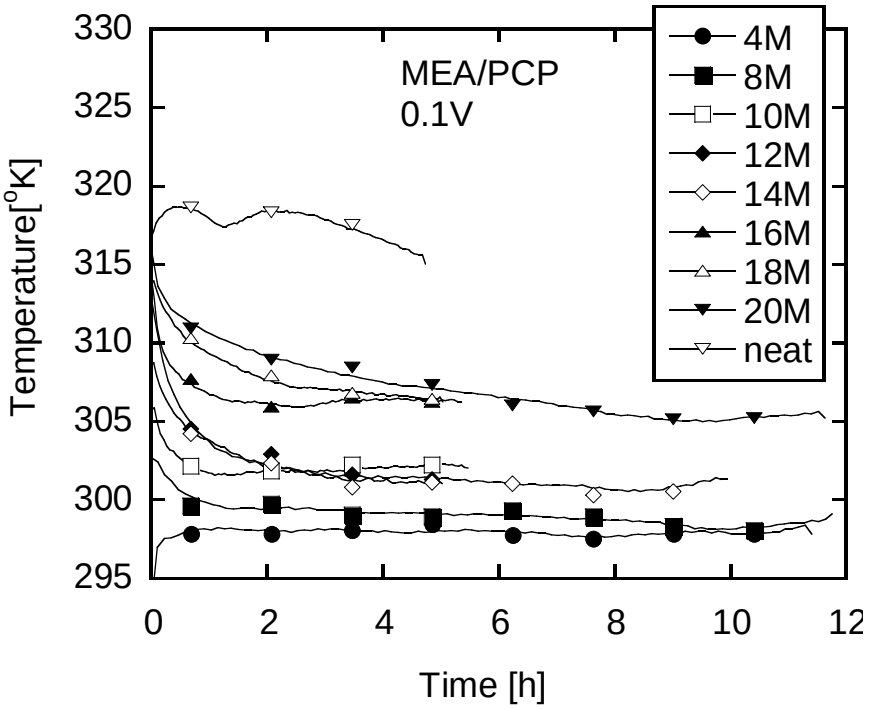

Figure 3-8: Variations in operating cell temperature of passive DMFC with porous plate, MEA/PCP, under cell voltage 0.1V

Figure 3-8 shows the cell temperature in the case of MEA/PCP with different methanol concentrations from 4M to neat methanol, corresponded to the i-t experiment shown in Figs. 3-6a and b. It was clearly shown, in this figure, that the employment of the PCP controlled the cell temperature low and constant compared to that in the case of MEA_C, where, the temperature of MEA/PCP at 8M was about 297K, but it was more than 315K for MEA_C at the same concentration. The temperature for MEA/PCP relatively decreased with time after several hours due to the decrease in MCO that resulted from the decrease of methanol concentration with time. Cell temperature increased with increasing methanol concentration and reached about 318K at the neat methanol.

The initial temperatures for MEA/PCP were higher than that for MEA_C due to MCO during the open circuit situation before i-t measurement. Before starting the i-t measurement, the cell, in the case of MEA/PCP, was kept as open circuit situation for a certain time from a few minutes to more than 1h according to methanol concentration in order to make the methanol concentration at the anode surface closing to that of the solution in the reservoir, after the injection of the solution with a certain methanol concentration to the reservoir. During this open circuit situation, temperature for MEA/PCP somewhat increased.

It was very clear from Figs 3-7 and 3-8 that the temperature profile coincided with the current profile, suggesting that the performance was sensitive to the temperature.

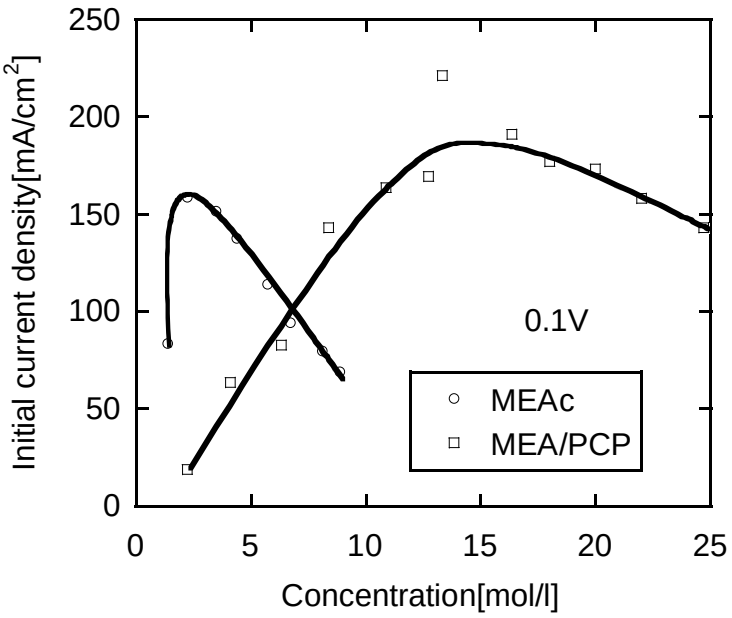

Figure 3-9: Effect of methanol concentration on initial current density for MEA with and without the porous plate

Figure 3-9 shows the effect of methanol concentration on the initial current density, the peak current density appeared within 5 minutes from the start, for MEA with and without the porous plate. The peak current density reached the maximum, 160 mA/cm^2, at 2M for MEA_C, and it was decreased with increasing the methanol concentration. On the other hand, in the case of MEA/PCP, the initial current density reached about 190mA/cm^2 at the methanol concentrations ranging from 12M to 20M. The similar peak current density but at different methanol concentration for MEA_C and MEA/PCP suggested that the mass transfer of methanol was restricted at MEA/PCP, but the electrode activity was reproduced with the high methanol concentrations at MEA/PCP.

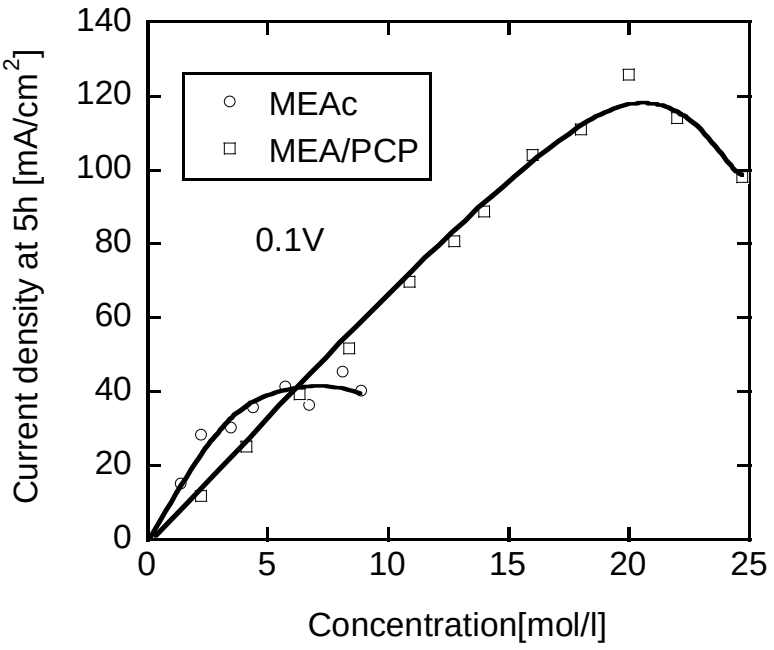

Figure 3-10: Effect of methanol concentration on steady current density for MEA with and without the porous plate

Figure 3-10 shows the effect of methanol concentration on the steady current density which was defined as the current density at 300 minutes from the start, for MEA_C and MEA/PCP. In the case of MEA_C, the steady current density increased with increasing methanol concentration from 1M to 4M and reached about 40mA/cm^2, this value was slightly increased with increasing concentration to 8M. On the other hand, in the case of MEA/PCP, the steady current density was increased with increasing the methanol concentration and reached about 130mA/cm^2 at 20M, which was three times higher than that in the case of MEA_C and was similar to the maximum current density at the initial for MEA_C. The proportional dependency of the current density on the concentration up to 20M meant, again, that the methanol supply to the anode was the rate limiting.

This figure clearly showed the significant effect of the employing PCP, i.e., very high methanol concentration like 20M could be used and the current density was three times higher than that for MEA_C

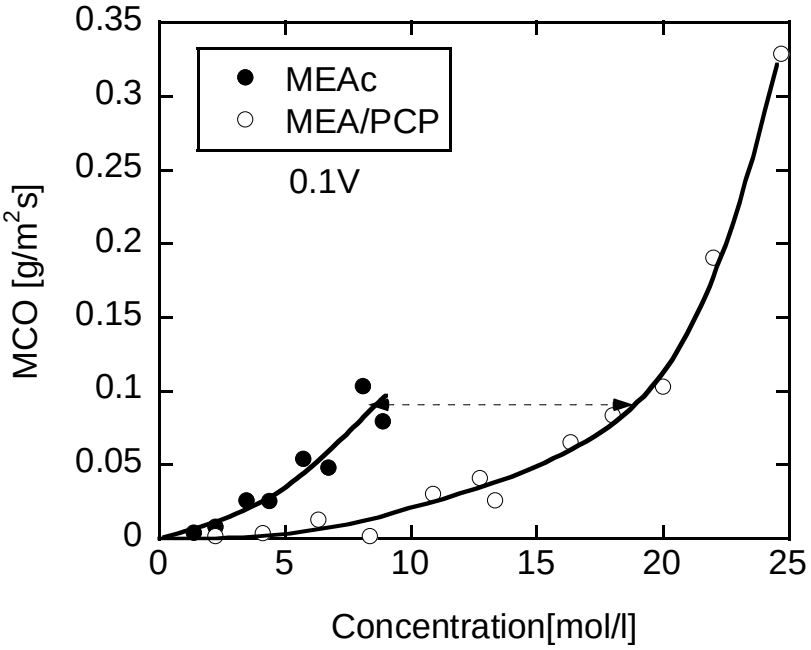

Figure 3-11: Effect of methanol concentration on methanol crossover for MEA with and without the porous plate

3.4. Permeation of methanol and water through membrane

Figure 3-11 shows the effect of methanol concentration on MCO as the methanol flux through the membrane, J_M defined by eq. (3-7), for MEA_C and MEA/PCP. As shown in the figure, MCO for both MEA_C and MEA/PCP increased with increasing the methanol concentration, but differently. It would be due to the increase of the driving force of the methanol transfer, i.e., difference in concentration of methanol between the anode surface and the cathode surface. It was very clear in the figure that MCO for MEA/PCP at any methanol concentrations was very small, about 1/10, in comparison to that for MEA_C. For example, MCO for MEA_C at 7M was nearly equivalent to that for MEA/PCP at 20M.

On the other hand, figure 3-12 shows the effect of methanol concentration on the water flux through the membrane, J_W defined by eq. (3-8), for MEA_C and MEA/PCP. As shown in the figure, the water flux for MEA_C was about 0.1g/(m^2s) and this value did not affected by methanol concentration. Whereas, in the case of MEA/PCP, the water flux decreased with increasing the concentration, and, noteworthily, it became negative from 6M and it further decreased as the methanol concentration increased. The negative flux meant back diffusion of water from the cathode to the anode. The magnitude of the back diffusion of water increased with increasing the concentration.

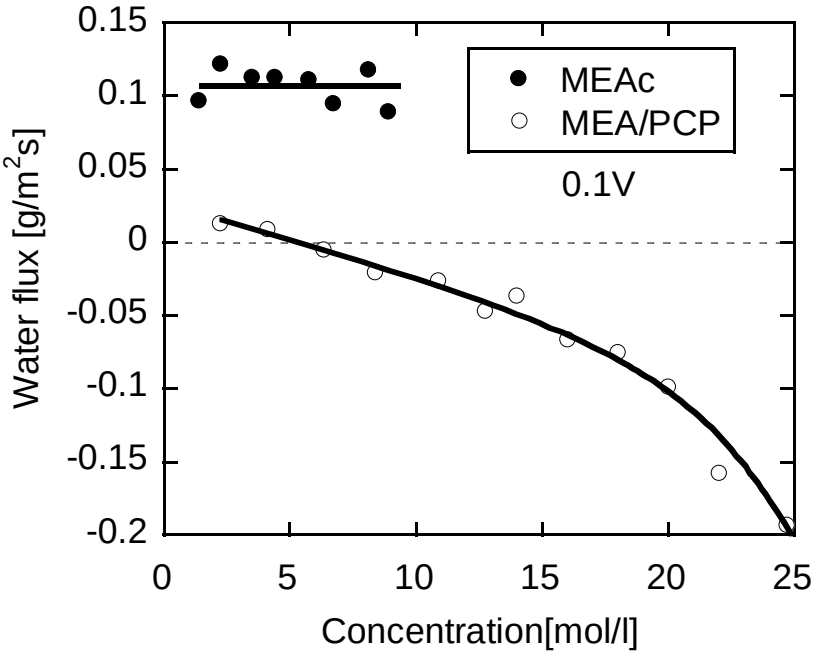

Figure 3-12: Effect of methanol concentration on water flux for MEA with and without the porous plate

This must be a result of the balance of water that consumed at the anode and that supplied from the reservoir and from the cathode through the membrane. Water can be supplied not only from the reservoir but also from the cathode where water is produced by ORR and by the oxidation of the permeated methanol. The back diffusion of water from the cathode was desirable for DMFC to prevent the cathode from flooding. Actually, neither water film nor water droplets were observed at all at the cathode surface during the i-t experiments for MEA/PCP, whereas, flooding was very clear at the cathode in case of MEA_C. This would be one of the main reasons for MEA/PCP to had superior i-t performances compared to that for MEA_C.

As shown in Figs. 3-11 and 3-12, it was clear that not only the methanol flux but also the water flux were significantly reduced by the employing of the PCP. In our previous paper, we made clear that PCP controlled methanol flux and water flux through the membrane in the open circuit conditions by the diffusion resistance of PCP[31]. Differently from the cases of open circuit conditions, we need to consider another effect of CO_2 gas that produced at the anode. The CO_2 gas would be accumulated in the space between the anode and the porous plate and also in a part of the pores of the PCP preparing a layer of CO_2 gas. And once the gas layer was formed, it was maintained during the experiment. This CO_2 gas layer must add an additional resistance to the mass transport, because the CO_2 have to

be transported from the anode to the outlet through the PCP in a counter flow to that of the methanol and the water, in this experiment. And also the methanol and the water have to be transported as gaseous materials in the gas layer with CO_2. Hence, these effects significantly reduced the rate of the mass transport of methanol and water from the reservoir to the anode, and resulted in very strong reduction of MCO and negative flux of water as shown in the figure. We would say that the PCP and the CO_2 gas layer acted as a barrier for the methanol and water transport, where PCP was necessary to prepare and stably maintained the CO_2 layer over the anode surface.

To check the effect of the CO_2 barrier on the cell performance, we changed the distance between the anode and the PCP by using two plates of current correctors at the anode.

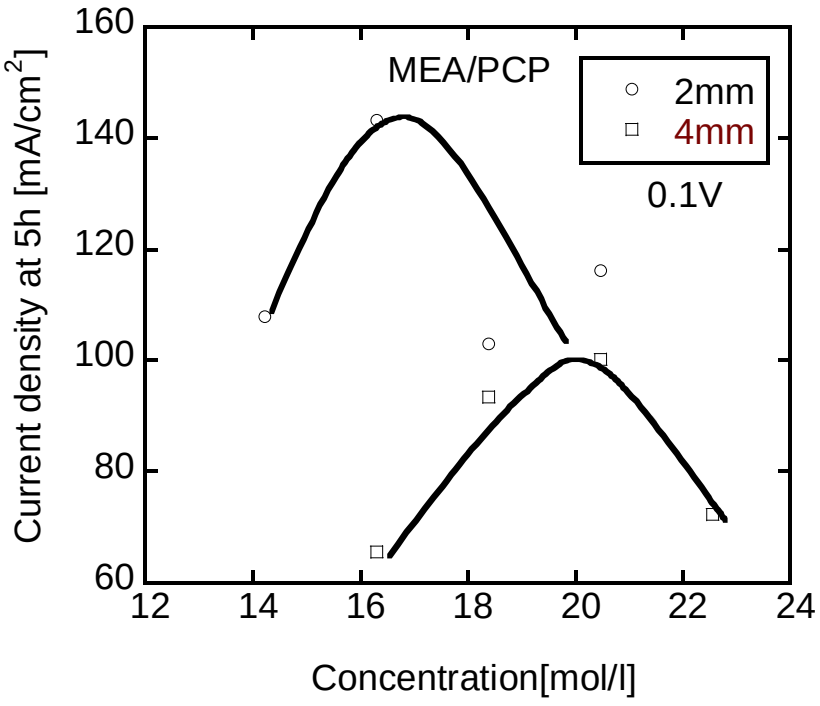

Figure 3-13: Effect of the distance between the anode and the porous plate on the performance of passive DMFC.

Figure 3-13 shows the effect of the distance between the PCP and the anode surface on the steady current density under cell voltage 0.1V. In this experiment, different MEA with a somewhat different catalyst loading from that used in the above figures was used. Then the result with 2mm distance was not the same as that shown in Fig. 3-10. From this figure, it was clear that, as the distance increased from 2mm to 4mm, the steady current density decreased from130 mA/cm^2 at 16M to 100mA/cm^2 at 20M. This could be

explained by, as the distance between the PCP and the anode surface increased, the resistance to the mass transfer increased, so the performance at a certain concentration decreased and the optimum concentration increased from 16M to 20M, to compensate the methanol supply from the reservoir.

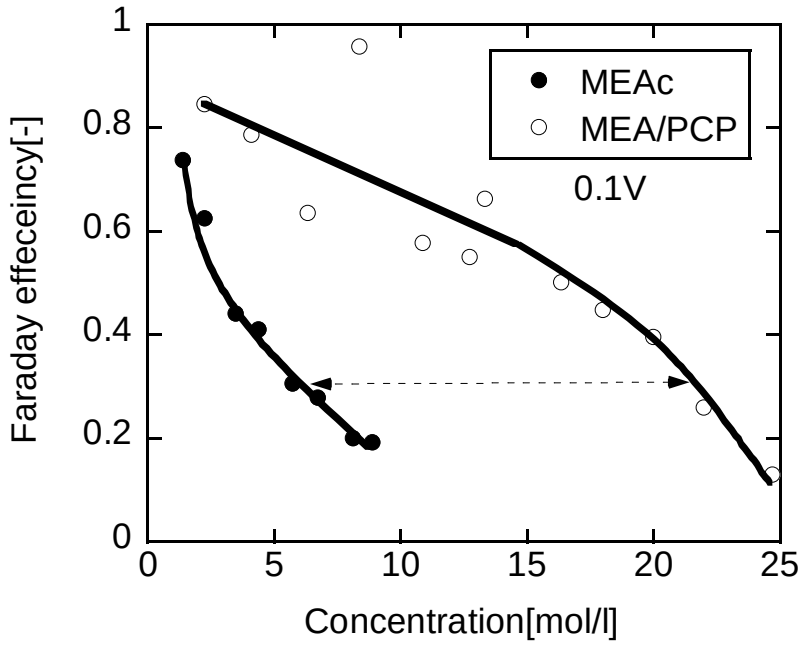

Figure 3-14: Effect of methanol concentration on faradic efficiency for MEA with and without the porous plate.

Figure 3-14 shows the comparison in Faraday efficiency between MEA_C and MEA/PCP corresponding to the results shown in Figs. 3-5 to 3-12. Although Faraday efficiency, larger or fewer, decreased with increasing methanol concentration due to MCO. However, it should be noted that, it in case of MEA/PCP was very much larger than that in the case of MEA_C in all the range of the methanol concentration measured. In the case of MEA_C, Faraday efficiency decreased from 75% at 1M to about 30% at 5M. Contrary to this, it only decreased from 80% at 2M to 60% at 14M in the case of MEA/PCP. And Faraday efficiency for MEA_C at 5M was nearly the same as that at 22M for MEA/PCP. This was a direct result of controlling MCO by employing PCP showing that the methanol was efficiently converted to power output, and also very high methanol concentration could be used efficiently.

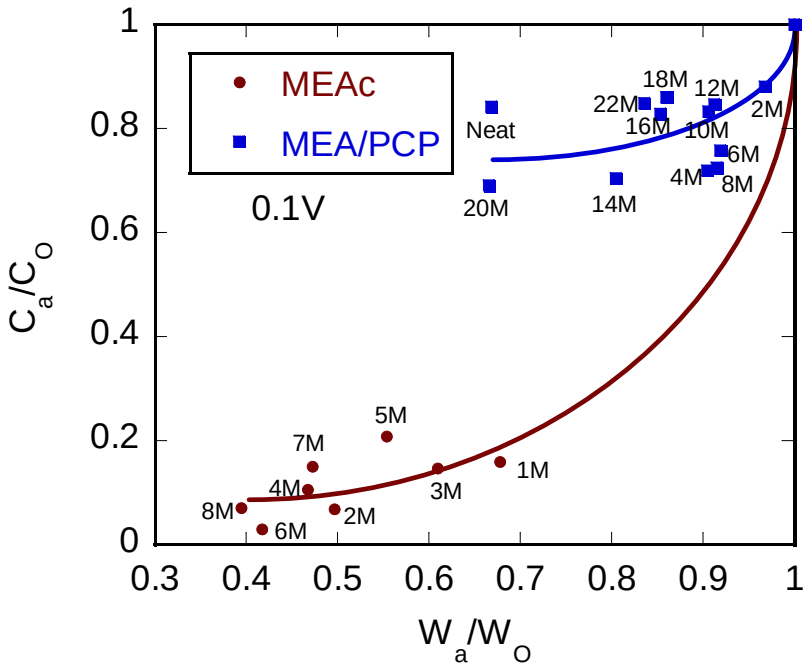

Figure 3-15: Relationship between the decrease in the weight and that in the methanol concentration for the methanol solution remaining in the reservoir during the experiment for MEA with and without the porous plate

The efficient utilization of the methanol in MEA/PCP was also explained in Figure 3-15 that shows relationships between W_a/W_o and C_a/C_o for the i-t experiments corresponding to Fig. 3-14. We can see in this figure that how the concentration and the weight of the inputted methanol solution changed during the i-t experiments for both of MEA_C and MEA/PCP. As we shown above, the employment of the porous plate made the utilization of high methanol concentrations possible efficiently by controlling the mass transport from the reservoir to the anode. The employment of PCP is quite effective to achieve an efficient DMFC and important technique to increase its power density. The back diffusion of water from cathode to anode was confirmed at high methanol concentrations. This back diffusion of water though Nafion membrane, i.e., its high water permeability, would be essential to achieve a high performance with this type of mechanism using the porous plate.

4. Conclusions

Performance of the passive DMFC with and without PCP was investigated under closed circuit conditions with different methanol concentrations ranging from 1M to neat methanol, and the following conclusions were drawn.

1) Mass transfer both of methanol and water from the reservoir to the anode were significantly restricted by the employment of PCP at the anode side. It was considered that the CO_2 gas layer formed between the anode and PCP restricted the mass transfer, and the PCP stably maintained the CO_2 layer over the anode.

2) As a result of the mass transfer restrictions by the employing of PCP, high methanol concentrations, even neat methanol, could be used efficiently. This results in a high power density of DMFC.

3) Back diffusion of water from the cathode to the anode was confirmed at relatively high methanol concentrations for the DMFC with PCP. This was desired to prevent the cathode from flooding and increase the cell performance.

5. References

1. H. Chang, J.R. Kim, J.H. Cho, H.K. Kim, K.H. Choi, *Solid State Ionics* **148** (2002) 601–606.
2. Blum, T. Duvdevani, M. Philosoph, N. Rudoy, E. Peled, *J. Power Sources* **117** (2003) 22–25.
3. D. Kim, E.A. Cho, S.A. Hong, I.H. Oh, H.Y. Ha, *J. Power Sources* **30** (2004) 172–177.
4. Z. Guo, Y. Cao, *J. Power Sources* **132** (2004) 86–91.
5. T. Shimizu, T. Momma, M. Mohamedi, T. Osaka, S. Sarangapani, *J. Power Sources* **137** (2004) 277–283.
6. H. Qiao, M. Kunimatsu, T. Okada, *J. Power Sources* **139** (2005) 30.
7. Q. Ye, T.S. Zhao, *J. Power Sources* **147** (2005) 196–202.
8. B. Kho, I. Oh, S. Hong, H.Y. Ha, *Electrochim. Acta* **50** (2004) 781.
9. A.S. Arico, S. Srinivasan, V. Antonucci, *Fuel Cells* **1** (2001) 133–161.
10. T. Schultz, K. Su Zhou, Sundmacher, *Chem. Eng. Technol*. **24** (2001) 1223–1233.
11. J.G. Liu, T.S. Zhao, R. Chen, C.W. Wong, *Electrochem. Commun.* **7** (2005) 288.
12. J.G. Liu, T.S. Zhao, Z.X. Liang, R. Chen, *J. Power Sources* **153** (2006) 61–67.
13. S. Surampudi, S.R. Narayanan, E. Vamos, H. Frank, G. Halpert, A. LaConti, J. Kosek, G.K. Surya Prakash, G.A. Olah, *J. Power Sources* **47** (1994) 377–385.
14. M.K. Ravikumar, A.K. Shukla, *J. Electrochem. Soc.* **143** (1996) 2601–2606.
15. S.R. Yoon, G.H. Hwang, W.I. Cho, I.-H. Oh, S.-A. Hong, H.Y. Ha, *J. Power Sources* **106** (2002) 215–223.
16. R. Chen, T.S. Zhao, *J. Power Sources* **152** (2005) 122–130.
17. B. Bae, B.K. Kho, T. Lim, I. Oh, S. Hong, H.Y. Ha, *J. Power Sources* **158** (2006) 1256–1261.
18. J.T. Wang, S. Wasmus, R.F. Savinell, *J. Electrochem. Soc.* **143** (1996) 1233–1239.

19. E. Peled, T. Duvdevani, A. Aharon, A. Melman, *Electrochem. Solid State Lett.* **3** (2000) 525–528.

20. M.V. Fedkin, X. Zhou, M.A. Hofmann, E. Chalkova, J.A. Weston, H.R. Allcock, S.N. Lvov, *Mater. Lett.* **52** (2002) 192–196.

21. T. Yamaguchi, M. Ibe, B.N. Nair, S. Nakao, *J. Electrochem. Soc.* **149** (2002) A1448–A1453.

22. M.L. Ponce, L. Prado, B. Ruffmann, K. Richau, R. Mohr, S.P. Nunes, *J. Membr. Sci.* **217** (2003) 5–15.

23. A.S. Arico, P. Creti, P.L. Antonucci, V. Antonucci, *Electrochem. Solid State Lett.* **1** (1998) 66–68.

24. C. Yang, S. Srinivasan, A.S. Arico, P. Creti, V. Baglio, V. Antonucci, *Electrochem. Solid State Lett.* **4** (2001) A31–A34.

25. N. Jia, M.C. Lefevre, J. Halfyard, S. Qi, P.G. Pickup, *Electrochem. Solid State Lett.* **3** (2000) 529–531.

26. I.J. Hobson, H. Ozu, M. Yamaguchi, M. Muramatsu, S. Hayase, *J. Mater. Chem.* **12** (2002) 1650–1656.

27. W.C. Choi, J.D. Kim, S.I. Woo, *J. Power Sources* **96** (2001) 411– 414.

28. S.R. Yoon, G.H. Hwang, W.I. Cho, I.-H. Oh, S.-A. Hong, H.Y. Ha, *J. Power Sources* **106** (2002) 215–223.

29. Y.K. Xiu, K. Kamata, T. Ono, K. Kobayashi, T. Nakazato, N. Nakagawa, *Electrochemistry 73* (2005) 67–70.

30. N. Nakagawa, K. Kamata, A. Nakazawa, M. Ali Abdelkareem, K. Sekimoto, **Electrochemistry 74** No.3 (2006) 221-225.

31. N. Nakagawa, M. Ali Abdelkareem, K. Sekimoto, *J. Power Sources* **160** (2006) 105–115.

32. G.Q. Lu, C.Y. Wang, T.J. Yen, X. Zhang, *Electrochim. Acta* **49** (2004) 821.

33. C.Y. Chen, P. Yang, *J. Power Sources* **123** (2003) 37–41.

34. R. Chen, T. S. Zaho and J. G. Liu, *J. Power Sources*, **157** (2006) 351–357.

35. J. Liu, G. Sun, F. Zhao, G. Wang, G. Zhao, L. Chen, B. Yi, Q. Xin, *J. Power Sources* **133** (2004) 175–180.

36. S. Yao, X. Tang , C.Hsieh, Y. Alyousef, M. Vladimer, G.Fedder, C. Amon , *Energy* **31** (2006) 636–649.

CHAPTER 4

Effect of Oxygen and Methanol Supply Modes on the Performance of a DMFC Employing a Porous Plate

1. Introduction

As a result of the high energy density of DMFCs, they are considered to be a promising candidate to provide power to electrical vehicles, small and large scale power stations and even portable electrical applications such as laptops and mobile phones. Unfortunately, tell now the energy density of the DMFCs is low due to the methanol crossover and the high over voltage at the electrodes [1-4]. As a result of methanol crossover, the highest performance of the DMFC obtained at very low methanol concentration 6wt% in the active type or 15 wt% in passive type [5-9]. To overcome the methanol crossover, a large number of studies [10–14] were carried out for developing or modifying the proton-conducting membrane [15-21]. Only a few papers have considered reducing the ability for methanol crossover by mass transport control in the backing layer [22-25].

We demonstrated, in chapter (3) that under closed circuit conditions, the PCP and the CO_2 gas layer that formed between the anode and the porous plate stably controlled the mass transport of methanol and water from the reservoir to the anode, and this facilitated operation with very high concentrations of methanol even neat methanol. When high concentrations of methanol were used with the porous plate, the Faraday efficiency was kept high and back diffusion of water from the cathode to the anode through the membrane occurred, resulting in no flooding at the cathode. The objective of this chapter is to clarify the effects of oxygen and methanol supply modes that affect the mass transfer rate between the MEA and outside of it on the type of DMFC using a PCP. Another objective is to show the superior characteristics of this type of DMFC.

The flooding, which is a well-known problem in the passive DMFCs [26, 27], causes blocking of the oxygen supply to the cathode resulting in a decrease in the power density as a result of water accumulation at the cathode. This occurs when the rate of water production is faster than the rate of water removal at the cathode. Hence, the flooding relates to the methanol and water fluxes through the membrane and the rate of the oxygen reduction reaction, i.e., current density, and the rate of water evaporation at the cathode, i.e., flow rate, temperature and humidity of the cathode gas. The evaporation of water from

the cathode under air-breathing condition is usually very small, so flooding easily takes place. Flooding can be avoided by blowing air or oxygen to the cathode where the rate of evaporation is greatly increased [27, 23]. Another main problem encountered in a passive DMFC is the depletion of methanol at the anode by the methanol crossover; the long-time operation of a passive DMFC was affected by the methanol supply rather than the air supply [19]. To avoid this problem, fresh methanol must be flowed continuously at the anode side.

In this chapter, the effects of the oxygen and methanol supply modes on the current density, temperature and the fluxes of methanol and water through the MEA were investigated for DMFCs with and without the PCP. The differences in those variables at different supply modes were discussed from the viewpoints of occurrence of flooding and methanol depletion.

2. Experimental

2.1. MEA preparation

The conventional MEA, MEAc, was prepared in the same manner described in chapter (3)

2.2 Porous carbon plate, PCP

A porous carbon plate, PCP, made of a composite of carbon nanotubes and amorphous carbon, supplied from Mitsubishi Pencil Co., Ltd., with 1.0mm thickness was used in this study. The microstructure of the PCP analyzed by a mercury porosimeter (Pascal 140 + 440, Thermo Finnigan, Inc.) revealed that it had 0.713cm^3/g in total cumulative pore volume, 1.49μm in average pore diameter, and 0.514 in total porosity. The PCP was hydrophobic and its water absorptivity as defined in chapter (2) was nearly zero. The PCP was placed on an anode current corrector and used as mentioned below.

2.3 Cell structures with and without a PCP and oxygen/methanol supply modes

Figure 4-1 shows a DMFC, used in this experiment, with the porous carbon plate. In the anode compartment, a methanol reservoir, 12 dm^3, with two stainless steel pipes for flowing methanol was prepared. On the cathode side, there was a cathode chamber with two stainless steel pipes for flowing O_2. This chamber was removed in the air-breathing mode. The MEA was sandwiched between two current collectors, which were plates of stainless steel of 2mm thickness and open holes with a 73% open ratio. The MEA with the

plates was fixed with the anode chamber in the air-breathing mode and was fixed between the anode and cathode chambers in the other operation modes.

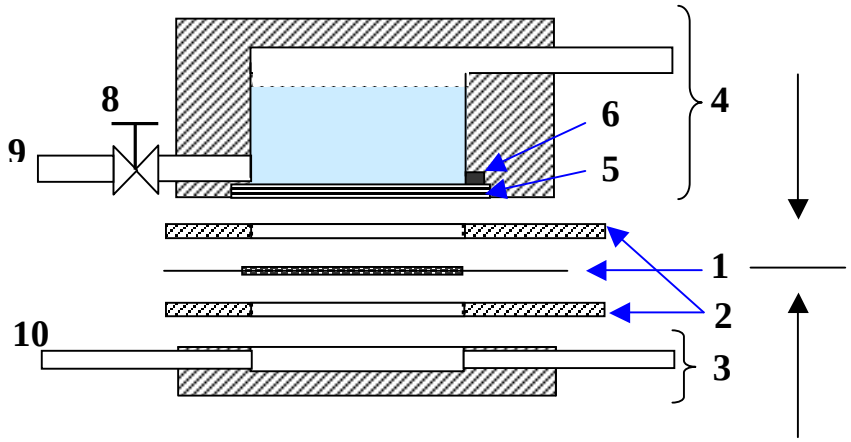

1. MEA
2. Current collectors (2mm thick.)
3. Cathode chamber
4. Anode chamber
5. Porous plate, PCP
6. Rubber sheet
7. Aqueous methanol solution
8. Valve
9. Pipe for flowing methanol
10. Pipe for flowing oxygen

Figure 4-1: Schematic diagram of a DMFC with or without porous plate.

When a PCP was used, the PCP was placed on the anode current collector by exposing the upper surface in the methanol solution. This configuration forced the methanol to pass through the porous plate then through the openings in the anode current collector to reach the anode catalyst layer. Under closed circuit conditions, the openings of the anode current collector and a part of the pores of the PCP would be filled with CO_2 produced at the anode, and hence, a CO_2 gas layer would be formed between the anode and the methanol solution. In this case, both the PCP and the CO_2 gas layer obstruct methanol transport from the reservoir to the anode. Without the PCP, the CO_2 gas layer is not formed, and CO_2 easily escapes through the openings of the current collector to the reservoir in a form of bubbles. This situation allows direct contact with the anode for the solution and then a high methanol transport. The cell was arranged horizontally keeping the reservoir upside to ensure a constant contact between the solution and the PCP and/or anode.

The methanol solution was supplied either in a passive mode or an active mode. The passive mode was defined as no flow of methanol to the anode and was realized by an injection of 6 to 7 cc of methanol solution into the reservoir. In the active mode, methanol solution was introduced to the reservoir through the lower tube at a rate of 1.5 ml/min using a pump (Iwaki, SDK-081). On the other hand, as a mode of oxygen supply, air-breathing was defined as just exposing the cathode to ambient air without the cathode chamber. By using the cathode chamber for the oxygen flow, oxygen was supplied at different flow rates, 0.1l/min and 1l/min.

The methanol concentrations used in this study were chosen to be 2M (mol/l) for the MEA without PCP, MEA_C, and 16M for the MEA with PCP, MEA/PCP, where the DMFC power output became a maximum for each type of MEA [24].

2.4 Measurement of the cell performance

In this study, all the experiments were conducted under ambient conditions (293K and 1atm), methanol solution at a certain concentration was fed into the reservoir, and left in the cell for a few minutes until the PCP became saturated with methanol. The time progress of the current density, i-t characteristics, at 0.1V was measured using an electrochemical measurement system (HAG-5010, Hokuto Denko Co., Ltd.). Where both flooding and depletion of methanol at the anode side would be very clear at higher current densities so we operated under 0.1V. The temperature of the cell was also measured using a thermocouple placed between the surface of anode current collector and the porous plate. The methanol and water fluxes during the i-t experiments were evaluated by measuring the weight and concentration of the methanol solution before and after the i-t experiments as described in chapter (3).

3. Results and discussion

3.1. Influence of methanol/oxygen supply modes on the performance of the conventional MEA, MEAc

3.1.1. Performance with a passive methanol supply with different oxygen supplies

Figure 4-2 shows the time progress of the current density, i-t curves, for the DMFC without the PCP with a passive methanol supply and different oxygen supply modes; air-breathing, oxygen flow at 0.1l/min and 1l/min. As shown in the figure, under the air-

breathing conditions, the current density was initially as high as 160mA/cm2 but it rapidly decreased to about 40mA/cm^2 within one hour.

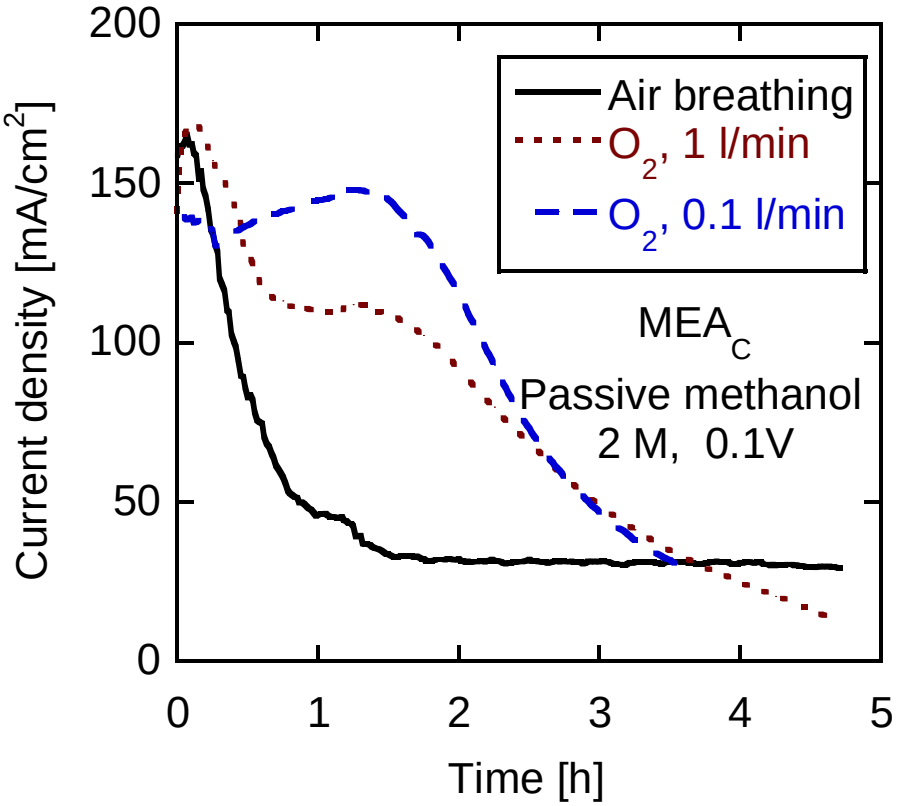

Figure 4-2: Current profile during continuous operation of a DMFC without porous plate, MEA_C, operated with different oxygen supplying modes under cell voltage 0.1V and 2M.

For the oxygen flow at 0.1l/min and 1l/min, the current density remained constant around 140mA/cm^2 and 110mA/cm^2, respectively, for about two hours, then decreased to a value similar to that for the air-breathing condition. The rapid reduction of the current density during the air-breathing would be related to the flooding at the cathode as reported [26, 27]. Water produced at the cathode would block the feeding of air at the cathode. Under the O_2 flow modes, water removal from the cathode by evaporation would be enhanced and so the current density remained at a high value [27].

The decrease in current density with time was also affected by the depletion of methanol at the anode. For the air-breathing, the volume and concentration of the methanol solution initially were 6.2 cm^3 and 2.1mol/l, respectively, and these values were finally reduced to 3.9 cm^3 and 0.2mol/l, respectively. The percent of methanol consumed during the

experiment was calculated to be 95%. This was calculated to be 85% and 90 % for the oxygen flow at 0.1 l/min and 1l/min, respectively.

The current density decreased with the increasing oxygen flow from 0.1l/min to 1l/min may be related to a cooling effect [9] as shown below.

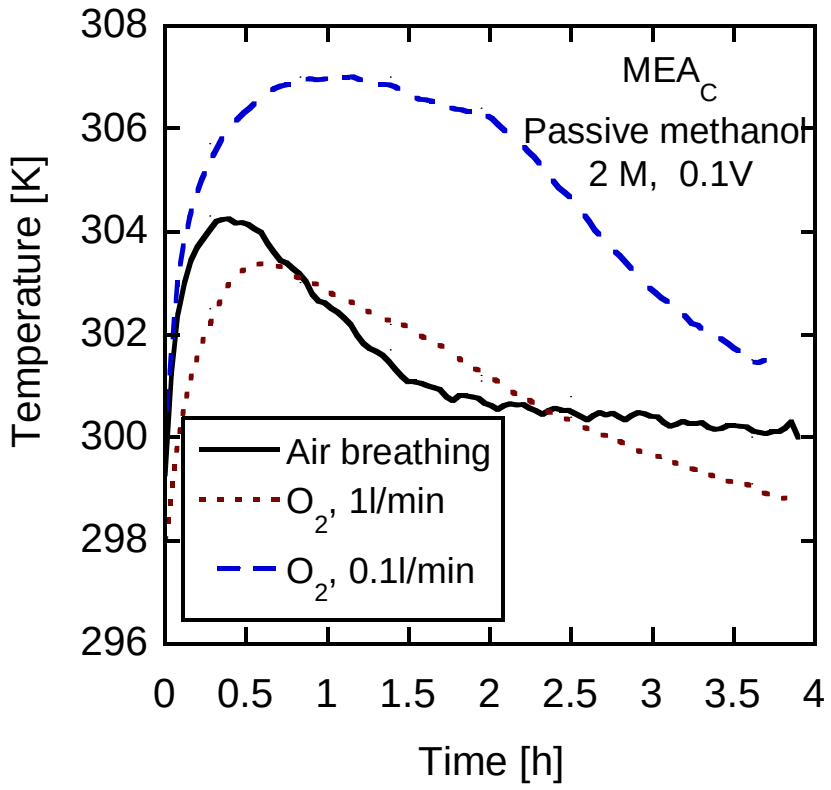

Figure 4-3: Variations in operating cell temperature of a DMFC without porous plate, MEA_C, operated with different oxygen supplying modes under cell voltage 0.1V and 2M.

Figure 4-3 shows the cell temperature in the experiment shown in Fig. 4-2. The highest cell temperature was obtained for the oxygen flowing at 0.1l/min, where it increased to 307K and was about 5K higher than those in the other supply modes. The lower temperature for the oxygen flow at 1l/min was considered a reason for the smaller current density compared to that at 0.1l/min, suggesting a cooling effect. The cell temperature was related to the rate of methanol crossover that induced an increase in the cell temperature by the exothermic oxidation reaction of the permeated methanol [26, 28-29]. The low temperature for the air-breathing mode may be attributed to the lower methanol crossover as shown below.

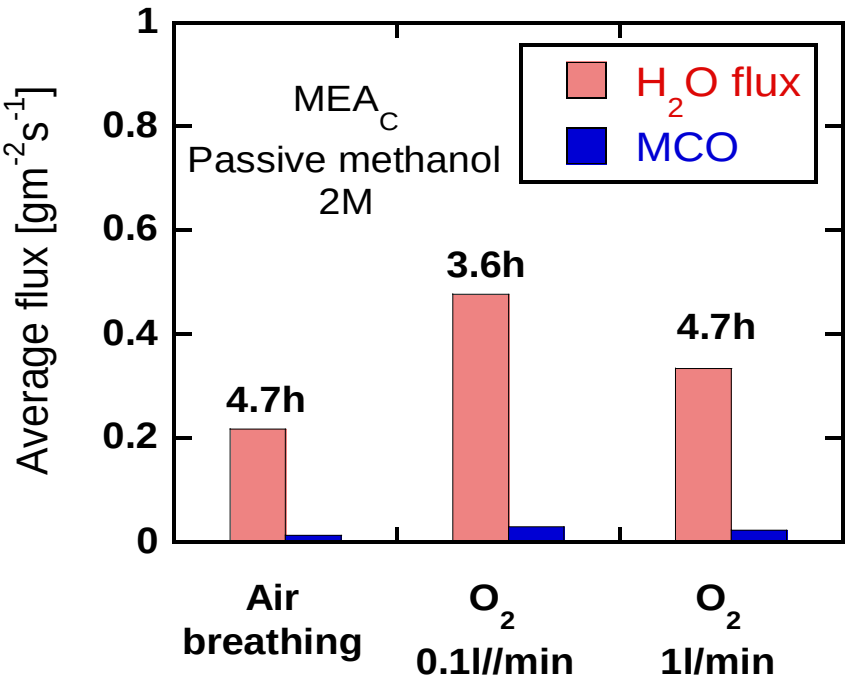

Figure 4-4: Effect of oxygen supplying mode on methanol and water fluxes of a DMFC without porous plate, MEA_C, under cell voltage 0.1V and 2M.

Figure 4-4 shows the effect of different oxygen supply modes on the methanol and water fluxes through the MEA during the i-t experiments shown in Fig. 4-2. As a result of the oxygen flowing, both the methanol and water fluxes through the MEA increased to one and a half or twice the value under the air-breathing mode. This should be due to the increased rate of evaporation of the solution at the cathode by the flowing oxygen, which in turn enhanced the driving force for mass transfer through the MEAC [36]. The average values of the methanol and water fluxes for 0.1l/min were higher than that at 1l/min, and this can be explained based on two reasons. First the higher temperature for 0.1l/min than that for 1l/min enhanced the mass transfer of methanol and water through the MEA; the second reason is that the higher current density induced a larger crossover with the proton transport from the anode to cathode [30].

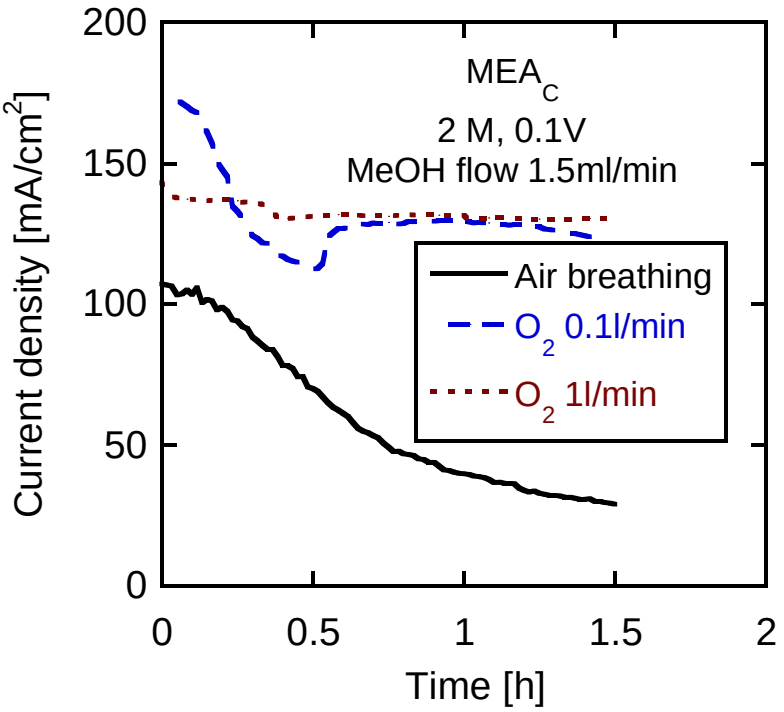

Figure 4-5: Current profile during continuous operation of a DMFC without porous plate, MEA$_C$, operated with different oxygen supplying modes under cell voltage 0.1V and flowing methanol 2M.

3.1.2. Performance with an active methanol supply with different oxygen supplies

Figure 4-5 shows the i-t curves for the DMFC without the PCP with flowing methanol and different oxygen supply modes. In the case of air-breathing, the current density was much lower than those with the oxygen flows through the operating time, and this decreased with time to less than 30mA/cm^2 which is slightly lower than that in the case of air-breathing and passive methanol shown in Fig. 4-2. Reduction in the current density under the air-breathing mode would be related to the flooding at the cathode. The methanol crossover might be increased resulting from no depletion of the methanol under this condition. On the other hand, with the oxygen flows, the current density was highly constant and similar in each case unrelated to the flow rates except for the initial period within 0.75h. The initial period would be needed to reach the steady state. The flow of both methanol and oxygen stabilized the current density because the flowing oxygen prevents flooding at cathode [26] by increasing the rate of water removal by evaporation, and flowing methanol prevents the depletion of methanol at the anode [19]. The negative effect of the increasing O_2 flow from 0.1l/min to 1l/min, observed in the passive methanol feeding, did not appear. This might be related to the high reaction rate, resulting from the

water removal by the oxygen supply at the cathode, which reduced the effect of the methanol crossover by consuming the methanol at the anode.

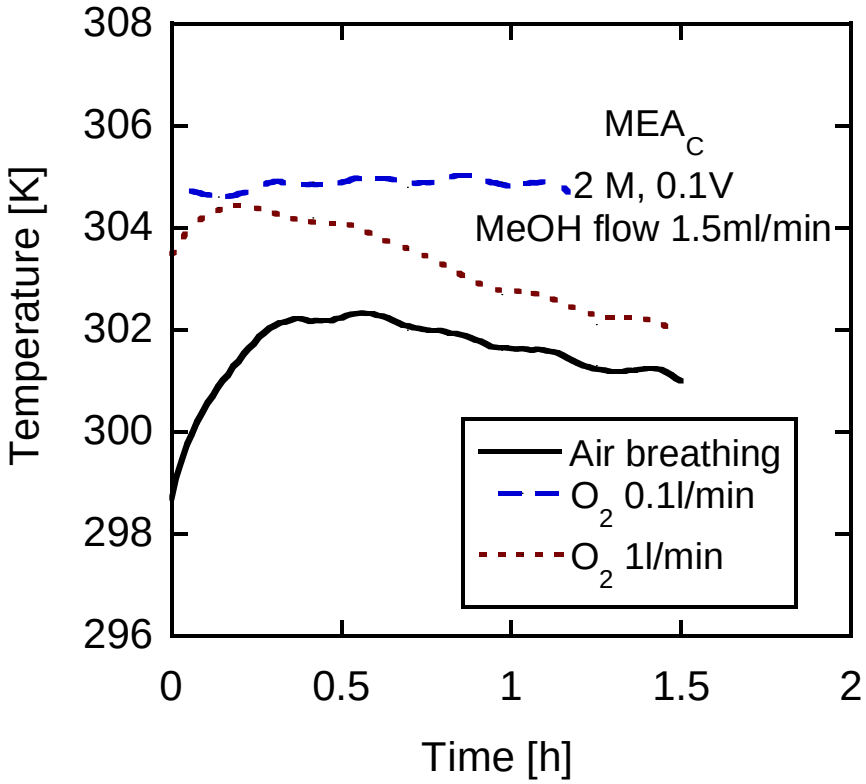

Figure 4-6: Variations in operating cell temperature of a DMFC without porous plate, MEA_C, operated with different oxygen supplying modes under cell voltage 0.1V and flowing methanol 2M.

Figure 4-6 shows the cell temperature in the i-t experiment shown in Figure 4-5. The cell temperature was the lowest in the case of air-breathing, and this might be related to the excessive flooding due to the methanol flow at the anode.

3.2. Influence of methanol/oxygen supply modes on the performance of MEA with PCP, MEA/PCP

3.2.1. Performance with the passive methanol supply with different oxygen supplies

Figure 4-7 shows the i-t curves for the DMFC with PCP, MEA/PCP, with the passive methanol supply and different oxygen supply modes. The flowing of oxygen for the MEA/PCP did not have a positive effect on the current density, in contrast to the conventional MEA as shown in Fig.4-2.

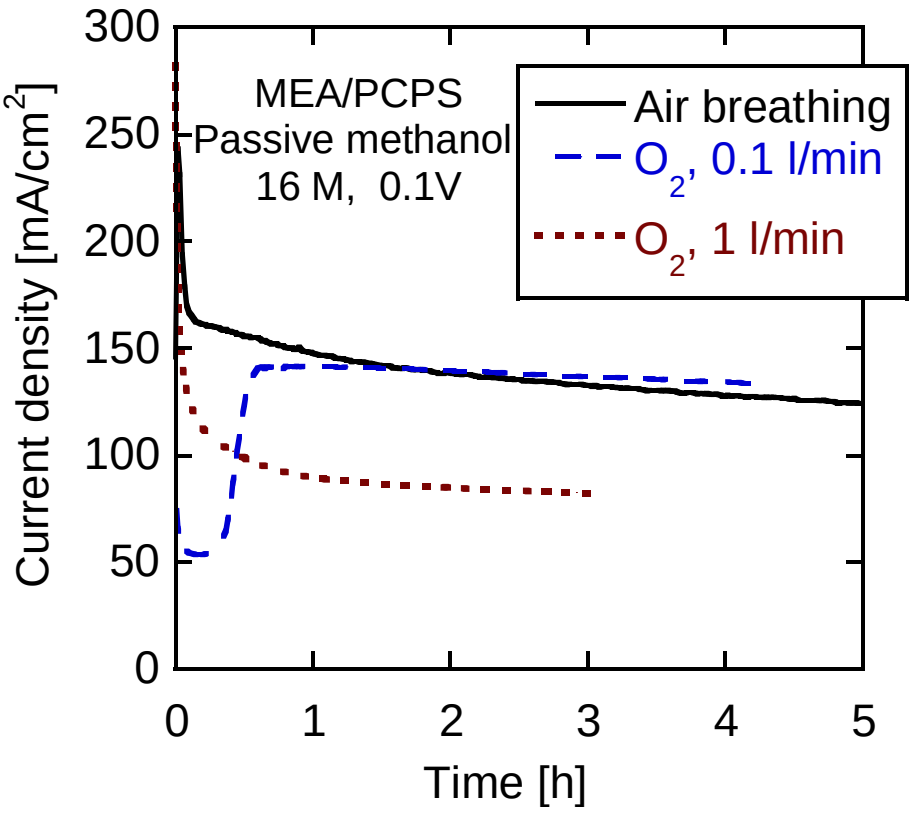

Figure 4-7: Current profile during continuous operation of a DMFC with porous plate, MEA/PCP, operated with different oxygen supplying modes under cell voltage 0.1V and 16M.

The current density with the air-breathing remained high and almost similar to that with an oxygen flow of 0.1l/min. The current densities for all of the oxygen supply modes slightly decreased with time due to the slightly decrease in the methanol concentration during that time. PCP prevented the methanol crossover and water flux through the MEA [24] resulting in a small methanol consumption during the experiment, i.e., 20% (during the 4.2h experiment) for the oxygen flow at 0.1l/min and 18% (3h) for the oxygen flow at 1l/min. Hence, the flowing of O_2 did not have a positive effect on the performance where the flooding was prevented. For the oxygen flow at 0.1l/min, although the current density was initially low which was affected by the initial condition, it increased and became almost constant after 0.7h. The current density decreased with the increase in oxygen flow rate from 0.1l/min to 1l/min. This reduction in current density would be related to a change in the mass transport through the membrane.

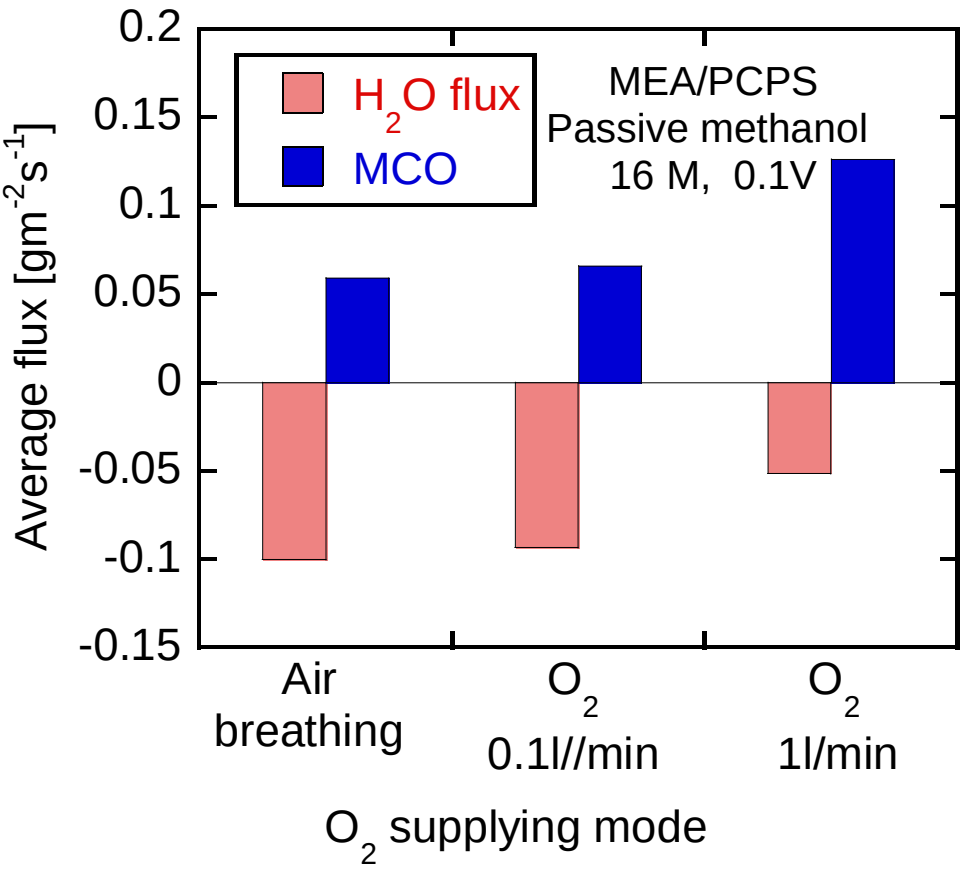

Figure 4-8: Effect of oxygen supplying mode on methanol and water fluxes of a DMFC with porous plate, MEA/PCP, under cell voltage 0.1V and 16M.

In fact, the methanol flux and the water flux with oxygen flowing at 1l/min were different from that at 0.1l/min and air-breathing as shown in Figure 4-8. The rate of water removal at the cathode by evaporation was increased substantially and was calculated to be almost 6 times that at 0.1l/min based on the dependency of the mass transfer coefficient on the gas flow rate, by the increase in the oxygen flow to 1l/min. This would cause a larger methanol flux and a low back diffusion of water. Fig. 4-8 shows that the increased oxygen flow from 0.1l/min to 1l /min reduced the back diffusion of water to half while the methanol flux was nearly doubled. In contrast, there was no big difference in the value of fluxes between air-breathing and the oxygen flow at 0.1l/min.

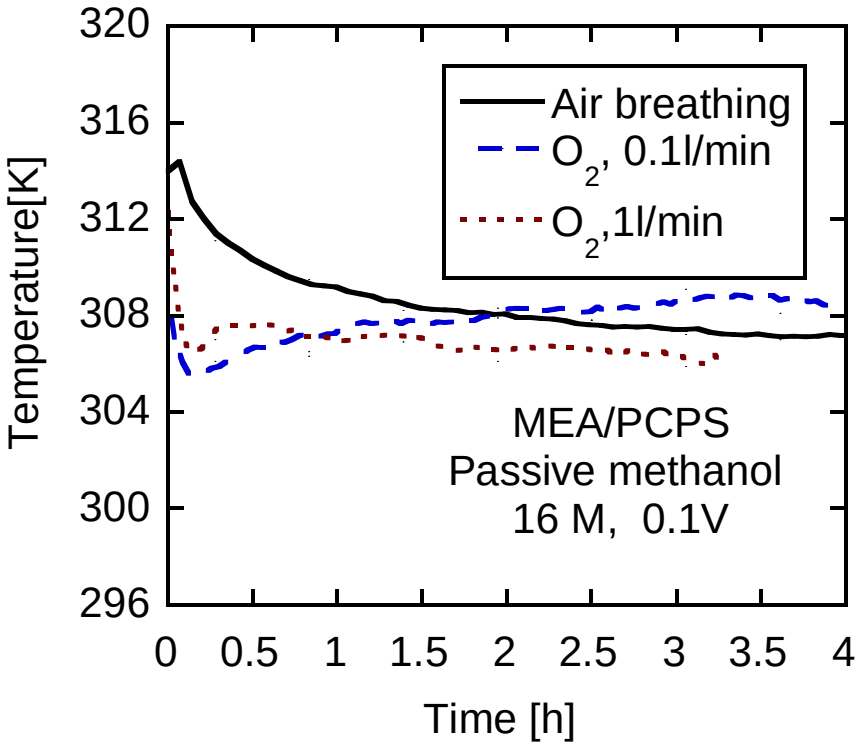

Figure 4-9: Variations in operating cell temperature of a DMFC with porous plate, MEA/PCP, with different oxygen supplying modes under cell voltage 0.1V and 16M.

Figure 4-9 shows the cell temperature in the experiment shown in Fig. 4-7. The flowing of oxygen and the oxygen supply modes did not affect the cell temperature where the PCP controlled the mass transport through the MEA.

3.2.2. Performance with the active methanol supply with different oxygen supplies

Figure 4-10 shows the i-t curves for the DMFC with PCP, MEA/PCP, with the active methanol supply and the different oxygen supply modes. There was no big difference in the performance with the air-breathing and the oxygen flow at 0.1l/min.

The performance between the passive methanol supply, shown in Fig. 4-7, and the active methanol, shown in Fig. 4-10, was quite similar in each case. Because the methanol transport from the reservoir to the anode was strongly controlled by the PCP in these experiments, the effect of the flow rate on the performance would be small. Strictly speaking, we understood that the current density for the air-breathing and the oxygen flow at 0.1l/min became constant during the experiment, and a decrease in the current density with time as shown in Fig. 4-7 was not observed in Fig. 4-10. This is because the depletion of the methanol in the reservoir did not occur under the active methanol conditions.

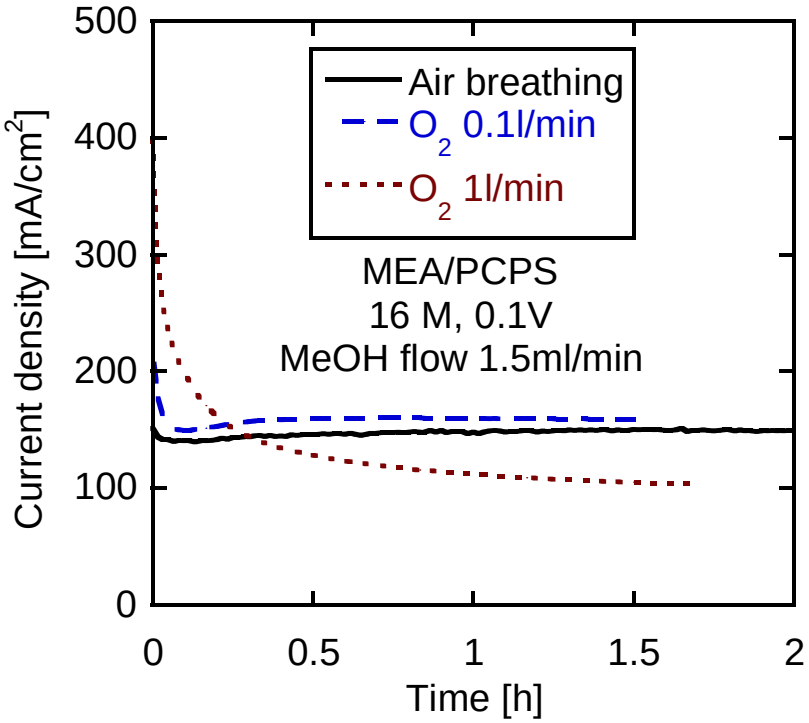

Figure 4-10: Current profile during continuous operation of a DMFC with porous plate, MEA/PCP, with different oxygen supplying modes under cell voltage 0.1V and flowing methanol 16M.

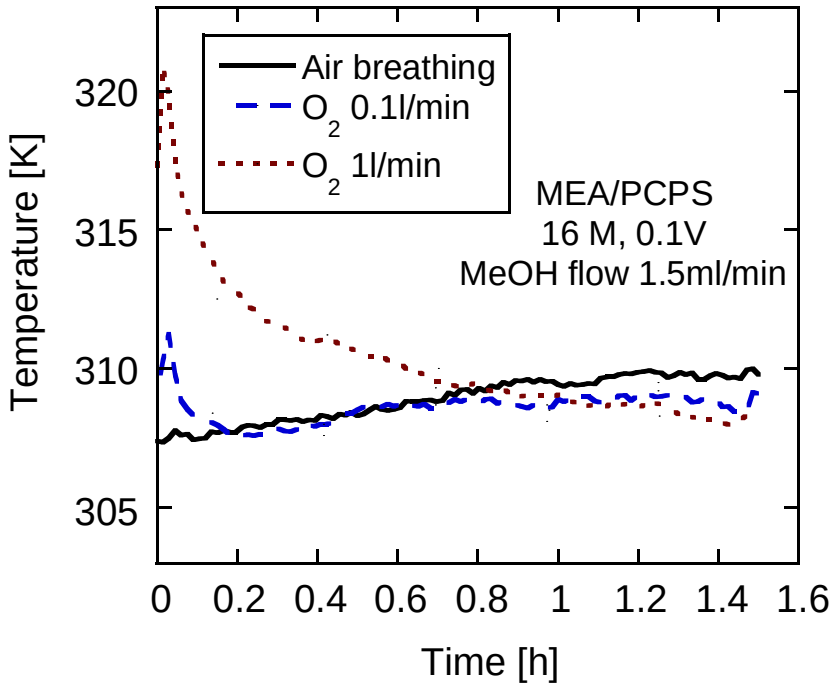

Figure 4-11: Variations in operating cell temperature of a DMFC with porous plate, MEA/PCP, operated with different oxygen supplying modes under cell voltage 0.1V and flowing methanol 16M.

In the case of the flowing oxygen at 1l/min, the current density was initially high, about 400mA/cm^2, but rapidly decreased. This high initial current density was related to the cell temperature which was about 320 K, almost 10K higher than those in the other cases as shown in Figure 4-11. The heat production by the oxidation of the initially accumulated methanol at the cathode under open circuit would be accelerated by the oxygen flow.

The above comparison in the DMFC performance between the MEA with and without the PCP made it clear that a very moderate supply of oxygen to the cathode, as with air-breathing, was appropriate for the MEA with the PCP. The employment of the PCP reduced the methanol crossover and prevented the MEA from flooding by controlling the mass transport of methanol and water by the PCP. Also the effect of the methanol flow rate on the cell performance was small compared to that of the MEA without the PCP. Such moderate methanol and water supplies would be desired for a practical DMFC system, because the excess power needed for the flow of oxygen and/or methanol can be minimized.

4. Conclusions

The performance of a DMFC with and without a PCP was investigated under different methanol/oxygen supply modes, passive and active supplies of methanol, and air-breathing and flowing supplies of oxygen, under ambient conditions using methanol concentrations of 2M for MEA without the PCP and 16M for that with the PCP. The following conclusions were drawn.

1) Both flooding at the cathode and depletion of methanol at the anode decreased the cell performance of the DMFC without the PCP. The Flow of both oxygen and methanol increased the current density.

2) The performance of the DMFC with a PCP was hardly affected by the flow either methanol or oxygen, due to the mass transport control by the PCP.

3) A moderate supply of oxygen to the cathode, such as air-breathing, was appropriate for the DMFC with a PCP.

4) Increasing the O_2 flow rate from 0.1l/min to 1l/min had a negative effect on cell performance both with and without a PCP, due to a cooling effect or a drying effect on the MEA.

References

1. A.S. Arico, S. Srinivasan, V. Antonucci, *Fuel Cells* **1** (2001) 133–161.
2. T. Schultz, K. Su Zhou, Sundmacher, *Chem. Eng. Technol.* **24** (2001) 1223–1233.
3. J.G. Liu, T.S. Zhao, R. Chen, C.W. Wong, *Electrochem. Commun.* **7** (2005) 288.
4. J.G. Liu, T.S. Zhao, Z.X. Liang, R. Chen, *J. Power Sources* **153** (2006) 61–67.
5. S. Surampudi, S.R. Narayanan, E. Vamos, H. Frank, G. Halpert, A. LaConti, J. Kosek, G.K. Surya Prakash, G.A. Olah, *J. Power Sources* **47** (1994) 377–385.
6. M.K. Ravikumar, A.K. Shukla, *J. Electrochem. Soc.* **143** (1996) 2601–2606.
7. S.R. Yoon, G.H. Hwang, W.I. Cho, I.-H. Oh, S.-A. Hong, H.Y. Ha, *J. Power Sources* **106** (2002) 215–223.
8. R. Chen, T.S. Zhao, *J. Power Sources* **152** (2005) 122–130.
9. B. Bae, B.K. Kho, T. Lim, I. Oh, S. Hong, H.Y. Ha, *J. Power Sources* **158** (2006) 1256–12261.
10. J.T. Wang, S. Wasmus, R.F. Savinell, *J. Electrochem. Soc.* **143** (1996) 1233–1239.
11. E. Peled, T. Duvdevani, A. Aharon, A. Melman, *Electrochem. Solid State Lett.* **3** (2000) 525–528.
12. M.V. Fedkin, X. Zhou, M.A. Hofmann, E. Chalkova, J.A. Weston, H.R. Allcock, S.N. Lvov, *Mater. Lett.* **52** (2002) 192–196.
13. T. Yamaguchi, M. Ibe, B.N. Nair, S. Nakao, *J. Electrochem. Soc.* **149** (2002) A1448–A1453.
14. M.L. Ponce, L. Prado, B. Ruffmann, K. Richau, R. Mohr, S.P. Nunes, *J. Membr. Sci.* **217** (2003) 5–15.
15. A.S. Arico, P. Creti, P.L. Antonucci, V. Antonucci, *Electrochem. Solid State Lett.* **1** (1998) 66–68.
16. C. Yang, S. Srinivasan, A.S. Arico, P. Creti, V. Baglio, V. Antonucci, *Electrochem. Solid State Lett.* **4** (2001) A31–A34.

17. N. Jia, M.C. Lefevre, J. Halfyard, S. Qi, P.G. Pickup, *Electrochem. Solid State Lett.* **3** (2000) 529–531.

18. I.J. Hobson, H. Ozu, M. Yamaguchi, M. Muramatsu, S. Hayase, *J. Mater. Chem.* **12** (2002) 1650–1656.

19. W.C. Choi, J.D. Kim, S.I. Woo, *J. Power Sources* **96** (2001) 411– 414.

20. S.R. Yoon, G.H. Hwang, W.I. Cho, I.-H. Oh, S.-A. Hong, H.Y. Ha, *J. Power Sources* **106** (2002) 215–223.

21. Y.K. Xiu, K. Kamata, T. Ono, K. Kobayashi, T. Nakazato, N. Nakagawa, *Electrochemistry* **73** (2005) 67–70.

22. N. Nakagawa, K. Kamata, A. Nakazawa, M. Ali Abdelkareem, K. Sekimoto, *Electrochemistry* **74** No.3 (2006) 221-225.

23. N. Nakagawa, M. Ali Abdelkareem, K. Sekimoto, *J. Power Sources* **160** (2006) 105–115.

24. M. Ali Abdelkareem, N. Nakagawa, *J. Power Sources* **162** (2006) 114-123.

25. G.Q. Lu, C.Y. Wang, T.J. Yen, X. Zhang, *Electrochim. Acta* **49** (2004) 821.

26. R. Chen, T.S. Zaho, J.G. Liu, J. Power Sources, *J. Power Sources* **157** (2006) 351–357.

27. C.Y. Chen, P. Yang, *J. Power Sources* **123** (2003) 37–41.

28. J.G. Liu, T.S. Zaho, Z.X. Liang, R. Chen, *J. Power Sources* **153** (2006) 61– 67.

29. J. Liu, G. Sun, F. Zhao, G. Wang, G. Zhao, L. Chen, B. Yi, Q. Xin, *J. Power Sources* **133** (2004) 175–180.

30. S. Yao, X. Tang, C.Hsieh, Y. Alyousef, M. Vladimer, G.Fedder, C. Amon , *Energy* **31** (2006) 636–649.

CHAPTER 5

The Role of Carbon Dioxide Layer Prepared By a Porous Carbon Plate in a Passive DMFC as a Mass Transport Barrier

1. Introduction

Direct methanol fuel cells (DMFCs) are a promising power sources for the mobile electric devices and automobiles because of their high theoretical energy densities, low operating temperatures and simple design. However, the energy density of the DMFCs currently under development is still far from that expected due to the methanol crossover and the high over voltage at the electrodes [1-4]. Methanol crossover, MCO, from anode to cathode significantly reduced the cell potential, lowered fuel utilization and lowered methanol concentration resulting in the optimum concentration of 2 to 3mol/L [5, 6] under active conditions and about 5mol/L [7–9] under passive conditions. To overcome the methanol crossover, a large number of studies [10–14] were carried out for developing a new membrane and modifying the existing membranes. On the other hand, the authors proposed a novel electrode structure employing a porous carbon plate, PCP, for anode in order to control the methanol crossover [15-19]. Such attempt by controlling the methanol transport by modifying a part of electrode components was seen in some recent reports [20-22].

In chapter (2) we have demonstrated, that a passive DMFC with a porous carbon plate, PCP, under open circuit conditions significantly reduced the methanol transport from methanol reservoir to the anode surface. The separation of methanol through this type of passive DMFC under open circuit conditions was explained by diffusion control of the methanol transport by the PCP depending on the properties of the porous material, i.e., thickness, porosity and water absorptivity of the porous material. In chapter (3) the performance was tested under closed circuit conditions, the PCP and the CO_2 gas layer that formed between the anode and the porous plate stably controlled the mass transport of methanol and water from the reservoir to the anode, and this facilitated operation with very high concentrations of methanol, even neat methanol.

In this chapter, we will study the importance of the existence of the gas barrier on the performance of this type of passive DMFCs, the relation between the gas discharge through or not through the PCP and the DMFC performance was investigated for the

passive DMFC with PCPs with different pore structures. When the gas was not discharged through the PCP, its pressure was controlled and its effect on the performance was studied. The results were discussed on the basis of the effect of pore structure of PCP on the transport of methanol through the PCP to the anode.

2. Experimental

2.1. MEA preparation

The conventional MEA, which uses Pt and Pt-Ru black as the catalyst for the cathode and anode, respectively, was prepared and fabricated in the same manner as described in chapter (3). The catalyst loading was 10mg/cm^2 in each electrode. The same MEA was used for the different PCPs shown below.

2.2 Porous carbon plates, PCP

The porous carbon plates, PCPs, used for anode in this study was supplied from Mitsubishi Pencil Co., Ltd., the properties and pore structure of these porous carbon plates were listed in Table 5-1.

Table 5-1: Properties of the carbon plates used

PCP	δ (mm)	α_W (-)	Pore structure measured by the mercury porosimeter			By the Perm-porometer	
			V_P (cm^{3}g^{-1})	$d_{P,ave}$ (μm)	ε (-)	$P_{b.p.}$(kPa)	$dp_{,b.p.}$ (μm)
PCPY	1.0	0.40	0.543	42.3	0.417	3.05	14.8
PCPS	1.0	0.15	0.556	1.425	0.457	42.76	1.05

δ: Thickness; α_W: Water absorptivity; V_P: Total cumulative volume; d_P: Pore diameter;

ε: Total porosity; $P_{b.p}$: Bubble point pressure; $dp_{,b.p}$: Bubble point pore diameter

One of the porous carbon plates, PCPS, was made of graphite carbon and amorphous carbon and had a small pore size about 1μm in diameter. Another porous carbon plate, PCPY, was made of amorphous carbon and had a large pore size over 40 μm. The microstructure of these porous plates was measured by using a mercury porosimeter, (Pascal 140 + 440, Thermo Finnigan, Inc.). Perm-porometer (Porous Materials Inc.) was also used to measure the bubble point pressure and the bubble pore diameter, using

Galwick solution with surface tension 0.0157 N/m, the surface tension of this solution was near of that of methanol 0.022 N/m.

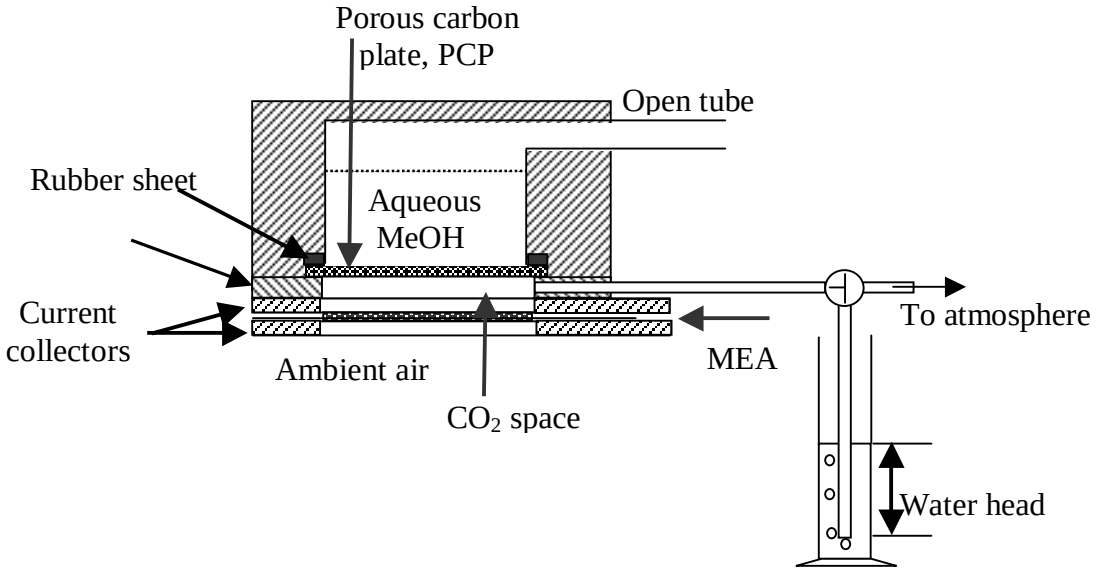

Figure 5-1 Schematic diagram of passive DMFC with porous plate and CO_2 control arrangements

2.3 Passive DMFC with PCP

MEA with the porous carbon plate was set in a plastic holder as shown in Figure 5-1. In the anode compartment, a methanol reservoir, 12cm^3, was prepared. The MEA was sandwiched between two current collectors, which were stainless steel plates of 2mm thickness with open holes with 73% open ratio for the passages of fuel and oxidant. The cell was arranged horizontally by keeping the reservoir upside to ensure a consistent contact between the solution and PCP.

2.4 CO_2 discharge and pressure control

For the DMFC with PCP shown in Fig. 5-1, CO_2 gas that produced at the anode was accumulated and the CO_2 gas layer was formed between the porous plate and the anode under closed circuit conditions and this gas layer obstruct methanol transport from the reservoir to the anode [17]. To investigate the effect of the pore structure of the PCP on the formation of the CO_2 layer, rote of CO_2 discharge not through the PCP was prepared, and then, the effect of the gas discharge through this additional rote was investigated. To do this, a spacer of 5mm thickness with a thin tube with 3mm o.d. for gas discharge was fixed between the anode current collector and the PCP as shown in Fig. 5-1. This tube was

connected to a three way valve of which one outlet was opened to the atmosphere and another one was connected to a tube immersed in water with a certain head. When the valve connected the line immersed in water, the pressure of the CO_2 gas layer was controlled by the water head, and CO_2 discharged through either PCP or the immersed tube depending on the water head. For PCPY, CO_2 discharged through the immersed tube when the height of water head was less than 17cm that was the bubble point of the plate with the methanol solution. While for PCPS, CO_2 went through the immersed tube at all the height used in this experiment.

2.5 Measurement of the cell performance and fluxes through the PCP

All the experiments were conducted in a complete passive mode with the surrounding air at ambient conditions (293K and 1atm). After feeding a methanol solution, 6 to 7cm^3, with a certain concentration into the reservoir by a syringe through the injection tube, time progress of the current density, i-t characteristics, at 0.1V was measured using an electrochemical measurement system (HAG-5010, Hokuto Denko, Co., Ltd.). The temperature of the cell was also measured using a thermocouple placed between the anode current collector and the porous plate. At the end of the i-t experiments, the average methanol and water fluxes through PCP during the i-t experiments were calculated based on the weight loss of the cell holder and concentration change of the methanol solution before and after the i-t experiments as described in chapter (3). The methanol flux across PCP means the methanol crossover itself when the valve closed. However, it means the sum of the methanol crossover and the methanol went out through the tube.

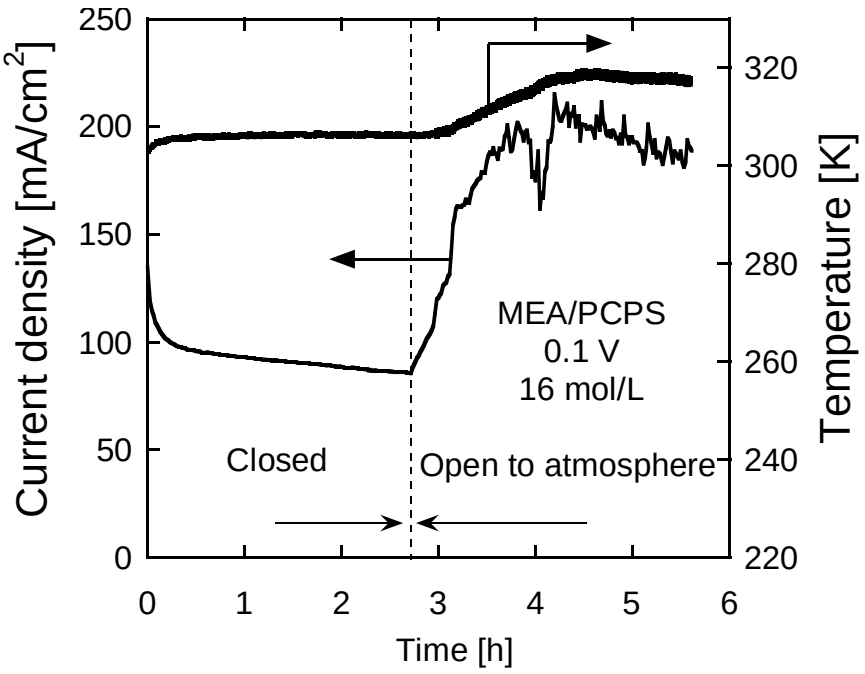

Figure 5-2 Current profile during continuous operation of passive DMFC with PCPS, MEA/PCPS, at cell voltage of 0.1V and 16M with different valve operations, closed and open to the atmosphere

3. Results and discussion

3.1. Effect of valve operation, open and close

Figure 5-2 shows the effect of the valve operation, close and open to the atmosphere, for the passive DMFC with the porous plate, PCPS, on the current density at 0.1V and 16mol/L. At the beginning, the valve was closed. The current density was initially high 140mA/cm^2 and decreased to 100mA/cm^2 within a few minutes, then slightly decreased within 2.7h to 90mA/cm^2. During this time, the cell temperature was almost constant at 305K. The initial decrease in current density was due to the controlled rate of the methanol transfer by the CO_2 gas layer formed between PCP and the anode surface [17]. At this condition with PCPS, the current density was controlled by the rate of methanol supply to the anode [19]. When the valve was opened to the atmosphere at 2.7h, current density increased up to about 200mA/cm^2 and the cell temperature increased up to 318K. These increases were caused by the higher methanol supply caused by the valve opening to the atmosphere, where the gas accumulated in the CO_2 gas layer discharged to the atmosphere through the tube. Therefore the resistance to the methanol transport through the PCP decreased and a larger amount of methanol reached to the anode surface resulting in larger current density.

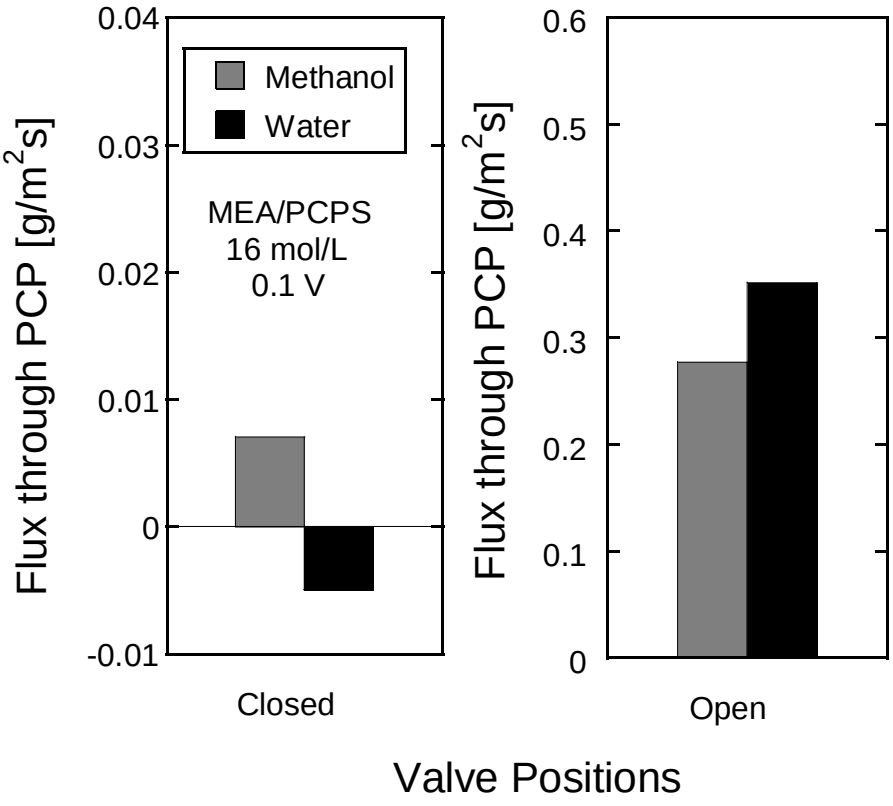

Figure 5-3 The effect of the valve operation on the methanol and water fluxes across PCPS, at cell voltage of 0.1V and 16M.

However, at the same time, the cell temperature increased, flooding appeared at the cathode surface and fluctuations were seen in the current density suggesting that a large methanol crossover occurred.

Figure 5-3 shows the methanol and water fluxes through the PCP for the i-t experiments shown in Fig. 5-2. As clear from the figure, the methanol flux increased with the valve opening from 0.007 g/m^2s to 0.277 g/m^2s, while, the back diffusion of water, the negative flux of water, appeared only in case of the complete inclusion of the CO_2. This clearly showed the blocking of the CO_2 gas generated at the anode from escaping from the space between the PCP and the anode to the outside significantly controlled the methanol flux through the PCP. Although the methanol flux at the valve opening was relatively high, the methanol solution in the reservoir remained for a couple of hours after the opening suggesting the resistance of PCPS to the flow of the methanol solution was relatively high.

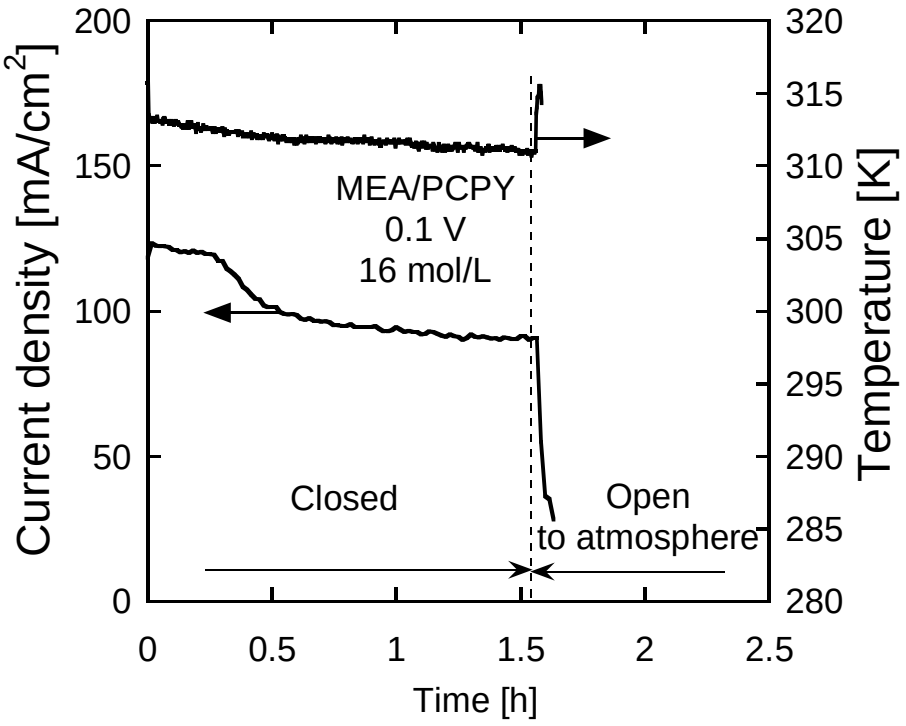

Figure 5-4 Current profile during continuous operation of passive DMFC with PCPY, MEA/PCPY, at cell voltage of 0.1V and 16M with different valve operations, closed and open to the atmosphere.

Figure 5-4 shows the effect of the valve operation on the performance for the passive DMFC using PCPY at 0.1V and 16 mol/L. When the valve was closed, the current density became stable at 100mA/cm^2 after 1.5h. It rapidly decreased to less than 20mA/cm^2 within a few minutes when the valve was opened to the atmosphere. At this condition, methanol solution in the reservoir flowed out through the PCP and then through the open tube within a few minutes showing that the resistance of PCPY for the fluid flow was relatively small. The calculated fluxes in the case of Fig. 5-4 were shown in Figure 5-5. The very large fluxes of methanol and water through PCPY resulted in a large methanol crossover to the MEA then the current density reduced very rapidly and flooding at cathode appeared. The sudden increase of the cell temperature just after the valve opening as shown in Fig. 5-4 also supported the large methanol crossover. PCPY which had large size of pore diameter, 42μm, could not resist methanol transport by the permeation when CO_2 escaped to the atmosphere.

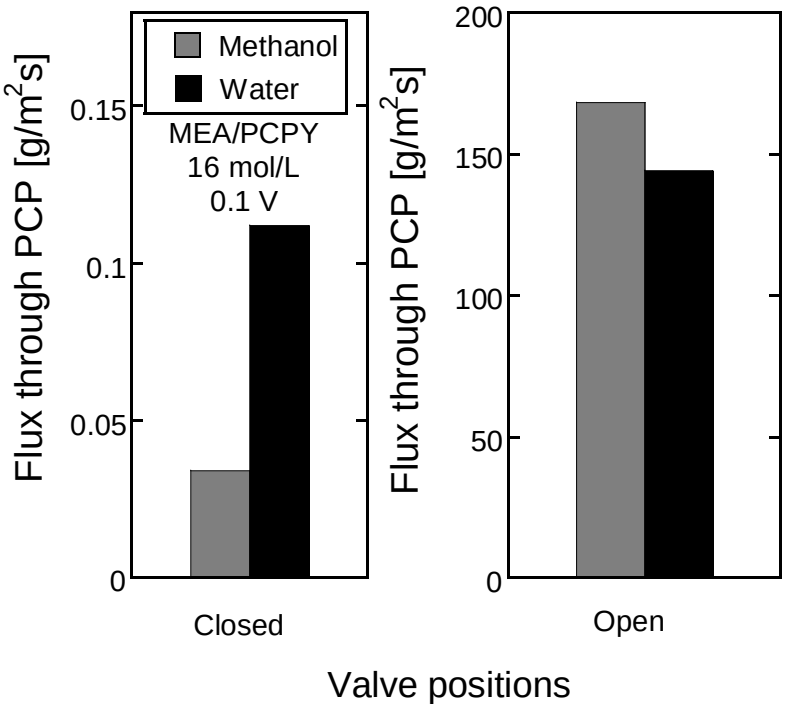

Figure 5-5 The effect of the valve operation on the methanol and water fluxes across PCPY, at cell voltage of 0.1V and 16M.

3.2. The effect of the pressure of the CO_2 gas layer

Figure 5-6 shows the variations in the current density for DMFC with PCPS at different CO_2 pressures measured by opening the three way valve to the tube immersed in the water and changing the water head. The current density at five hours in the i-t experiment was nominated as the steady current density and plotted against CO_2 pressure at different methanol concentrations 10mol/L and 20mol/L. It was clear that the current density was not affected by the pressure of the CO_2 gas layer within the measured range.

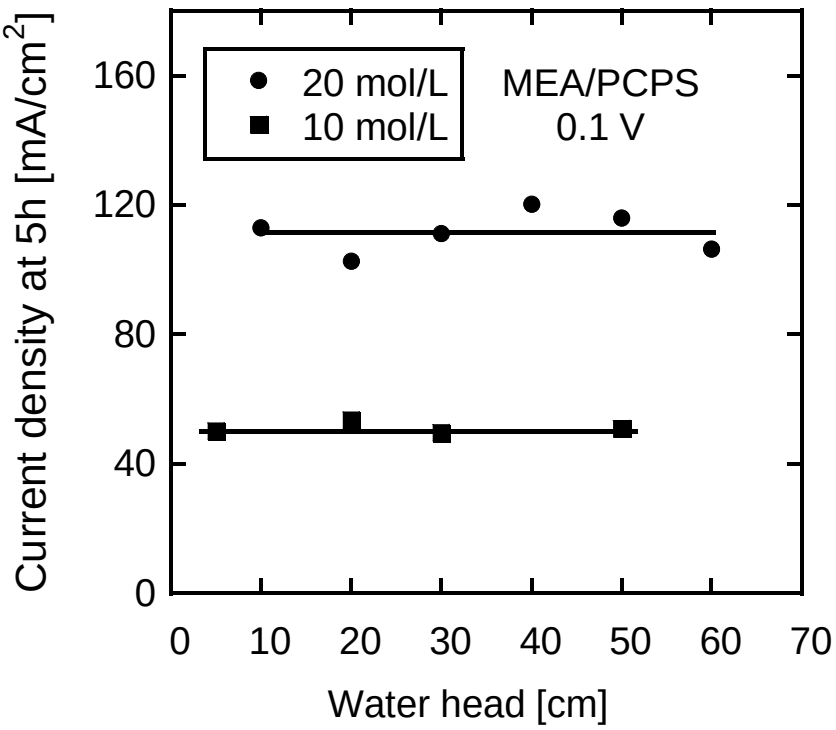

Figure 5-6 Effect of CO_2 gas pressure on the steady current density for MEA/PCPS at 0.1V and different methanol concentrations, 10M and 20M.

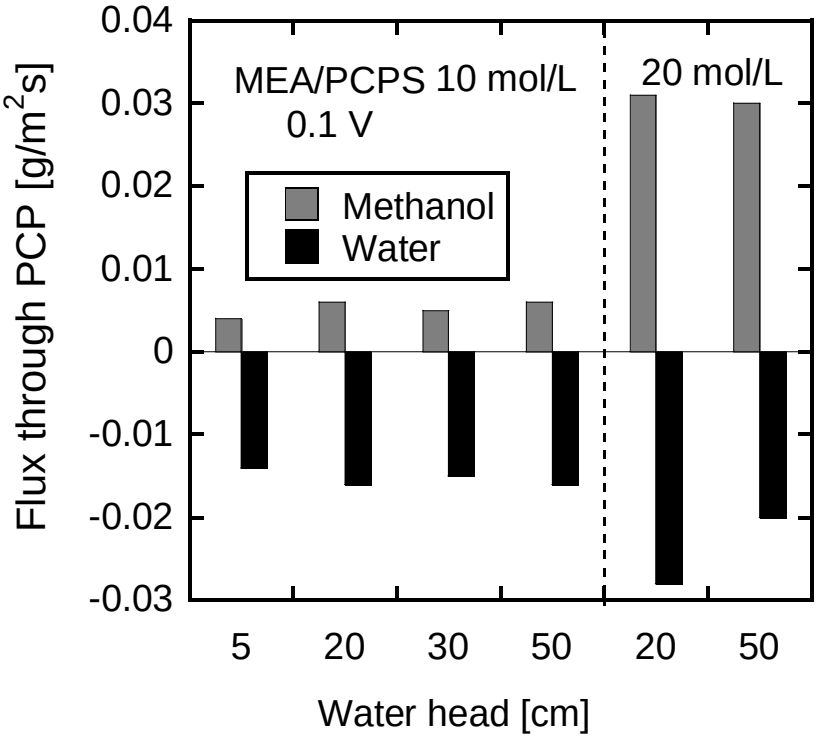

Figure 5-7 Effect of CO_2 gas pressure on the methanol and water fluxes across PCPS, at 0.1V using different methanol concentrations, 10M and 20M.

In this range, the methanol and water fluxes were almost independent on the pressure as shown in Figure 5-7. From this figure, we could understand that the rate of methanol supply to the anode through the PCP and the gas layer was kept constant, and the current density was not affected by the changes of the pressure. The negligible effect of the pressure was reasonable, because of the small pressure changes in this case, less than one order of magnitude, comparing to that affected the DMFC performance reported [23,24]. The DMFC with PCPS was operated under limiting current conditions in the methanol concentrations below 20 mol/L as shown in our previous paper [19]. This was clearly shown in Fig. 5-6 where the current density was proportional to the methanol concentration, 50mA/cm^2 at 10mol/L and 100mA/cm^2 at 20M. By comparing the current density at 16mol/L shown in Fig. 5-2, 90mA/cm^2 at 2.5h in the case of the valve closed situation and 200mA/cm^2 at 4h in the case of the valve open situation, it was suggested that the gas pressure as small as 5cm H_2O (0.5kPa) was enough to prevent the methanol solution from the flow down through the PCP and from a direct contact to the anode. The porous carbon plate PCPS that had a small pore size and a high bubble point pressure could control the methanol flux very strictly.

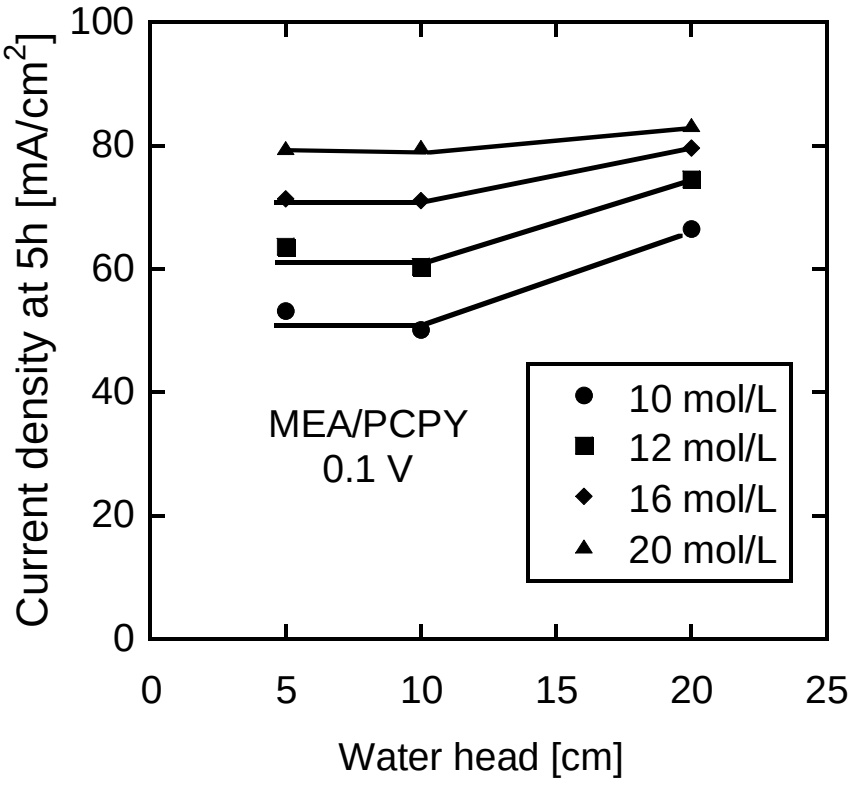

Figure 5-8 Effect of CO_2 gas pressure on the steady current density for MEA/PCPY at 0.1V and different methanol concentrations, 10, 12, 16 and 20M.

Figure 5-8 shows the variations in the current density for DMFC with PCPY at different CO_2 pressures and methanol concentrations. The current density increased with increasing the concentration, but not linearly proportional to the methanol concentration, on contrast to the case of PCPS shown in Fig. 5-6. The non linear dependency of the current density on the methanol concentration suggested that the current density was not under the limiting current conditions. This could be confirmed in Figure 5-9 which shows the fluxes of methanol and water through the PCP for the case of Fig. 5-8. The methanol flux was almost double of that in case of PCPS at the same methanol concentration, while the fluxes were very much reduced by pressurizing the gas between the PCP and the anode even with a small water head height than the case of the direct discharge of the CO_2 to the atmosphere, Fig. 5-5.

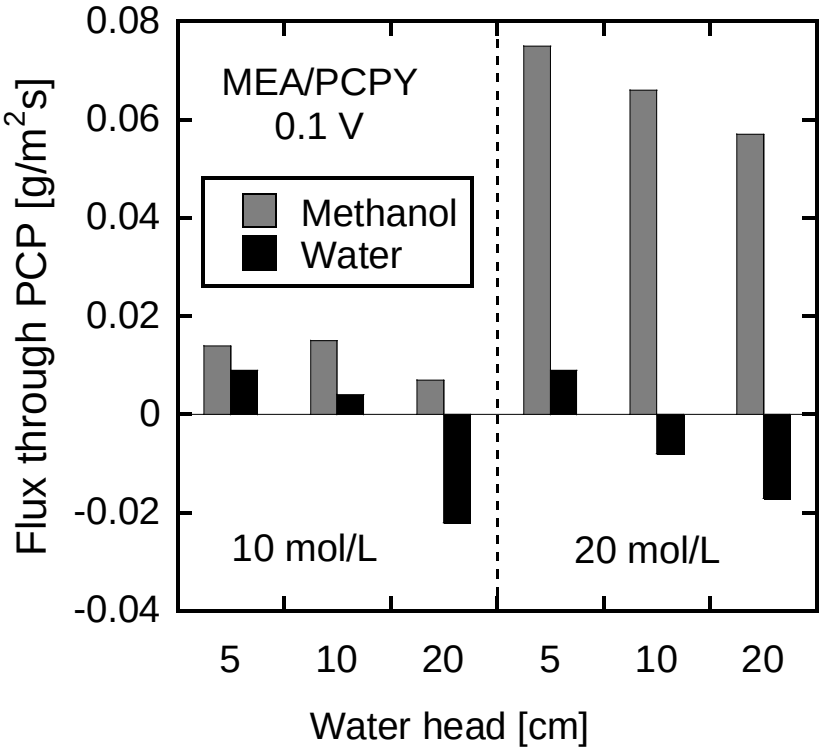

Figure 5-9 Effect of CO_2 gas pressure on the methanol and water fluxes across PCPY at 0.1V using different methanol concentrations, 10M and 20M.

In the experiments shown in Fig. 5-8, gas bubbles discharged through the tube immersed in the water at 5 and 10cm water head, while it discharged through the PCP at 20cm water head. The current density was not affected by increasing CO_2 pressure from 5 to 10cm but it increased at 20cm. This would be resulted from the complete formation of the gas barrier at 20cm thereby methanol flux through the PCP reduced as shown in figure 5-9 so

the performance increased. In the cases of the CO_2 gas discharged through the tube immersed in the water, very tinny droplets of solution as a humid were seen on the inner surface of the hose. On the other hand the comparison of the different PCPs under the situation of the complete formation of the gas barrier it was clear that the bubble discharge through the PCP accelerated the methanol and water fluxes through the PCP when the pore diameter is large, like 40μm. Where a bubble discharged out the surface of the PCP, the same solution volume will replace it in the PCP therefore accelerating the flux of the solution through the PCP and this not happen in case of PCPS with the small pore diameter.

4. Conclusions

The effect of CO_2 discharge from the CO_2 gas layer formed between the anode surface and the PCP was investigated in order to clear the effect of the PCP and the CO_2 gas layer on the performance and mass transfer in a passive DMFC using different types of PCPs with different pore structures, and the following conclusions were drawn;

1) The formation of CO_2 gas layer was very important for the strong obstructing the methanol transport to the anode surface where the gaseous methanol diluted in the CO_2 gas contacted. The resistance to the methanol transport across the PCP was affected by the pore structure of the PCP, i.e., pore size and the bubble point pressure.

2) When the pore size was large, 42μm, the bubble through the PCP accelerated the methanol transport.

3) The changes of the CO_2 pressure affect the performance only when they affect the methanol and water fluxes through the PCP within the measured pressure range.

5. References

1. A.S. Arico, S. Srinivasan, V. Antonucci, *Fuel Cells* **1** (2001) 133–161.
2. T. Schultz, K. Su Zhou, Sundmacher, *Chem. Eng. Technol.* **24** (2001) 1223–1233.
3. J.G. Liu, T.S. Zhao, R. Chen, C.W. Wong, *Electrochem. Commun.* **7** (2005) 288.
4. J.G. Liu, T.S. Zhao, Z.X. Liang, R. Chen, *J. Power Sources* **153** (2006) 61–67.
5. S. Surampudi, S.R. Narayanan, E. Vamos, H. Frank, G. Halpert, A. LaConti, J. Kosek, G.K. Surya Prakash, G.A. Olah, *J. Power Sources* **47** (1994) 377–385.
6. M.K. Ravikumar, A.K. Shukla, *J. Electrochem. Soc.* **143** (1996) 2601–2606.
7. S.R. Yoon, G.H. Hwang, W.I. Cho, I.-H. Oh, S.-A. Hong, H.Y. Ha, *J. Power Sources* **106** (2002) 215–223.
8. R. Chen, T.S. Zhao, *J. Power Sources* **152** (2005) 122–130.
9. B. Bae, B.K. Kho, T. Lim, I. Oh, S. Hong, H.Y. Ha, *J. Power Sources* **158** (2006) 1256–12261.
10. J.T. Wang, S. Wasmus, R.F. Savinell, *J. Electrochem. Soc.* **143** (1996) 1233–1239.
11. E. Peled, T. Duvdevani, A. Aharon, A. Melman, Electrochem. *Solid State Lett.* **3** (2000) 525–528.
12. M.V. Fedkin, X. Zhou, M.A. Hofmann, E. Chalkova, J.A. Weston, H.R. Allcock, S.N. Lvov, *Mater. Lett.* **52** (2002) 192–196.
13. T. Yamaguchi, M. Ibe, B.N. Nair, S. Nakao, *J. Electrochem. Soc.* **149** (2002) A1448–A1453.
14. M.L. Ponce, L. Prado, B. Ruffmann, K. Richau, R. Mohr, S.P. Nunes, *J. Membr. Sci.* **217** (2003) 5–15.
15. N. Nakagawa, K. Kamata, A. Nakazawa, M. Ali Abdelkareem, K. Sekimoto, *Electrochemistry* **74** No.3 (2006) 221-225.
16. N. Nakagawa, M. Ali Abdelkareem, K. Sekimoto, *J. Power Sources* **160** (2006) 105–115.
17. M. Ali Abdelkareem, N. Nakagawa, *J. Power Sources* **162** (2006) 114-123.

18. M. Ali Abdelkareem, N. Nakagawa, *J. Power Sources* **165** (2007) 685-691.

19. M. Ali Abdelkareem, N. Nakagawa, *J. Power Sources* **172** (2007) 659-665.

20. F. Liu, G. Lu, C. Wang, *J. Electrochem. Soc.* **153** (2006) A543–A553.

21. C. Chung, W. Kim, H. Choi, Y. Lee, S. Cho, J. Nam, Direct Methanol Fuel Cell Having Reduced Crossover of Methanol and Comprising a Layer of Material for Controlling the Diffusion Rate of Fuel, *U.S. Patent No.* **0026286A1.**

22. Z. Guo, A. Faghri , *J. Power Sources* **160** (2006) 1142-1155.

CHAPTER 6

Factors Affecting Methanol Transport in a Passive DMFC Employing a Porous Carbon Plate

1. Introduction

Nowadays, the technology for portable applications (computers, mobile phones, etc.) is in constant evolution for the development of smaller and lighter devices with more performing integrated functions. As a consequence, the on board energy density is a key parameter which has to be taken into account [1]. Up to now, lithium based technology is currently used (volumic energy close to 500 Wh L^{-1}) [2,3], but mini fuel cells seem to be a very promising alternative as power supply for the next generation systems. In spite of its high specific energy (32 Wh g^{-1}) [4] and because of storage problems in portable systems, the use of hydrogen as fuel is dismissed [5]. Liquid fuels as alcohols seem better adapted to the targeted technology. Indeed, alcohols are easy to store and have a relatively good energy density: 6.1 Wh g^{-1} (4800 Wh L^{-1}) and 8.6 Wh g^{-1} (6800 Wh L^{-1}) for methanol and ethanol, respectively [6].

Nevertheless, several problems have to be overcome. Low power densities are still currently obtained in DMFC due to the methanol crossover and low reaction kinetics [7-9]. To overcome the methanol crossover, a large number of studies were carried out whether for developing a new proton-conducting membrane with a low methanol permeability and high proton conductivity or modifying of the existing membranes [10–21]. A few reports have considered reducing the ability for methanol crossover by mass transport control in the backing layer [22-27].

Lu et al., added a compact micro porous layer to the backing structure as a barrier to the mass transport of methanol across the MEA. Thereby the rate of methanol crossover was reduced, but the maximum methanol concentration that can be used was as low as 8M [22]. Recently, Guo et al., controlled the mass transport of methanol and water by storing them in hydrophobic and hydrophilic porous media respectively and they succeeded in using neat methanol but with the addition of water from time to time, and they did not considered the effect of CO_2 under the closed circuit conditions on the mass transport of the solution [27]. Others have considered the control of methanol transport from the

reservoir to the anode surface via pervaporation membranes where methanol was supplied in the gaseous phase [28].

In chapter (2) we have studied the effect of the porous material properties on the methanol and water fluxed across this novel DMFC under open circuit conditions, and results show that the separation of methanol through was dependent on the properties of the porous material, i.e., thickness, porosity and water absorptivity of the porous material.

And we confirmed in chapter 5 that , the formation of CO_2 gas layer was very important for the strong obstructing the methanol transport to the anode surface where the gaseous methanol diluted in the CO_2 gas contacted.

In this chapter, we investigated the effect of pore structure and thickness of the porous plate on the mass transport of methanol from the methanol reservoir to the anode surface under closed circuit conditions, and how these properties affect the cell performance and MCO. Also, the effect of the gas barrier thickness on the methanol transport and cell performance was investigated. We will discuss the mechanism for the restriction of the methanol transport in the case of DMFC using PCP.

2. Experimental

2.1. MEA preparation

The conventional MEA, which uses Pt and Pt-Ru black as the catalyst for the cathode and anode, respectively, was prepared and fabricated in the same manner as described in chapter (3). The catalyst loading was 10-12mg/cm^2 in each electrode.

Table 6-1: Properties of the carbon plates used:

PCP	δ (mm)	α_W (-)	Pore structure measured by the mercury porosimeter			By the Perm-porometer	
			V_P (cm^3g^{-1})	$d_{P,ave}$ (μm)	ε (-)	$P_{b.p.}$(kPa)	$dp_{,b.p.}$ (μm)
PCPY1	1.0	0.40	0.543	42.3	0.417	3.05	14.8
PCPY2	2.0	0.21					
PCPS1	1.0	0.15	0.556	1.425	0.457	42.76	1.05

δ: Thickness; α_W: Water absorptivity; V_P: Total cumulative volume; d_P: Pore diameter;

ε: Total porosity; $P_{b.p}$: Bubble point pressure; $dp_{,b.p}$: Bubble point pore diameter

2.2 Porous carbon plates, PCP

The porous carbon plate, PCP, used for anode in this study was supplied from Mitsubishi Pencil Co., Ltd., the properties and pore structure of these porous carbon plates were listed in Table 1. The porous carbon plates were categorized into two types: the S type, PCPS, which was made of graphitic carbon and amorphous carbon and the Y type, PCPY, which was made of amorphous carbon. The microstructure of these porous plates was measured by using a mercury porosimeter, (Pascal 140 + 440, Thermo Finnigan, Inc.). Perm-porometer (Porous Materials Inc.) was used to measure bubble point pressure, bubble pore diameter, using Galwick solution with surface tension 15.7 dyne/cm, and the resistivity of the two types of PCPs to air flow.

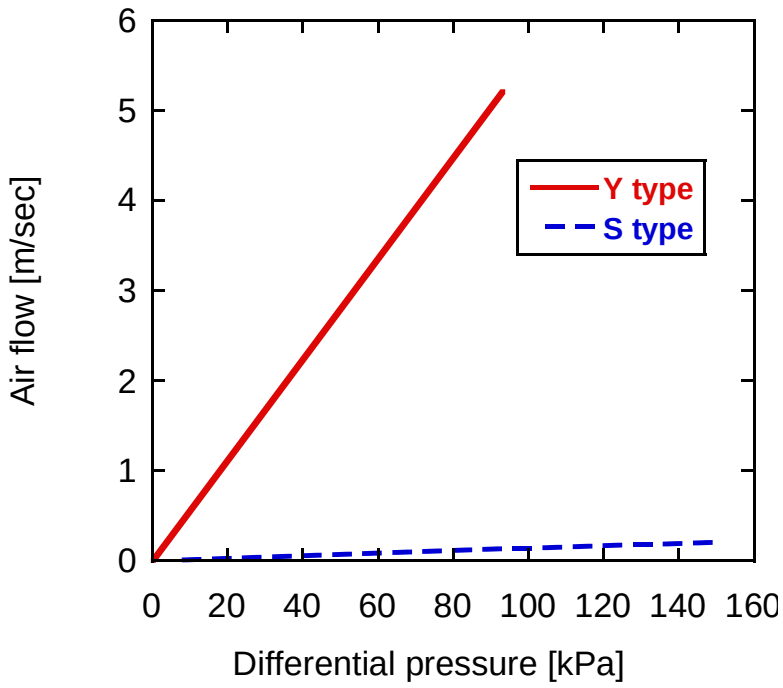

Figure 6-1: Effect of PCP type on the air flow resistivity.

Figure 6-1 clearly showed that the resistivity for the air flow of the PCPS was larger than that of PCPY type due to its smaller pore diameter. As shown in Table 6-1, PCPY had larger pore diameter than that for PCPS, and PCPY was used in two thickness 1mm, PCPY1 and 2mm, PCPY2 to investigate the effect of the PCP thickness. Water absorptivities, as defined in chapter (2), of the different PCPs were measured and also shown in Table 6-1.

2.3 Passive DMFC with PCP

MEA with the porous carbon plate was set in a plastic holder as shown in Figure 6-2. In the anode compartment, a methanol reservoir, 12cc, was prepared. The MEA was sandwiched between two current collectors, which were stainless steel plates of 2mm thickness with open holes for the passages of fuel and oxidant. The open ratio of the area for the active electrode was 73%. The cell was arranged horizontally keeping the reservoir upside to ensure a constant contact between the solution and the PCP.

2.4 Operation under the barrier of gas with different thicknesses

As a result of the configuration mentioned above, methanol had to pass through the porous plate then through the openings of the anode current collector. Under closed circuit conditions, the openings of the anode current collector were filled with CO_2 gas which is enclosed between the porous plate and the anode. Therefore, a layer of CO_2 gas was formed between the porous plate and the anode, and this gas layer obstruct methanol transport from the reservoir to the anode, methanol have to be transported through the gas layer as vapor. To show the effect of the thickness of this gas barrier on the performance of passive DMFC, different thicknesses of this gas barrier were prepared by changing the thickness of the anode current collector, i.e., 1mm, 2mm, 3mm and 7mm.

1. MEA
2. Current collectors (2mm thick.)
3. Porous carbon plate, PCP
4. Rubber sheet
5. Aqueous methanol solution
6. Open tube

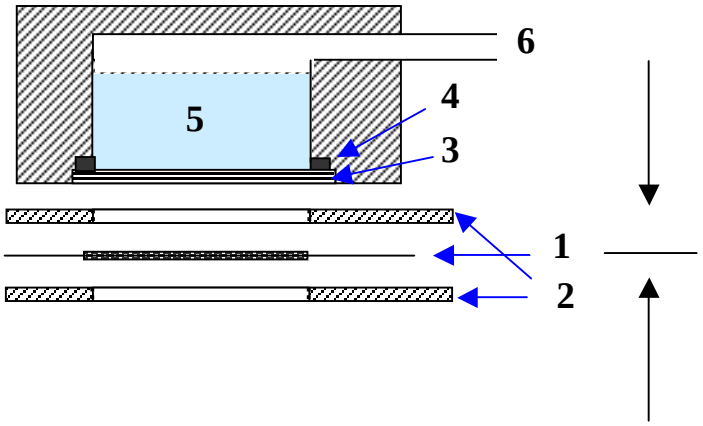

Figure 6-2: Schematic diagram of passive DMFC with porous plate.

2.5 Measurement of the cell performance

In this study, all the experiments were conducted in a complete passive mode with the surrounding air at ambient conditions (293K and 1atm). Methanol solution, 6 to 7cc, with different concentration, from 2M to neat methanol, was fed into the reservoir by a syringe through the open tube. We avoided the MEA from direct contact with the solution for a long time, when the methanol concentration was high. Current-voltage, i-V, characteristics were measured by the linear sweep voltammetry from the OCV to zero with the scan rate 1mV/sec. After that, time progress of the current density, i-t characteristics, at the different cell voltages 0.1, 0.2 and 0.3V was measured for 5h to 12h. These measurements were conducted by using an electrochemical measurement system (HAG-5010, Hokuto Denko, Co., Ltd.). The temperature of the cell was also measured using a thermocouple placed between the surface of anode current collector and the porous plate.

At the end of the i-t experiments for a certain methanol concentration, the weight loss of the entire cell holder was measured and the methanol concentration of the remained solution in the reservoir was also measured by a gas chromatography. From the results, methanol and water fluxes during the i-t experiment were calculated as shown below. And then, the remained solution was removed from the reservoir, and a new solution with another concentration was injected in the cell. And hence, the same measurements were conducted for the new solution.

2.6 Evaluation of the methanol, water fluxes and energy density

The average methanol and water fluxes during the i-t experiments were calculated based on the weight loss and concentration change of the methanol solution before and after the i-t experiments as well as the amount of methanol and water electrochemically reacted at the anode as described in chapter (3). Methanol and water reacted at the anode were calculated with the assumption that every molecule of methanol was completely converted to carbon dioxide producing 6 electrons and no intermediates. Faraday efficiency for each concentration was calculated by dividing the reacted methanol at the anode by the total methanol loss during the i-t experiment as described in chapter (3).

Energy density was calculated on the basis of the volume of methanol solution input and completely consumed at the anode, evaluating the results from 2M to a certain methanol concentration according to the following equation:

$$\text{Energy density} = \eta_f \, \eta_v \, \Delta G \, C_{max}$$

Where:

ΔG: Gibbs free energy of the oxidation reaction of methanol to produce CO_2 and water, 726kJ/mol, C_{max}: maximum methanol concentration could be used at certain cell voltage; η_f: the average faraday efficiencies of all methanol concentration which could be used at a definite cell voltage; η_v: voltage efficiency calculated by dividing the operated cell voltage, i.e. 0.1, 0.2 or 0.3V by the theoretical cell voltage of DMFC, 1.18V.

3. Results and discussion

3.1. Time progress of the current at different constant cell voltages

Figure 6-3 shows the variations in current density at 0.1V for MEA/PCPS1 with different methanol concentrations ranged from 4M to 22M. Current density initially somewhat decreased and within few minutes it became nearly constant with time. The difference between the initial and the nearly stable current density was increased with increasing methanol concentration; i.e., in the case of 20M it was initially about 270mA/cm^2 and decreased within five minutes to 170mA/cm^2. The initial decrease in current density would be caused by the initial methanol accumulated at the anode surface under the open circuit conditions, where PCP was left in contact with methanol solution until saturation before flowing current, during this time large MCO occurred and cell temperature was initially

high [25]. The value of the nearly stable current density was increased with increasing methanol concentration where it increased from about 20mA/cm^2 at 4M to about 170mA/cm^2 at 22M. The current density was nearly constant with time due to the employment of the PCP, which constantly regulated the methanol transfer rate from the reservoir to the anode and prevented the excess loss of methanol by MCO [25].

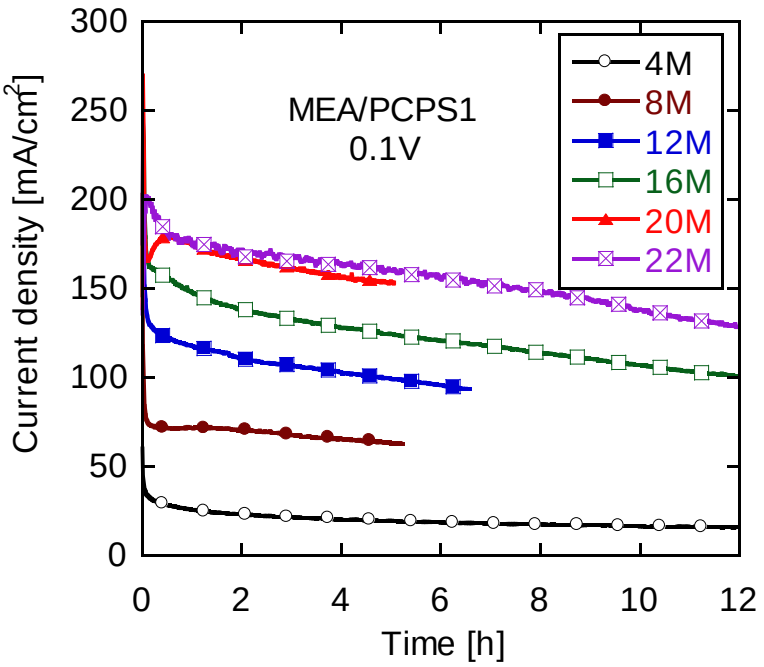

Figure 6-3: Current profile during continuous operation of passive DMFC with PCPS1, MEA/PCPS1, at cell voltage of 0.1V.

Figure 6-4 shows the variations in current density at 0.3V for MEA/PCPY1 with different methanol concentrations. Current density increased with increasing methanol concentration up to 18M then decreased with further increase in methanol concentration. At 22M, the initial performance was very high, showing about 60mW/cm^2, but it decreased with time, and a constant power density around 30mW/cm^2 could be obtained. Fluctuations with a certain frequency in current density appeared at high methanol concentrations at more than 14M. The initial decrease in current would be related to the same reasons shown above for PCPS1, but it took here longer time for the current density to be stable. This longer time should be due to the larger pore diameter of PCPY1 therefore lower resistivity to methanol transfer. The decrease in current density with increasing methanol concentration from 18M to 22M would be caused by the high MCO at 22M than 18M, as the dependency of MCO on the methanol concentration will be shown later. The fluctuations in current could not be related to the flooding, because

neither water film nor water droplets were found in all of the experiments. The fluctuation may be related to the evolution of CO_2 bubbles from the porous plate which in turn will affect the methanol transfer across the PCP, this process occurred periodically so fluctuations appeared in the current density.

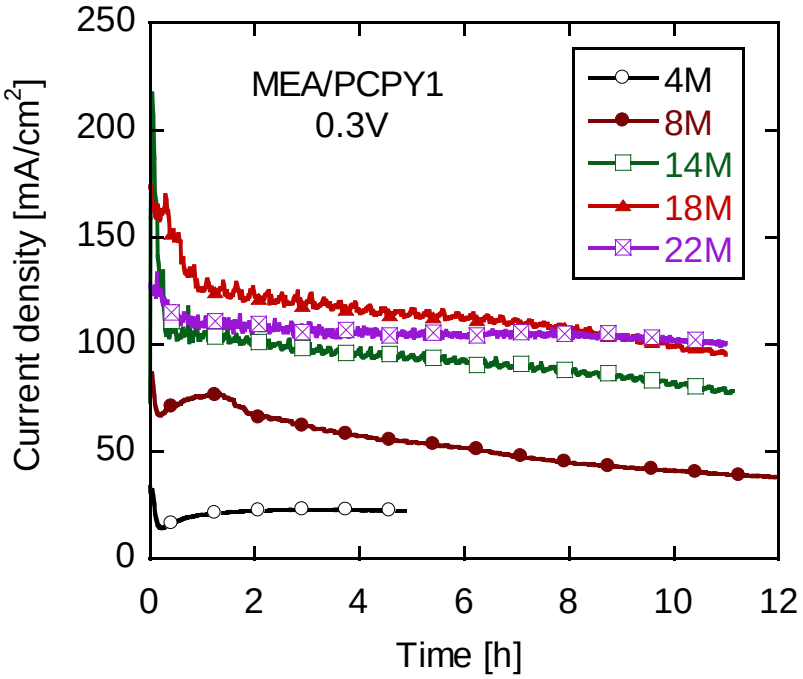

Figure 6-4: Current profile during continuous operation of passive DMFC with PCPY1, MEA/PCPY1, at cell voltage of 0.3V.

3.2. Effect of pore structure and thickness of PCP on current density and MCO at different cell voltages

The different types of the porous plates, PCPY1, PCPY2 and PCPS1 were used under the different cell voltages 0.1, 0.2 and 0.3V with different methanol concentrations. In these experiments, current density at 5h from the start was defined as a stable current density, $i_{5h,}$ and it was plotted at the different cell voltages against methanol concentration for the different PCPs, as shown in figures 6-5, 6-7, and 6-8.

Figure 6-5 shows the effect of pore structure and thickness of the PCP on the stable current density, i_{5h}, under 0.1V. The stable current density was linearly increased with increasing the concentration up to 60mA/cm^2, and there was no difference in the value of i_{5h} for the different PCPs. On the other hand, above 60mA/cm^2, every PCP had its own slope. The three PCPs were operated under limiting current conditions which was clear

from the linear dependency of i_{5h} on the methanol concentration. The stepper slope of the line shows the smaller rate of the methanol transport. This regime verified that the rate of the methanol transport was dependent on the current density, and pore structure and thickness of the PCP.

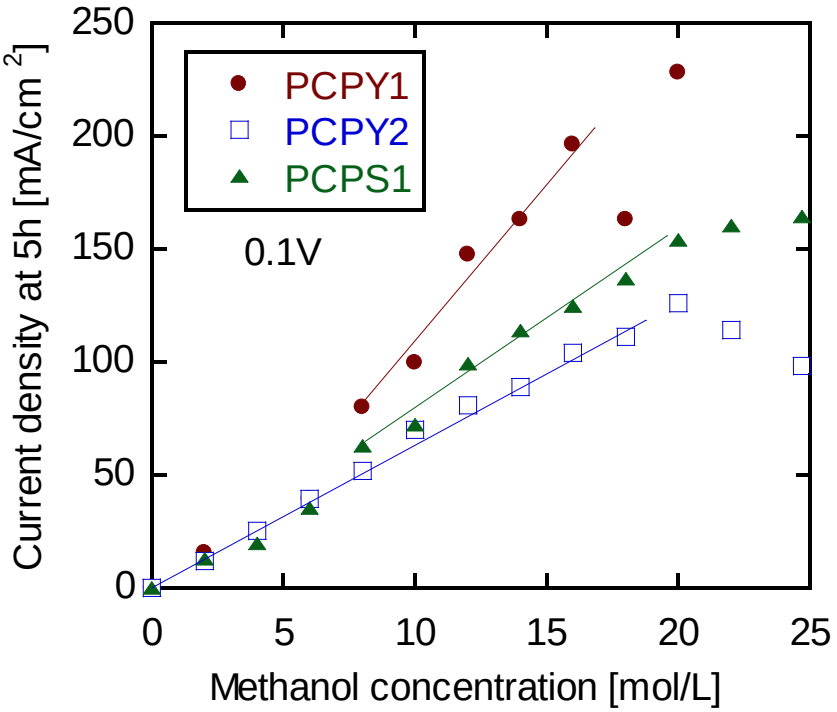

Figure 6-5: Effect of pore structure and thickness of PCP on the stable current density, i_{5h}, at 0.1V.

Figure 6-6 shows the effect of pore structure and thickness of the PCP on MCO during the i-t experiments shown in figure 6-5. MCO was similar to each other for the different PCPs in the range of low methanol concentration, which showed similar current densities among them as shown in figure 6-5. And a higher MCO for PCPY1 compared to PCPY2 was obtained in the range of high methanol concentration.

Under closed circuit conditions, the openings of the anode current collector were filled with CO_2 gas. Therefore, a layer of CO_2 gas was formed between the porous plate and the anode, and this gas layer obstruct methanol transport, methanol diffused in the gaseous state, from the reservoir to the anode surface. At low current densities, no CO_2 bubbles come out through the PCP where the CO_2 gas layer had not the enough pressure to force the solution out from the pores of the PCP and CO_2 transported by dissolving in the

methanol solution through the PCP. Where the liquid/gas interface was found at the bottom surface of the PCP, therefore, the thickness of the gas layer was similar for each PCP and a similar resistivity for methanol transport.

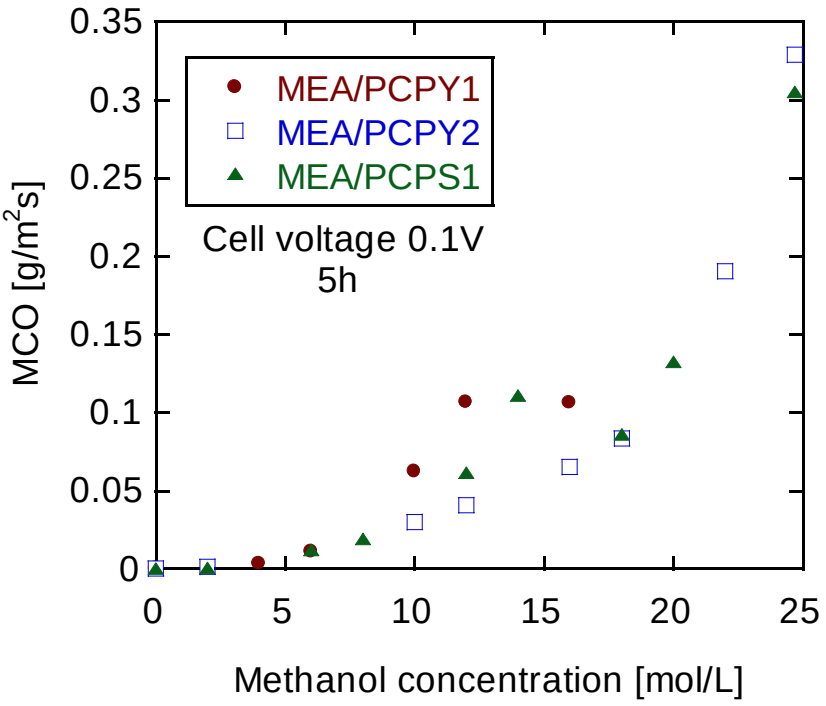

Figure 6-6: Effect of pore structure and thickness of PCP on MCO at 0.1V.

The resistance of the PCP with this gas layer was very high in comparison with the PCP alone, therefore no clear difference between the different types of the PCP in this range. But as the current density increased, the pressure of the gas layer increased as well as the surface tension of the methanol solution decreased due to the increase in methanol concentration. Therefore CO_2 bubbles could push the solution out from some pores of the PCP and escaped out through the PCP. At this point, the pressure of CO_2 gas layer in the barrier decreased instantaneously. This may induce entering some solution through pores instead of the gas out. This situation would be largely dependent on the properties of the PCP, where gas was easily escaped through thinner plates with large pore diameter than through thicker plates with small pore diameter, and this situation, in turn, would affect the resistivity of the gas layer. PCPY1 had large pore diameter, small thickness and low bubble point pressure, so it showed the lowest resistivity for the gas removal. Therefore, the higher methanol transport for PCPY1 would cause the steep slope of the line at high current densities as shown in Fig. 6-5. On the other hand, PCPY2 and PCPS1 had higher resistivity due to the large thickness or the small pore diameter, respectively; therefore

both of them would maintain high resistivity for methanol transport across the PCP as clear from their gentle slopes of the lines as shown in Fig. 6-5.

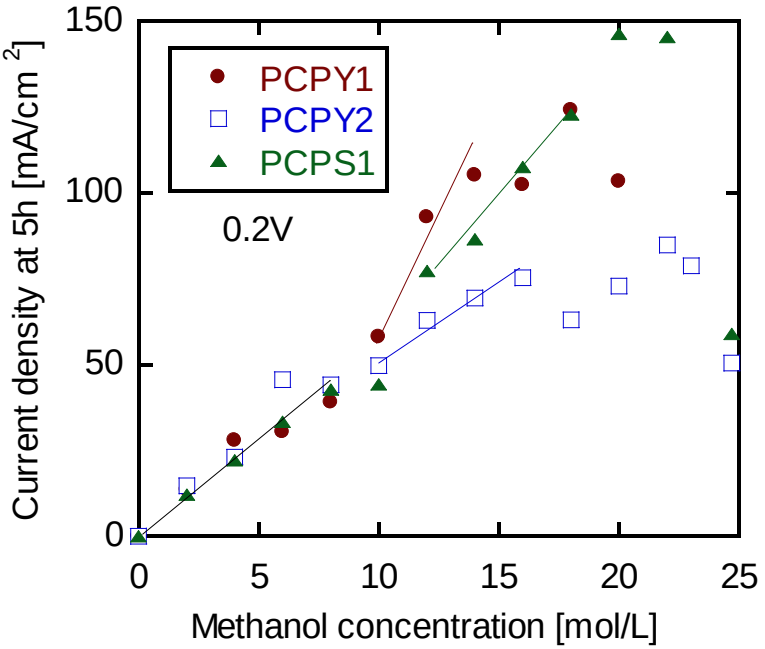

Figure 6-7: Effect of pore structure and thickness of PCP on the stable current density, i_{5h}, at 0.2V.

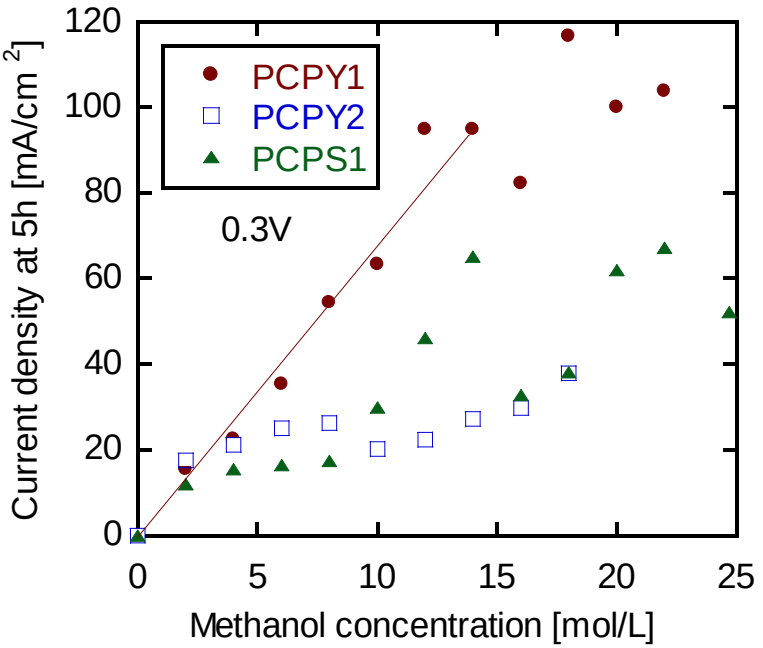

Figure 6-8: Effect of pore structure and thickness of PCP on the stable current density, i_{5h}, at 0.3V.

Figure 6-7 shows the effect of pore structure and thickness of the PCP on the stable current density, i_{5h}, under 0.2V. Similar behavior as that shown in Fig. 6-5 was obtained but with lower values of current densities, where i_{5h} was linearly increased with increasing the concentration and up to 60mA/cm^2, and all of PCPs had a similar slope. But this slope was different from one PCP to another at higher current densities. At this cell voltage, 0.2V, the three PCPs still operated under limiting current conditions, which was clear from the linear dependency of i_{5h} on methanol concentration, but with smaller values of current densities than that for 0.1V. For the same reasons discussed at Fig. 6-5, the pore structure and thickness of the PCP did not affect the performance in the low current densities range and affected it at higher current densities, above 60mA/cm^2.

Figure 6-8 shows the effect of pore structure and thickness of the PCP on the stable current density, i_{5h}, under 0.3V. In this figure, it was clear that the straight relationship between i_{5h} and methanol concentration appeared only for PCPY1 up to 12M. This suggested that the operation under limiting current still appeared for PCPY1 but not appeared for PCPY2 and PCPS1. This would be resulted from the different activities of the electrodes for each MEA. Although MCO for PCPY1 was high, but the reactivity of the electrodes for PCPY1 was high, then it showed the straight relationship.

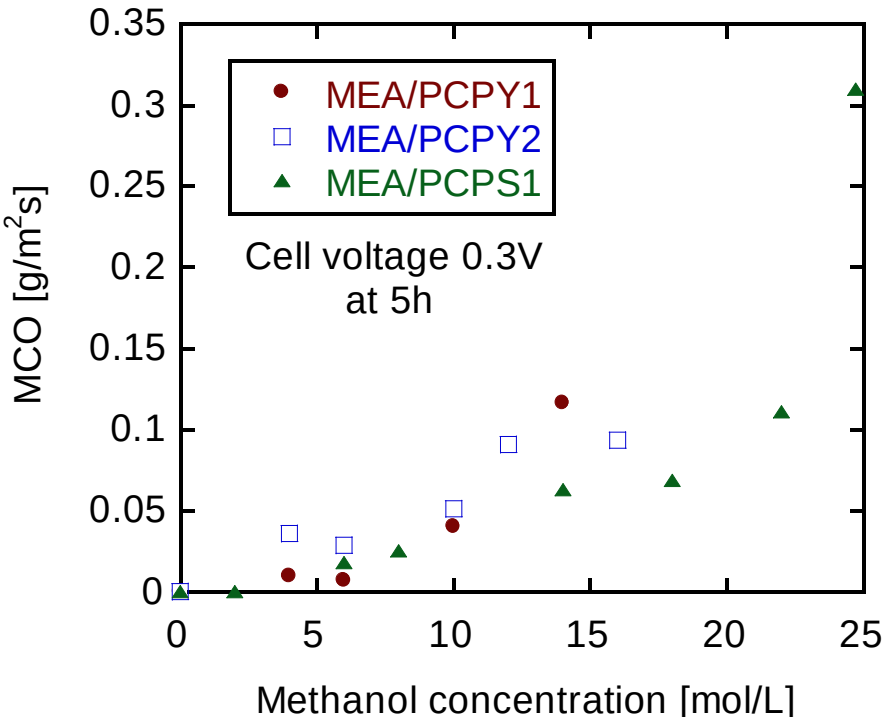

Figure 6-9: Effect of PCP pore structure and thickness on MCO at 0.2V.

Figure 6-9 shows the effect of pore structure and thickness of the PCP on MCO during the i-t experiments shown in Fig. 6-8. No clear difference in MCO among the different types of the PCPs was found although a higher MCO for PCPY1 was supposed.

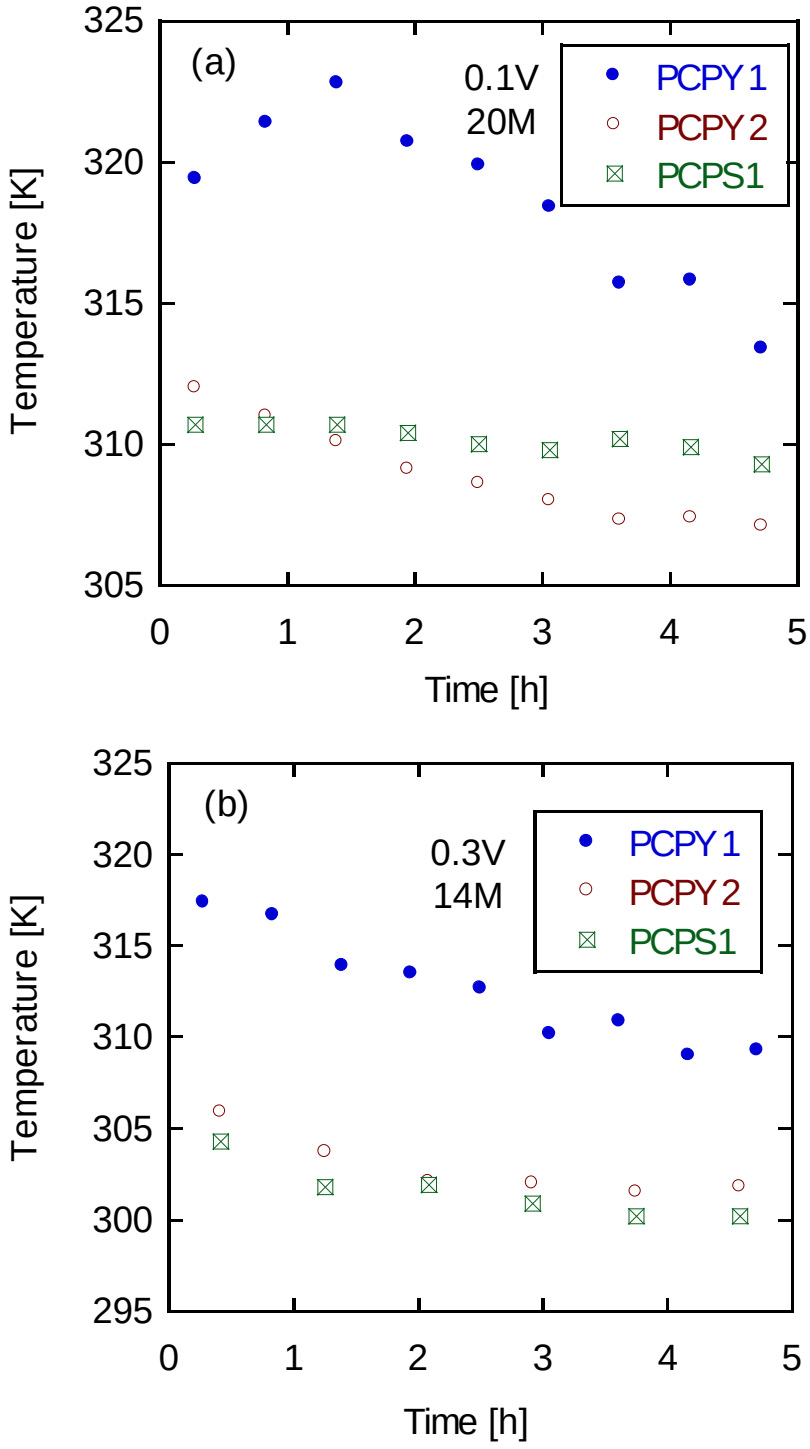

Figure 6-10: Variations in operating cell temperature of passive DMFC with different porous plates during i-t measurements:

(a) At 0.1V and 20M **(b) At 0.3V and 14M**

Figures 6-10a and b show the temperature profile during the i-t experiments at 0.1V and 0.3V for the different types of PCPs, respectively. At 14 and 20M, the cell temperature for PCPY2 and PCPS1 was nearly the same and it was lower than that for PCPY1 by about

ten degrees. The increase in cell temperature for PCPY1 than that for PCPY2 and PCPS1 would be related to MCO which was higher in case of PCPY1 than that for the other two PCPs.

3.3. Effect of the thickness of the gas layer on current density and MCO

Figure 6-11 shows the effect of the thickness of the gas layer between the PCP and the anode on the stable current density. With increasing the methanol concentration, the stable current density increased up to 130mA/cm^2 for 1mm thickness at 16M and up to 80mA/cm^2 for 7mm thickness at 20M. Up to 16M, i_{5h} was decreased with increasing the barrier thickness from 1mm to 7mm. The reduction in i_{5h} with increasing the thickness of the gas barrier would be due to the increase in the resistivity of the gas layer.

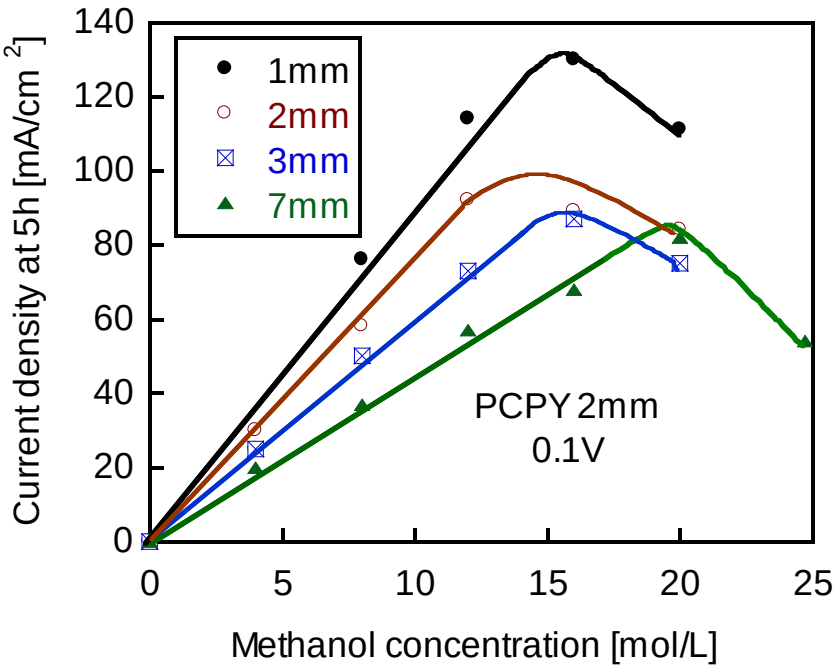

Figure 6-11: Effect of gas layer thickness on the stable current density, i_{5h}, using PCPY2 at 0.1V.

Figure 6-12 shows the effect of gas barrier thickness on the average MCO during the i-t experiments using PCPY2 at 0.1V and 20M. MCO was decreased from 1.31 g/m^{2}s to 0.064 g/m^{2}s with increasing the gas barrier thickness from 1mm to 7mm. The reduction in MCO with increasing the gas barrier thickness was due to the increased resistivity to methanol transport across this gas layer.

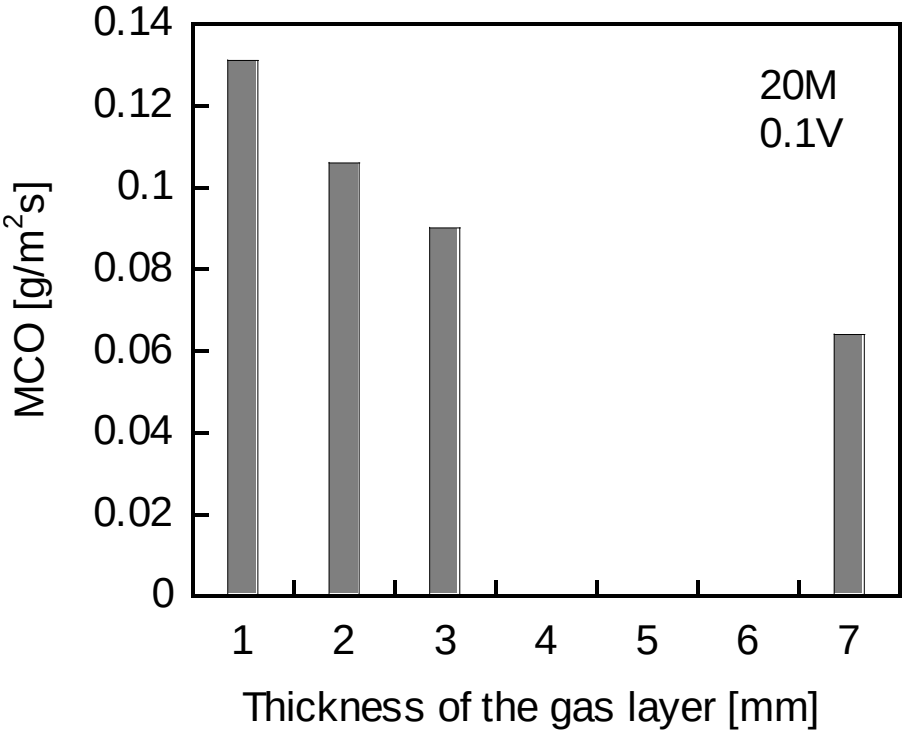

Figure 6-12: Effect of gas layer thickness on MCO at 0.1V.

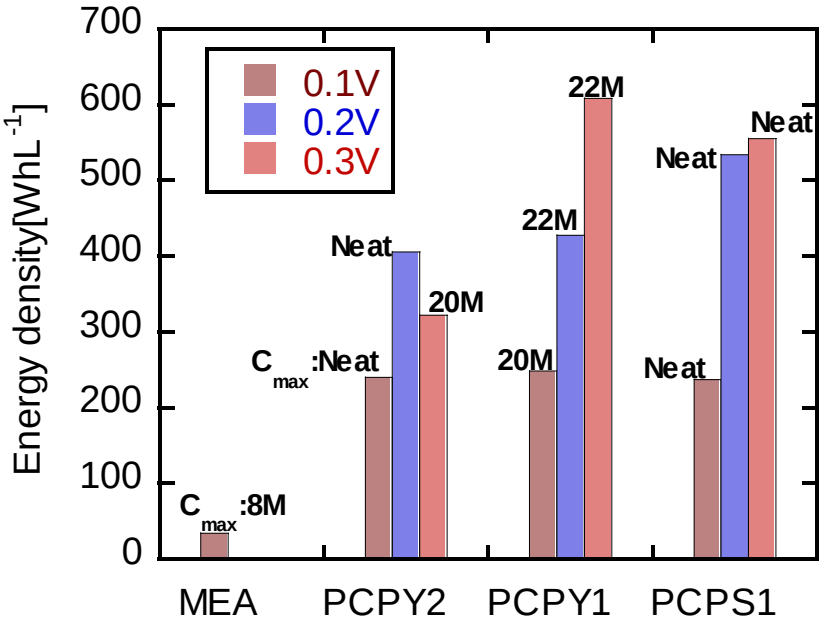

Figure 6-13: Effect of PCP pore structure and thickness on the energy density of passive DMFC at different cell voltages.

3.4. Effect of PCP pore structure and thickness on energy density

Figure 6-13 shows the effect of PCP pore structure and thickness on the energy density at the different cell voltages 0.1V, 0.2V and 0.3V as well as that of conventional MEA at 0.1V. Energy density increased largely as a result of using the PCP. It was increased more than seven times than that for without PCP. The increase in energy density for PCP would be resulted from the controlling of MCO by the PCP therefore faraday efficiency was increased as well as voltage efficiency was increased by working at high cell voltage. Energy density was the highest in case of PCPS1 and PCPY1 at 0.3V, and this would be caused by the high cell efficiency for PCPS1 and PCPY1 due to good control of MCO or high cell temperature, respectively.

4. Conclusions

The effect of pore structure and thickness of the PCP as well as the gas layer thickness on the mass transfer and performance of passive DMFC under different cell voltages 0.1, 0.2 and 0.3V using different methanol concentrations ranging from 2M to neat methanol have been investigated, and the following conclusions were obtained.

1) As a result of the mass transfer restrictions by employing the PCP, high methanol concentrations could be used efficiently producing relatively high constant power density, 30mW/cm^2 in case of PCPY1 at 0.3V and 22M for more than 10hrs.

2) The thickness of the gas layer which was formed between the PCP and the anode surface was one of the most important factors in resisting methanol transport. The effect of the PCP structure and thickness on the cell performance appeared at relatively high current densities.

3) It was demonstrated that using of PCP is quite effective to achieve high energy density for passive DMFCs, and higher resistance to the methanol transport across the gas barrier could be obtained by increasing its thickness.

5. References

1. C. Coutanceau, R.K. Koffi, J.-M. Leger, K. Marestin, R. Mercier, C. Nayoze, P. Capron, *J. Power Sources* 1**60** (2006) 334–339.

2. M. Broussely, G. Archdale, *J. Power Sources* **136** (2004), p. 386.

3. K. Takei, K. Ishihara, K. Kumai, T. Iwahori, K. Miyake, T. Nakatsu, N. Terada, N. Arai, *J. Power Sources* **136** (2003) (119–121), p. 887.

4. C. Lamy, J.-M. Léger, *J. Phys. IV* **4** (1994) C1.

5. L. Zhou, *Renew. Sust. Energy Rev.* **9** (2005), p. 395.

6. F. Vigier, C. Coutanceau, A. Perrard, E.M. Belgsir, C. Lamy, *J. Appl. Electrochem.* **34** (2004), p. 439

7. M. Hogarth, R. Ralph, *Platinum Metals Rev.* **46** (2002), p. 146.

8. R. Chen, T.S. Zhao, *J. Power Sources* **152** (2005) 122–130.

9. B. Bae, B.K. Kho, T. Lim, I. Oh, S. Hong, H.Y. Ha, *J. Power Sources* **158** (2006) 1256–1261.

10. J.T. Wang, S. Wasmus, R.F. Savinell, *J. Electrochem. Soc.* **143** (1996) 1233–1239.

11. E. Peled, T. Duvdevani, A. Aharon, A. Melman, *Electrochem. Solid State Lett.* **3** (2000) 525–528.

12. M.V. Fedkin, X. Zhou, M.A. Hofmann, E. Chalkova, J.A. Weston, H.R. Allcock, S.N. Lvov, *Mater. Lett*. **52** (2002) 192–196.

13. T. Yamaguchi, M. Ibe, B.N. Nair, S. Nakao, *J. Electrochem. Soc.* **149** (2002) A1448–A1453.

14. M.L. Ponce, L. Prado, B. Ruffmann, K. Richau, R. Mohr, S.P. Nunes, *J. Membr. Sci.* **217** (2003) 5–15.

15. A.S. Arico, P. Creti, P.L. Antonucci, V. Antonucci, *Electrochem. Solid State Lett.* **1** (1998) 66–68.

16. C. Yang, S. Srinivasan, A.S. Arico, P. Creti, V. Baglio, V. Antonucci, *Electrochem. Solid State Lett.* **4** (2001) A31–A34.

17. N. Jia, M.C. Lefevre, J. Halfyard, S. Qi, P.G. Pickup, *Electrochem. Solid State Lett.* **3** (2000) 529–531.

18. I.J. Hobson, H. Ozu, M. Yamaguchi, M. Muramatsu, S. Hayase, *J. Mater. Chem.* **12** (2002) 1650–1656.

19. W.C. Choi, J.D. Kim, S.I. Woo, *J. Power Sources* **96** (2001) 411– 414.

20. S.R. Yoon, G.H. Hwang, W.I. Cho, I.-H. Oh, S.-A. Hong, H.Y. Ha, *J. Power Sources* **106** (2002) 215–223.

21. Y.K. Xiu, K. Kamata, T. Ono, K. Kobayashi, T. Nakazato, N. Nakagawa, *Electrochemistry* **73** (2005) 67–70.

22. G.Q. Lu, C.Y. Wang, T.J. Yen, X. Zhang, *Electrochim. Acta* **49** (2004) 821.

23. N. Nakagawa, K. Kamata, A. Nakazawa, M. Ali Abdelkareem, K. Sekimoto, *Electrochemistry* **74** No.3 (2006) 221-225.

24. N. Nakagawa, M. Ali Abdelkareem, K. Sekimoto, *J. Power Sources* **160** (2006) 105–115.

25. M. Ali Abdelkareem, N. Nakagawa, *J. Power Sources* **162** (2006) 114-123.

26. M. Ali Abdelkareem, N. Nakagawa, *J. Power Sources* **165** (2007) 685-691.

27. Z. Guo, A. Faghri , *J. Power Sources* **160** (2006) 1142-1155.

28. HaeKyoung Kim, *J. Power Sources* **162** (2006) 1232-1235.

CONCLUSIONS

A novel electrode structure has been proposed for controlling methanol crossover in passive direct methanol fuel cells. Different experiments have been carried out to clarify the fundamental basics, merits, and the main parameters affecting the performance of this type of fuel cells under both open and closed circuit conditions. The following conclusions were drawn.

Under open circuit conditions:

Methanol crossover in a passive DMFC using a porous plate as a support had been studied using different porous plates with different structures and different water absorptivities at different methanol concentrations and temperatures. The following conclusions were drawn.

1. The porous plates controlled and reduced the methanol crossover. As the material of the porous plate, both the porous carbon plate and the porous Al_2O_3 plate were useful.
2. The separation of methanol through this type of passive DMFC was explained theoretically and experimentally by the diffusion control of the methanol transport by the PCP depending on the properties of the porous material, i.e., thickness, porosity and water absorptivity of the porous material.

Under closed circuit conditions:

Performance of the passive DMFC with and without PCP was investigated under closed circuit conditions with different methanol concentrations ranging from 1M to neat methanol, using different types of porous materials i.e., different structures, thicknesses, different gas barrier existing and not existing, thicknesses, pressures, as well as different operating voltages. The following conclusions were drawn.

1. Mass transfer of both of methanol and water from the reservoir to the anode were significantly restricted by the employment of PCP at the anode side. As a result of the mass transfer restrictions by the employing of PCP, high methanol concentrations, even neat methanol, could be used efficiently. This results in a high power density of DMFC.

2. Back diffusion of water from the cathode to the anode was confirmed at relatively high methanol concentrations for the DMFC with PCP. This was desired to prevent the cathode from flooding and increase the cell performance.

3. Both flooding at the cathode and depletion of methanol at the anode decreased the cell performance of the DMFC without the PCP. The Flow of both oxygen and methanol increased the current density. On the other hand the performance of the DMFC with a PCP was hardly affected by the flow either methanol or oxygen.

4. A moderate supply of oxygen to the cathode, such as air-breathing, was appropriate for the DMFC with a PCP.

5. The formation of CO_2 gas layer was very important for strong obstructing the methanol transport to the anode surface where the gaseous methanol diluted in the CO_2 gas contacted. The resistance to the methanol transport across the PCP was affected by the pore structure of the PCP, i.e., pore size and the bubble point pressure.

6. When the pore size was large, 42μm, the bubble through the PCP accelerated the methanol transport. The changes of the CO_2 pressure affect the performance only when they affect the methanol and water fluxes through the PCP within the measured pressure range.

7. The thickness of the gas layer formed between the PCP and the anode surface was one of the most important factors in resisting methanol transport. The effect of the PCP structure and thickness on the cell performance appeared at relatively high current densities.

8. When the PCPs with different pore size were compared, difference in the resistance for the methanol transport through the PCP and the gas layer appeared only at high current densities, over 60mA/cm^2, where CO_2 bubbles evolved through the PCP. This suggested that the resistance for the methanol transport was related to the CO_2 gas discharge through the PCP depending on the pore structure of the PCP.

9. It was demonstrated that using of PCP is quite effective to achieve high energy density for passive DMFCs. Higher resistance to the methanol transport across the gas barrier could be obtained by increasing its thickness.

ACKNOWLEDGMENT

This thesis is dedicated to ALLAH Subhanahu wa Ta`aalaa whose guidance, help and grace was instrumental in making this humble work a reality. I have many people to thank for their assistance.

I would like to express my deepest appreciation to Professor N. Nakagawa for his brilliant guidance and earnest supervision not only throughout the duration of this study but also in all my general life aspects. He all time give and still giving his teach, care and help throughout the course of my studies in Gunma University and living in Japan.

Many thanks to Professor S. Katsura, J. Ozaki, T. Oshima and R. Noda for reviewing this thesis and giving many valuable comments and advice on my study that greatly helped me to improve this thesis.

I am also really grateful to Dr. T. Nakazato for his helpful advices and kind supports in my study. I am also grateful to Ms. K. Saito for her much help in daily work and missing her after she changed her position and left our lab.

A cordial thank to K. Sekimoto, N. Morohashi, and N. Masumi for their active cooperation and support in the experiment even during the hard times, and also to everyone of Prof. Nakagawa laboratory who gave me useful and helpful assistance in various ways in past few years. With best wishes to everyone in his incoming job or study.

A lot of thanks for all of the Gunma University staff for their help during my study and also for all of the Japanese for their kindness and help during my daily life in Japan.

A lot of thanks for my lovely country, Egypt, which give me this chance of teaching abroad and supporting me financially during this study. Also a lot of thanks to all the members of the Cultural Bureau, Embassy of Egypt, Tokyo, for their sincere cooperation and help.

I would like to thank my parents for all their support, encouragement, sincere heart dawat and prayers. I would also like to thank all my friends whatever their nationalities in Kiryu campus for creating an interesting atmosphere and bring a lot of happiness to me every day.

I give my profound and deepest thanks to my wife for her help and encouragements and providing the suitable atmosphere for my study.

List of Publications and Presentations Related To the Thesis

Publications related to the thesis:

Chapter two

1. Nobuyoshi NAKAGAWA, **Mohammad Ali Abdelkareem**, Kazuya SEKIMOTO, "Control of methanol transport and separation in a DMFC with a porous support", *Journal of Power Sources*, **160,** 105-115 (2006).

Chapter three

2. **Mohammad Ali Abdelkareem**, Nobuyoshi NAKAGAWA, "DMFC employing a porous plate for an efficient operation at high methanol concentrations", *Journal of Power Sources*, 162 (2006) 114-123.

Chapter four

3. **Mohammad Ali Abdelkareem**, Nobuyoshi NAKAGAWA, "Effect of oxygen and methanol supply modes on the performance of a DMFC employing a porous plate", *Journal of Power Sources*, **165**, 685-691(2007).

Chapter five

4. Nobuyoshi NAKAGAWA, **Mohammad Ali Abdelkareem**, "The role of carbon dioxide layer prepared by a porous carbon plate in a passive DMFC as a mass transport barrier", *Journal of Chemical Engineers of Japan*, **40**, (2007), 1199-1204

Chapter six

5. **Mohammad Ali Abdelkareem**, Nobuto Morohashi, and Nobuyoshi Nakagawa, "Factors affecting methanol transport in a passive DMFC employing a porous carbon plate", *Journal of Power Source* **172** (2007) 659-665.

Other publications related to the background of the thesis:

1. Nobuyoshi NAKAGAWA, Kosuke KAMATA, Akimichi NAKAZAWA, **Mohammad Ali Abdelkareem**, Kazuya SEKIMOTO, "Methanol crossover controlled by a porous carbon plate as a support", *Electrochemistry*, **74,** 221-225 (2006).
2. Tsutomu NAKAZATO, Naoya HIRAO, **Mohammad Ali Abdelkareem**, Akimichi NAKAZAWA, and Nobuyoshi NAKAGAWA, "Methanol Diffusion through a Porous Plate in Anode Backing of a Passive Direct Methanol Fuel Cell under Closed Circuit Conditions", *Journal of Chemical Engineers of Japan*, **40**, (2007), 1108-1112

Conference papers

International

1. **Mohamad Ali Abdelkareem**, Kazuya Sekimoto, Nobuyoshi Nakagawa, "Methanol Crossover Through a Passive DMFC Using Porous Support", 4th International Fuel Cell Workshop 2005, Kofu, Yamanashi, Japan (Sep. 23-24, 2005)
2. **Mohamad Ali Abdelkareem**, N. Nakagawa; "DMFC performance at high methanol concentrations" battery symposium, The 47th Battery Symposium in Japan 20-22 Nov. 2006, Tokyo
3. Nobuyoshi Nakagawa, **Mohammad Ali Abdelkareem**, "The role of Carbon Dioxide Layer Prepared by a Porous Carbon Plate in a Passive DMFC as a Mass Transport Barrier", International Symposium on Innovative Materials for Processes in Energy Systems, IMPRES, 28-31 October, 2007, Kyoto Research Park, Kyoto, Japan, Oral
4. **Mohammad Ali Abdelkareem,** Nobuyoshi Nakagawa, "Methanol Transport in a Passive Dmfc Employing a Porous Carbon Plate", 2007 AIChE Annual Meeting, Nov. 4-9, 2007, Salt Lake City, Utah, Oral.
5. Nobuyoshi Nakagawa, **Mohammad Ali Abdelkareem**, "ROLE OF CARBON DIOXIDE LAYER TO INCREASE ENERGY DENSITY OF A PASSIVE DMFC", Power MEMS 2007, Nov. 28-29, Freiburg, Germany, poster

Domestic

1. **Mohammad Ali Abdelkareem**、関本和也、中川紳好：MCO through a novel DMFC using porous carbon support and factors affecting on it、化学工学会第37回秋季大会、G123、岡山大学、2005年9月15-17日
2. **Mohammad Ali Abdelkareem**, Kazuya Sekimoto, Nobuyoshi Nakagawa：Effect of porous plate and electrolyte membrane on methanol crossover through a novel passive DMFC, 第46回電池討論会、1F-16、名古屋（2005年11月16-18日）
3. 平尾直也、Mohammad Ali Abdlekareem、中川紳好、"多孔質支持体を用いるDMFCの発電特性"、化学工学会第71年会、M214，2006年3月28-30日、東京工大
4. 関本和也、Mohammad Ali Abdlekareem、中川紳好、"多孔質支持体を用いるDMFCのメタノールクロスオーバー"、化学工学会第71年会、M215，2006年3月28-30日、東京工大
5. Mohammad Ali Abdelkareem，平尾直也，中川紳好、"The Effect of Using Porous Plate on the Performance of Passive DMFC"、電気化学73回大会、1P32、2006年4月1-3日、首都大学東京

6. 中川紳好、Mohammad Ali Abdelkareem、”多孔質板の利用によるクロスオーバー低減と高濃度メタノール運転”，第 13 回燃料電池シンポジウム講演予稿集，B35，2006 年 5 月 16-17 日、タワーホール船堀

7. Mohammad Ali Abdelkareem、関本和也、中川紳好，“Separation of methanol and water in a passive DMFC using a porous plate at open circuit conditions”，分離技術会年会 2006，技術・研究発表講演要旨集,S7-01，2006 年 6 月 2-3 日,早稲田大学理工学部

8. Mohammad Ali Abdlekareem，中川紳好，”Efficient DMFC using high methanol concentration”、化学工学会第 38 回秋季大会、0303，2006 年 9 月 16-18 日、福岡大

9. 中川紳好、Mohammad Ali Abdelkareem，“多孔質体を利用した新規 DMFC の高濃度メタノール運転特性”，高分子討論会、1T08，2006 年 9 月 20-22 日、富山大

10. 川人慎平、澤田真一、八巻徹也、浅野雅春、石黒弘規、Mohammad Ali Abdelkareem、中川紳好、寺井隆幸、鈴木晶大、前川康成、”架橋フッ素系高分子電解質膜の DMFC 性能”、2006 年電気化学会秋季大会、2C25，2006 年 9 月 14-15 日、京都（同志社大）

11. Mohammad Ali Abdelkareem, Nobuyoshi Nakagawa，“DMFC performance at high methanol concentrations”，The 47th Battery Symposium in Japan，1B-25，November 20-22，Tokyo

12. 川人慎平、澤田真一、八巻徹也、浅野雅春、石黒弘規、Mohammad Ali Abdelkareem、中川紳好、鈴木晶大、寺井隆幸、前川康成，“架橋ポリテトラフルオロエチレン電解質膜を用いた DMFC の性能評価”，第 47 回電池討論会、2B-03，11 月 20-22 日、東京

13. 中川紳好、Mohammad Ali Abdelkareem、”新規電極構造体における物質移動規制と DMFC の高性能化”、化学工学会第 72 年会、D301，2007 年 3 月 21 日、京都大

14. 増見直人、Mohammad Ali Abdelkareem、中里勉、野田玲治、中川紳好、”新規電極構造体を有するパッシブ DMFC の動作特性”、化学工学会第 72 年会、D304，2007 年 3 月 21 日、京都大

15. Mohammad Ali Abdlekareem、中川紳好、”The role of carbon dioxide layer prepared by a porous carbon plate in a passive DMFC as a mass transport barrier”、化学工学会第 39 回秋季大会、E121，2007 年 9 月 13 日、北海道大.

16. 中川紳好、Mohammad Ali Abdelkareem “パッシブ DMFC における高濃度メタノールの利用”，日本化学会第一回関東支部大会，1A3-13、2007 年 9 月 27 日、首都大東京.